To the Graduate Council:

I am submitting herewith a thesis written by J. Conrad Wysor entitled "Control of the AEDC-PWT 16-ft Transonic Wind Tunnel for Subsynchronous Operation." I have examined the final copy of this thesis for form and content and recommend that it be accepted in partial fulfillment of the requirements for the degree of Master of Science, with a major in Electrical Engineering.

Roy D. Joseph

Roy D. Joseph, Major Professor

We have read this thesis
and recommend its acceptance:

James W. Cunningham

Bruce W. Bomar

Accepted for the Council:

Lee Winkel

Vice Provost
and Dean of the Graduate School

# CONTROL OF THE AEDC PWT 16-FT TRANSONIC WIND TUNNEL FOR SUBSYNCHRONOUS OPERATION

A Thesis

Presented for the

Master of Science

Degree

The University of Tennessee, Knoxville

J. Conrad Wysor

May 1991

ACKNOWLEDGMENTS

The author wishes to thank Calspan Field Services for the opportunity to pursue educational opportunities at UTSI, and the officials of Calspan and the United States Air Force for permission to use the information presented herein. The author is also thankful to the members of his Committee, Drs. R. D. Joseph, J. W. Cunningham, and B. W. Bomar, for their help and support in this project, and to the author's family for their encouragement and support.

## ABSTRACT

This study was undertaken to develop a control algorithm which could maintain a set Mach number during subsynchronous operation of the AEDC PWT 16T wind tunnel to within 3 percent of its setpoint. The PWT Main Drive induction motors, the liquid rheostat positioning system, and the 16T compressor were modeled and studied using a computer simulation. By linearizing the system model, classical design techniques were used to design a controller. Due to the nature of the system, an adaptive proportional controller was sufficient to accomplish the control objectives. This controller was designed to minimize the overshoot of the closed loop system and maintain the setpoint Mach number with no steady state error. The adaptive proportional gain control algorithm is dependent on the tunnel total pressure, the test section Mach number, and the number of induction motors used to drive the compressor. The controller was designed to maintain a damping ratio of approximately 0.8. A computer simulation of the system with the controller implemented showed that the Mach number could be maintained with zero steady state error and an overshoot of less than two percent for a 10 percent step change in the operating set point.

TABLE OF CONTENTS


| CHAPTER | | PAGE |
|---|---|---|
| I. | INTRODUCTION | 1 |
| | Description of Tunnel 16T | 1 |
| | Problem Statement | 1 |
| | Approach | 4 |
| II. | MODEL DEVELOPMENT | 6 |
| | Rheostat Positioning System | 6 |
| | Induction Motors | 21 |
| | 16T Compressor | 26 |
| III. | CONTROLLER DEVELOPMENT | 42 |
| | Linearization of Model | 42 |
| | Development of Control Algorithm | 54 |
| IV. | RESULTS | 68 |
| V. | CONCLUSIONS AND RECOMMENDATIONS | 74 |
| BIBLIOGRAPHY | | 78 |
| APPENDIXES | | 80 |
| A. | Derivation of Induction Motor Time Constant | 81 |
| B. | Effects of the Mass of the Air in the Tunnel Circuit | 86 |
| C. | Additional Simulation Results | 103 |
| VITA | | 118 |

# LIST OF TABLES

TABLE PAGE


2-1. Liquid Rheostat Positioning System Values . . . . . 16

2-2. Induction Motor Values . . . . . 25

2-3. Compressor Values . . . . . 37

# LIST OF FIGURES


| FIGURE | | PAGE |
|---|---|---|
| 1-1. | 16T Wind Tunnel Configuration | 2 |
| 1-2. | Schematic of Subsynchronous Control of Main Drive | 5 |
| 2-1. | Rototrol and DC Motor Electrical Schematic | 7 |
| 2-2. | Liquid Rheostat Mechanical Schematic | 13 |
| 2-3. | Change in Electrolyte Resistance with Temperature | 14 |
| 2-4. | Liquid Rheostat Positioning System Simulation Results | 18 |
| 2-5. | Liquid Rheostat Electrode Velocity | 18 |
| 2-6. | Liquid Rheostat Positioning System Simulation Results for Master/Slave Operation | 20 |
| 2-7. | Induction Motor Equivalent Circuit for One Phase | 22 |
| 2-8. | Variation of Compressor Stator Blade Angle with Test Section Mach Number | 27 |
| 2-9. | 16T Subsynchronous Operating Limits | 28 |
| 2-10. | Test Section Mach Number as a Function of Compressor Shaft Speed | 32 |
| 2-11. | Compressor Pressure Ratio as a Function of Test Section Mach Number | 32 |
| 2-12. | Compressor Efficiency as a Function of Test Section Mach Number | 33 |
| 2-13. | $f(\omega_m)$ as a Function of Compressor Shaft Speed | 35 |
| 2-14. | Open Loop Simulation Flow Diagram | 39 |
| 2-15. | Open Loop Response to a Step Input for Two Motor Operation and $PT_T$=2000 lb/ft$^2$ | 40 |
| 3-1. | Variation of Time Constant $\tau_c$ with Total Pressure for Mach 0.4, Two Motor Operation | 50 |

LIST OF FIGURES (Continued)


3-2. Variation of Time Constant $\tau_c$ with Compressor Shaft Speed for a Total Pressure of 1000 lb/ft$^2$, Two Motor Operation . . . . . 50

3-3. Block Diagram of Linearized Model . . . . . 55

3-4. Block Diagram for Closed Loop Control of Mach Number . . 57

3-5. w-Plane Bode Plot for Mach 0.4 and a Total Pressure of 2000 lb/ft$^2$ with Two Motors . . . . . 60

3-6. Damping Ratio versus Phase Margin for a Second Order System . . . . . 62

3-7. w-Plane Bode Plot with Proportional Gain $K_p$ for Mach 0.4 and a Total Pressure of 2000 lb/ft$^2$ with Two Motors . . . . . 64

3-8. Change in Controller Gain $K_p$ for Mach 0.4 and a Total Pressure of 2000 lb/ft$^2$ with Two Motors . . . . . 65

3-9 Control Algorithm Flow Diagram . . . . . 67

4-1. Closed Loop Simulation Flow Diagram . . . . . 69

4-2. Simulation Results for a Total Pressure of 1000 lb/ft$^2$ at Mach 0.2 and One Motor Operation . . . . . 70

4-3. Simulation Results for a Total Pressure of 2000 lb/ft$^2$ at Mach 0.4 and Two Motor Operation . . . . . 70

4-4. Simulation Results for a Total Pressure of 1000 lb/ft$^2$ at Mach 0.6 and Two Motor Operation . . . . . 71

4-5. Simulation Results for a 10% Disturbance in Compressor Load at 2000 lb/ft$^2$, Mach 0.4, and Two Motor Operation . . . 73

4-6 Compressor Load Disturbance . . . . . 73

5-1. Control System Implementation . . . . . 77

B-1. 16T Wind Tunnel Dimensions . . . . . 92

LIST OF FIGURES (Continued)


B-2. Compressor Pressure Ratio $\lambda_c$(rpm) as a Function of Compressor Shaft Speed . . . . . 96

B-3. Steady State Compressor Pressure Ratio $\lambda_{ss}$(M) as a Function of Test Section Mach Number . . . . . 96

B-4. Tunnel Pressure Ratio $\lambda_T$(M) as a Function of Test Section Mach Number . . . . . 97

B-5. Effect of a 10 Percent Change in Compressor Shaft Speed for a Mach Number Operating Point of 0.2 . . . . . 98

B-6. Effect of a 10 Percent Change in Compressor Shaft Speed for a Mach Number Operating Point of 0.3 . . . . . 99

B-7. Effect of a 10 Percent Change in Compressor Shaft Speed for a Mach Number Operating Point of 0.4 . . . . . 100

B-8. Effect of a 10 Percent Change in Compressor Shaft Speed for a Mach Number Operating Point of 0.5 . . . . . 101

B-9. Effect of a 10 Percent Change in Compressor Shaft Speed for a Mach Number Operating Point of 0.6 . . . . . 102

C-1. Open Loop Response to a Step Input for One Motor Operation and $PT_T$ =1000 lb/ft$^2$. . . . . 104

C-2. Open Loop Response to a Step Input for One Motor Operation and $PT_T$ =2000 lb/ft$^2$. . . . . 105

C-3. Open Loop Response to a Step Input for One Motor Operation and $PT_T$ =3000 lb/ft$^2$. . . . . 106

C-4. Open Loop Response to a Step Input for Two Motor Operation and $PT_T$ =1000 lb/ft$^2$. . . . . 107

C-5. Open Loop Response to a Step Input for Two Motor Operation and $PT_T$ =2000 lb/ft$^2$. . . . . 108

C-6. Open Loop Response to a Step Input for Two Motor Operation and $PT_T$ =3000 lb/ft$^2$. . . . . 109

LIST OF FIGURES (Continued)


C-7. Simulation Results for a Total Pressure of 2000 lb/ft$^2$ at Mach 0.2 and One Motor Operation . . . . . 110

C-8. Simulation Results for a Total Pressure of 1000 lb/ft$^2$ at Mach 0.2 and Two Motor Operation . . . . . 110

C-9. Simulation Results for a Total Pressure of 2000 lb/ft$^2$ at Mach 0.2 and Two Motor Operation . . . . . 111

C-10. Simulation Results for a Total Pressure of 3000 lb/ft$^2$ at Mach 0.2 and Two Motor Operation . . . . . 111

C-11. Simulation Results for a Total Pressure of 1000 lb/ft$^2$ at Mach 0.3 and One Motor Operation . . . . . 112

C-12. Simulation Results for a Total Pressure of 2000 lb/ft$^2$ at Mach 0.3 and One Motor Operation . . . . . 112

C-13. Simulation Results for a Total Pressure of 1000 lb/ft$^2$ at Mach 0.3 and Two Motor Operation . . . . . 113

C-14. Simulation Results for a Total Pressure of 2000 lb/ft$^2$ at Mach 0.3 and Two Motor Operation . . . . . 113

C-15. Simulation Results for a Total Pressure of 3000 lb/ft$^2$ at Mach 0.3 and Two Motor Operation . . . . . 114

C-16. Simulation Results for a Total Pressure of 1000 lb/ft$^2$ at Mach 0.4 and One Motor Operation . . . . . 114

C-17. Simulation Results for a Total Pressure of 1250 lb/ft$^2$ at Mach 0.4 and One Motor Operation . . . . . 115

C-18. Simulation Results for a Total Pressure of 1000 lb/ft$^2$ at Mach 0.4 and Two Motor Operation . . . . . 115

C-19. Simulation Results for a Total Pressure of 3000 lb/ft$^2$ at Mach 0.4 and Two Motor Operation . . . . . 116

C-20. Simulation Results for a Total Pressure of 1000 lb/ft$^2$ at Mach 0.5 and Two Motor Operation . . . . . 116

LIST OF FIGURES (Continued)

C-21. Simulation Results for a Total Pressure of 2000 lb/ft$^2$ at Mach 0.5 and Two Motor Operation . . . . . 117

C-22. Simulation Results for a Total Pressure of 750 lb/ft$^2$ at Mach 0.6 and Two Motor Operation . . . . . 117

# LIST OF SYMBOLS

| | |
|---|---|
| $A_e$ | Area of liquid rheostat electrodes, $in^2$ |
| $A_T$ | Area of test section, $ft^2$ |
| a | Inverse of time constant $\tau_c$, $sec^{-1}$ |
| B | Number of induction motors |
| c | Speed of sound, ft/sec |
| $C_p$ | Specific heat at constant pressure, ft-lb/slug- $^oR$ |
| $C_1$ | Compressor speed function linearization constant |
| $C_2$ | Compressor speed function linearization constant, sec |
| $C_3$ | Compressor speed function linearization constant, $sec^2$ |
| $C_4$ | Mach number linearization constant |
| $C_5$ | Mach number linearization constant, sec |
| $C_6$ | Mach number linearization constant, $sec^2$ |
| $e_a$ | Rototrol terminal voltage, volt |
| $e_b$ | DC motor armature voltage, volt |
| $e_f$ | Rototrol field voltage, volt |
| f | DC motor viscous friction coefficient, ft-lb-sec |
| $f(\omega_m)$ | Compressor speed function |
| F(M) | Compressor Mach number function |
| GR | Gear ratio of DC motor driven gear box |
| $G_c(z)$ | Controller z-plane transfer function |
| $G_1(z)$ | Combined transfer function of plant and controller |
| $i_a$ | DC motor armature current, amp |
| $i_f$ | Rototrol field current, amp |

| | |
|---|---|
| $\bar{I}_r$ | Induction motor rotor current phasor refered to stator, amp |
| $I_r$ | Magnitude of induction motor rotor current refered to stator, amp |
| $J_{brake}$ | Moment of inertia of Main Drive brake, ft-lb-sec$^2$ |
| $J_c$ | Total moment of inertia on compressor shaft, ft-lb-sec$^2$ |
| $J_{comp}$ | Moment of inertia of compressor, ft-lb-sec$^2$ |
| $J_{ind}$ | Moment of inertia of induction motor rotor, ft-lb-sec$^2$ |
| $J_r$ | DC motor shaft moment of inertia, ft-lb-sec$^2$ |
| $J_{syn}$ | Moment of inertia of synchronous motor rotor, ft-lb-sec$^2$ |
| $K_a$ | Gain of Rototrol, volts/amp |
| $K_b$ | DC motor back emf constant, volt-rad/sec |
| $K_T$ | DC motor torque constant, ft-lb/amp |
| $K_1$ | Constant depending on operating point shaft speed and drive torque, ft-lb-sec |
| $K_2$ | Constant depending on operating point shaft speed, drive torque, and rheostat resistance, $(\Omega\text{-sec})^{-1}$ |
| $K_3$ | Constant depending on Mach number operating point and shaft speed, second |
| $K_4$ | Constant depending on operating point shaft speed, drive torque, and rhoestat resistance, $(\text{in-sec})^{-1}$ |
| $K_5$ | Constant for simplification, rad/(volt-sec) |
| $L_a$ | DC motor armature inductance, henry |
| $L_f$ | Rototrol field inductance, henry |
| M | Mach number |

| | |
|---|---|
| $\bar{M}$ | Mach number operating point |
| $\hat{M}$ | Mach number set point |
| $\dot{m}_c$ | Mass flow of air through compressor, lb/sec |
| $\dot{m}_T$ | Mass flow of air through test section, lb/sec |
| $p_i$ | Compressor inlet pressure, $lb/ft^2$ |
| $P_c$ | Power required to drive compressor, watt |
| $P_m$ | Power developed by induction motor, watt |
| $p_o$ | Compressor outlet pressure, $lb/ft^2$ |
| $P_T$ | Test section static pressure, $lb/ft^2$ |
| $PT_T$ | Test section total pressure, $lb/ft^2$ |
| $r_1$ | Induction motor intrernal stator resistance per phase, Ω |
| $r_2'$ | Induction motor internal rotor resistance per phase referred to stator, Ω |
| R | Liquid rheostat resistance per phase, Ω |
| R' | Liquid rheostat resistance per phase referred to the stator, Ω |
| $\bar{R}'$ | Liquid rheostat operating point resistance per phase referred to the stator, Ω |
| $R_a$ | DC motor internal armature resistance, Ω |
| $R_c$ | Gas constant, ft-lb/slug-°R |
| $R_{eq}$ | DC motor equivalent armature resistance, Ω |
| $R_f$ | Rototrol control field internal resistance, Ω |
| $R_{feq}$ | Equivalent Rototrol control field resistance, Ω |
| $r_e$ | Liquid rheostat electolyte resistivity, Ω-inch |
| $r_s$ | Radius of liquid rheostat drive sprocket, inch |

## LIST OF SYMBOLS (Continued)

| | |
|---|---|
| $R_1$ | Rototrol control field external resistance, Ω |
| $R_2$ | DC motor external armature resistance, Ω |
| slip | Induction motor slip |
| T | Controller sampling period, sec |
| $T_c$ | Torque required to drive compressor, ft-lb |
| $\bar{T}_c$ | Operating point compressor torque, ft-lb |
| $T_m$ | Torque developed by induction motor, ft-lb |
| $\bar{T}_m$ | Operating point torque developed by the induction motor, ft-lb |
| $T_r$ | Torque developed by DC motor, ft-lb |
| $T_T$ | Test section static temperature, °R |
| $TT_c$ | Total temperature at compressor inlet, °R |
| $TT_T$ | Total temperature at test section, °R |
| $\bar{V}_1$ | Induction motor stator voltage phasor per phase, volt |
| $V_1$ | Magnitude of induction motor stator voltage, volt |
| $v_T$ | Velocity of air in test section, ft/sec |
| $X_1$ | Induction motor stator reactance per phase, Ω |
| $X_2$ | Induction motor rotor reactance per phase, Ω |
| $X'_2$ | Induction motor rotor reactance per phase referred to stator, Ω |
| $X_{eq}$ | Equivalent motor reactance per phase, Ω |
| x | Liquid rheostat electrode distance from maximum position, inch |

| | |
|---|---|
| $x_{max}$ | Maximum distance between liquid rheostat electrodes, inch |
| y | Distance between liquid rheostat electrodes, inch |

Greek Symbols

| | |
|---|---|
| $\alpha$ | Turns ratio of induction motor windings |
| $\gamma$ | Specific heat ratio |
| $\Theta$ | DC pilot motor shaft angle, radian |
| $\eta_c$ | Compressor efficiency |
| $\tau_c$ | Time constant associated with accelerating compressor shaft, second |
| $\tau_m$ | DC motor time constant, second |
| $\tau_r$ | Induction motor time constant, second |
| $\lambda_c$ | Compressor pressure ratio |
| $\lambda_T$ | Tunnel pressure ratio |
| $\omega_m$ | Induction motor speed, rad/sec |
| $\bar{\omega}_m$ | Induction motor speed operating point, rad/sec |
| $\omega_s$ | Induction motor synchronous speed, rad/sec |
| $\rho$ | Density of air, $lb/ft^3$ |

# CHAPTER I

# INTRODUCTION

## Description of Tunnel 16T

The AEDC 16-ft transonic wind tunnel (16T) is a variable density continuous flow closed return wind tunnel with an operating range from Mach 0.2 to 1.6. The major components of the 16T wind tunnel are shown in Figure 1-1. The 16T compressor is a three-stage axial flow machine designed to deliver an inlet volume flow of 200,000 cfs at a pressure ratio of 1.385 [Parli, p. 1]*. The inlet guide vanes and stator blades are adjustable to provide the desired volume flow of air through the tunnel circuit. Control of the temperature is accomplished by an air to water heat exchanger down stream of the compressor. The test section of the 16T wind tunnel is a removable structure having a cross section of 16 ft x16 ft. Down stream of the test section is the diffuser which accounts for most of the losses in the tunnel. The diffuser is an annular type diffuser with a 3.5-degree effective half-angle of divergence. Pressure control of the tunnel is provided by the plenum evacuation system (PES) by pumping air into the tunnel or exhausting air to the atmosphere. The plenum evacuation system also provides a means of controlling the tunnel humidity by introducing dry makeup air into the tunnel [Stich, p.17] .

## Problem Statement

The 16T compressor is driven by two 83,000 hp synchronous motors and two

* Denotes reference listed in Bibliography

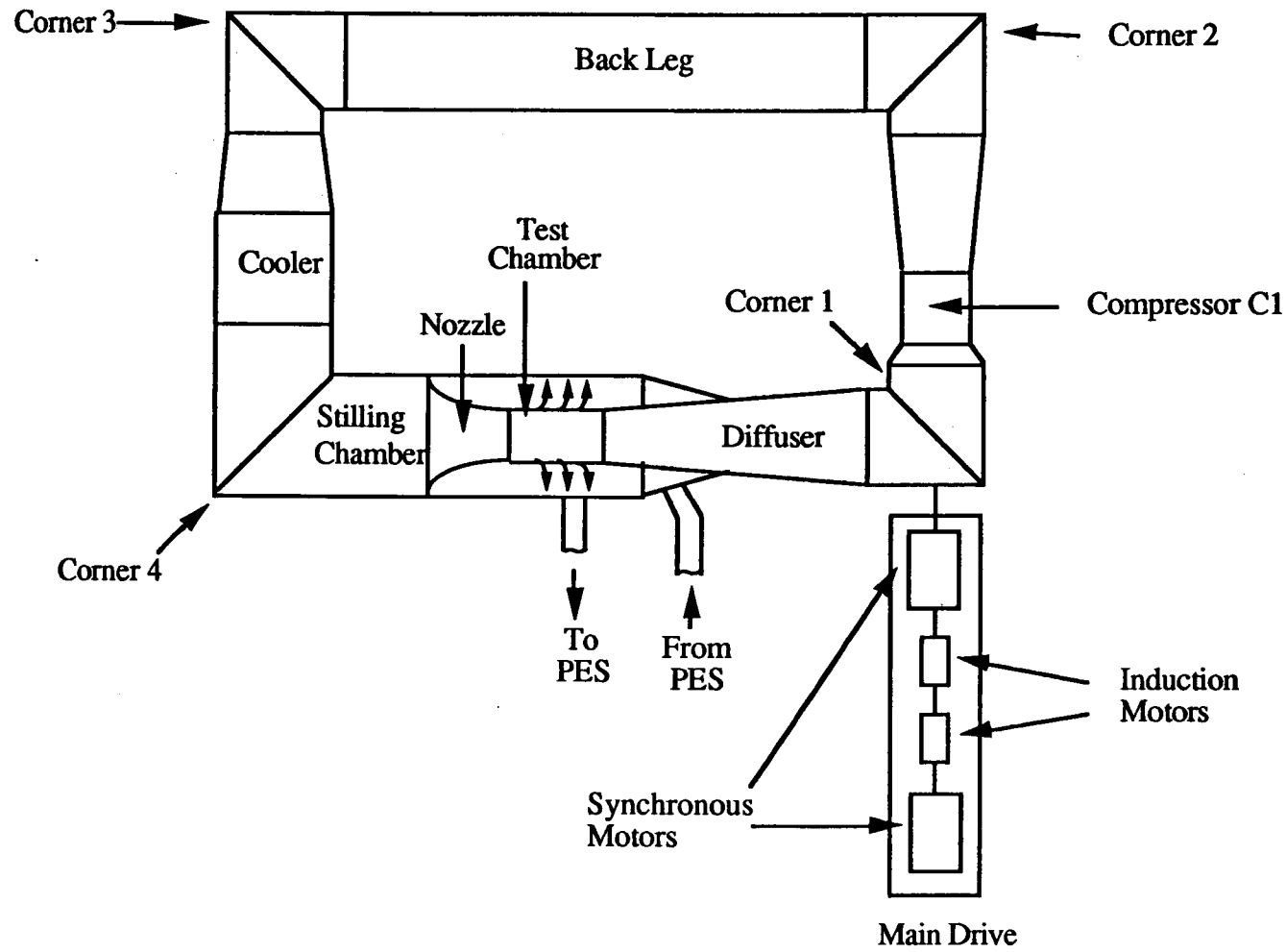



Figure 1-1. 16T Wind Tunnel Configuration

35,000 hp induction motors known as Main Drive. For subsonic operation at Mach numbers between 0.2 to 0.6, Main Drive is operated in the subsynchronous mode using only the induction motors. When testing is done at Mach numbers above 0.6, the compressor is driven by the two synchronous motors. When operating in the synchronous mode the induction motors are used to bring the compressor up to synchronous speed and provide additional power as needed depending on the test conditions.

When operating in the subsynchronous mode, the Mach number is controlled by setting the compressor stator blade angle and controlling the speed of the compressor drive induction motors. Depending on total pressure and the Mach number desired, one or both of the induction motors are used. The induction motors are brought up to speed using the existing control system used for bringing the drive up to synchronous speed. The control circuitry for bringing the induction motors up to speed limits the armature current of the motors and insures that the KVA rate limit is not exceeded. When the approximate operating speed is attained, control of the induction motors is switched from automatic to manual. Once in manual operation, the speed of the induction motors is controlled by raising or lowering the liquid rheostat electrode in the rotor circuit to regulate the rotor current. By lowering the electrode, the resistance in the rotor is decreased which increases the speed of the motor. Raising the electrode increases the resistance and decreases motor speed. During two motor operation the induction motors are operated in a master/slave mode. The liquid rheostat of the master motor is operated manually while a regulator circuit controls the slave motor liquid rheostat to maintain the same rotor current in both motors.

The control of the Mach number is presently achieved by one human operator watching the mach number readout and adjusting the speed of the drive motor by

raising or lowering the liquid rheostat electrode. Control in this manner is very demanding as it requires the operator to "bump" the liquid rheostat electrode up or down to maintain the test section Mach number. The Mach number must be controlled to within 3 percent of the setpoint while data is taken in the test section. If the Mach number falls outside this range, data taking must be discontinued until the Mach number is brought within tolerable limits.

## Approach

This study concerns only the subsynchronous operation of 16T. The purpose of this thesis is to construct a model of the liquid rheostat positioning system, the induction motors, and the 16T compressor using known or observed parameters of the components. This model will then be used to develop a control algorithm to maintain the test section Mach number within the tolerance range when Main Drive is run in the subsynchronous mode. The output of the controller will drive the liquid rheostat positioning control system. Figure 1-2 shows a schematic of the system including where the proposed controller will close the loop. The control algorithm will be designed to adapt to the changing operating conditions in the tunnel to maintain consistent system performance.

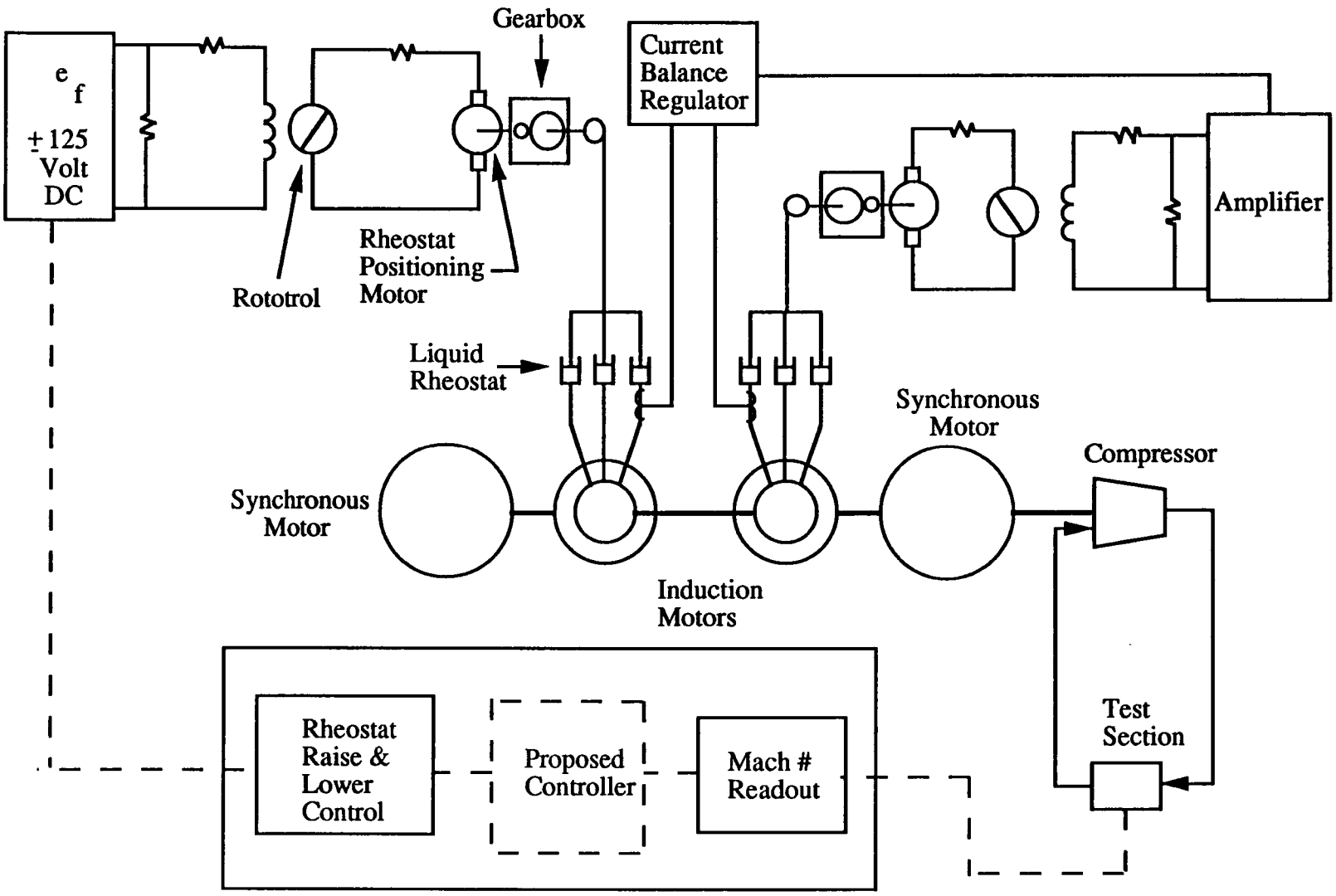



Figure 1-2. Schematic of Subsynchronous Control of Main Drive

# CHAPTER II

## MODEL DEVELOPMENT

The model of the system is divided into three major components: the liquid rheostat positioning system, the induction motors, and the 16T compressor. To obtain an accurate model of the system, its development is based on the observed performance of the liquid rheostat, manufacturers performance data on the induction motors, and on performance data obtained during an evaluation test for the the compressor during subsynchronous operation.

### Rheostat Positioning System

The control system for the liquid rheostat uses a 5 kW Rototrol driving a 2 hp DC motor which moves the electrode up or down as shown in Figure 1-2. The Rototrol is the Westinghouse trade name for a DC control generator. Driven at a constant speed by a small AC motor, the Rototrol has a control field winding which when energized produces a proportional output voltage. The output of the Rototrol drives the 2 hp DC electrode positioning motor which has a constant field current. The DC motor drives a sprocket and chain assembly through a 100:1 gear box to move the liquid rheostat electrodes up or down. There are three electrodes for each motor, one for each phase. A positive voltage applied to the a control field winding of the Rototrol moves the electrodes down while a negative voltage moves the electrodes up. An electrical schematic of the Rototrol and the rheostat positioning DC motor is shown in Figure 2-1.

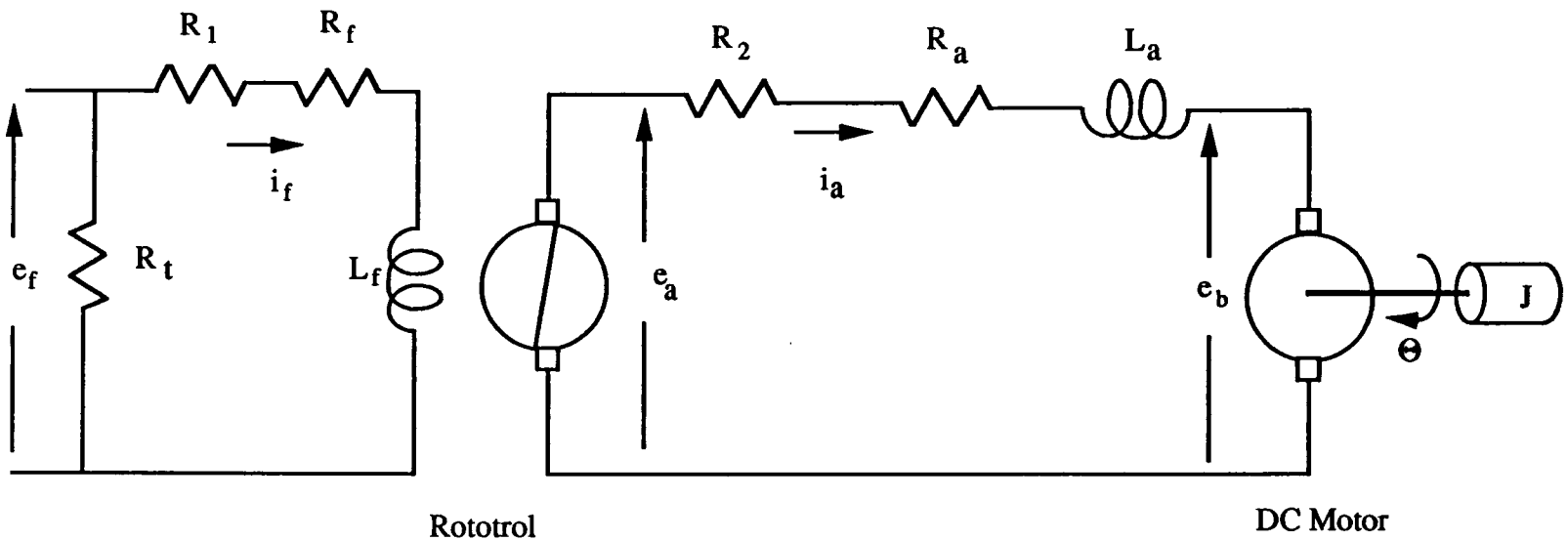



Figure 2-1. Rototrol and DC Motor Electrical Schematic

Summing voltages around the Rototrol control field gives

$$e_f = i_f(R_1 + R_f) + L_f \frac{di_f}{dt}. \tag{2-1}$$

The voltage output of the Rototrol is related to the control field current, $i_f$, by the gain of the Rototrol, $K_a$,

$$e_a = K_a i_f. \tag{2-2}$$

Rearranging Eq. (2-2) and differentiating with respect to time yields

$$\frac{di_f}{dt} = \frac{1}{K_a}\frac{de_a}{dt}. \tag{2-3}$$

Substituting Eqs. (2-2) and (2-3) into Eq. (2-1) gives a linear differential equation relating the input field voltage to the output voltage of the Rototrol,

$$\frac{de_a}{dt} + \frac{R_{feq}}{L_f} e_a = \frac{K_a}{L_f} e_f, \tag{2-4}$$

where

$$R_{feq} = R_f + R_1. \tag{2-5}$$

Taking the Laplace transform of Eq. (2-4) gives a transfer function relating the Rototrol terminal voltage to the control field voltage,

$$\frac{E_a(s)}{E_f(s)} = \frac{\frac{K_a}{R_{feq}}}{\frac{L_f}{R_{feq}}s + 1}. \qquad (2\text{-}6)$$

The output of the Rototrol drives the rheostat electrode positioning DC motor. The relationship between the output of the Rototrol and the input of the DC motor can be obtained by summing the voltages around the circuit in Figure 2-1. This gives

$$e_a = i_a(R_2 + R_a) + L_a\frac{di_a}{dt} + e_b. \qquad (2\text{-}7)$$

The DC motor terminal voltage, $e_a$, is related to the motor speed by the back emf constant of the motor, $K_b$, as

$$e_b = K_b\frac{d\Theta}{dt}. \qquad (2\text{-}8)$$

The torque developed by the DC motor, $T_r$, is related to the DC motor armature current by the motor torque constant, $K_T$,

$$T_r = K_T i_a. \qquad (2\text{-}9)$$

For mechanical rotational systems, Newton's law relating the acceleration of the motor shaft to the motor torque and the load on the shaft is [Meriam, p. 6]

$$J_r \frac{d^2\Theta}{dt^2} = \Sigma T. \qquad (2\text{-}10)$$

$J_r$ is the equivalent moment of inertia of the motor shaft and the liquid rheostat electrodes referred to the shaft through the gear box. Summing the torques on the motor shaft gives

$$\Sigma T = K_T i_a - f \frac{d\Theta}{dt}. \qquad (2\text{-}11)$$

The second term on the right side of Eq. (2-11) represents the frictional loads on the shaft where f is the viscous friction coefficient of the motor and the load referred to the shaft. Combining Eqs. (2-10) and (2-11) gives

$$J_r \frac{d^2\Theta}{dt^2} + f \frac{d\Theta}{dt} = K_T i_a. \qquad (2\text{-}12)$$

Combining Eqs. (2-7) ,(2-8), (2-12), and rearranging gives

$$\frac{J_r L_a}{K_T} \frac{d^3\Theta}{dt^3} + \frac{[L_a f + J_r(R_2 + R_a)]}{K_T} \frac{d^2\Theta}{dt^2} + \left[\frac{(R_2 + R_a)f}{K_T} + K_b\right] \frac{d\Theta}{dt} = e_a. \qquad (2\text{-}13)$$

Taking the Laplace transform of Eq. (2-13) gives a transfer function relating the angle of the motor shaft, $\Theta$, to the Rototrol terminal voltage, $e_a$,

$$\frac{\Theta(s)}{E_a(s)} = \frac{1}{s\left[\frac{J_r L_a}{K_T}s^2 + \frac{L_a f + J_r R_{eq}}{K_T}s + \frac{R_{eq} f}{K_T} + K_b\right]}, \tag{2-14}$$

where

$$R_{eq} = R_2 + R_a. \tag{2-15}$$

The inductance in the armature circuit, $L_a$, is usually very small and may be neglected, simplifying Eq. (2-14) to

$$\frac{\Theta(s)}{E_a(s)} = \frac{1}{s\left[\frac{J_r R_{eq}}{K_T}s + \left(\frac{R_{eq} f}{K_T} + K_b\right)\right]}. \tag{2-16}$$

If the viscous friction coefficient, f, is assumed to be small, Eq. (2-16) can be reduced to

$$\frac{\Theta(s)}{E_a(s)} = \frac{\frac{1}{K_b}}{s\left(\frac{J_r R_{eq}}{K_T K_b}s + 1\right)}. \tag{2-17}$$

Combining Eqs. (2-6) and (2-17) gives a transfer function relating the Rototrol control field voltage, $E_f(s)$, and the DC motor shaft angle $\Theta(s)$,

$$\frac{\Theta(s)}{E_f(s)} = \frac{\frac{K_a}{K_b R_{feq}}}{s\left(\frac{L_f}{R_{feq}}s + 1\right)\left(\frac{J_r R_{eq}}{K_T K_b}s + 1\right)}. \qquad (2\text{-}18)$$

The rotation of the shaft of the DC motor is translated into linear motion to move the rheostat electrode up and down. The gearbox driven by the DC motor turns a sprocket on which rides a chain. One end of the chain is attached to the electrodes and the other end is attached to a weight which counterbalances the weight of the electrodes. This is shown in Figure 2-2.

The distance the electrode moves is related to the rotation of the DC motor shaft by the gear ratio, GR, and the radius of the sprocket, $r_s$, as

$$x = \frac{r_s \Theta}{GR}. \qquad (2\text{-}19)$$

In its initial position, the liquid rheostat electrodes are the maximum distance apart. The distance between the electrodes, y, is the difference between the maximum electrode distance, $x_{max}$, and the distance moved as a result of the operation of the DC motor,

$$y = x_{max} - \frac{r_s \Theta}{GR}. \qquad (2\text{-}20)$$

The resistance of the liquid rheostat is directly proportional to the distance between the electrodes, y. This relationship as given by the liquid rheostat manufacturer [Westinghouse Main Drive Operators Manual-Section K] is

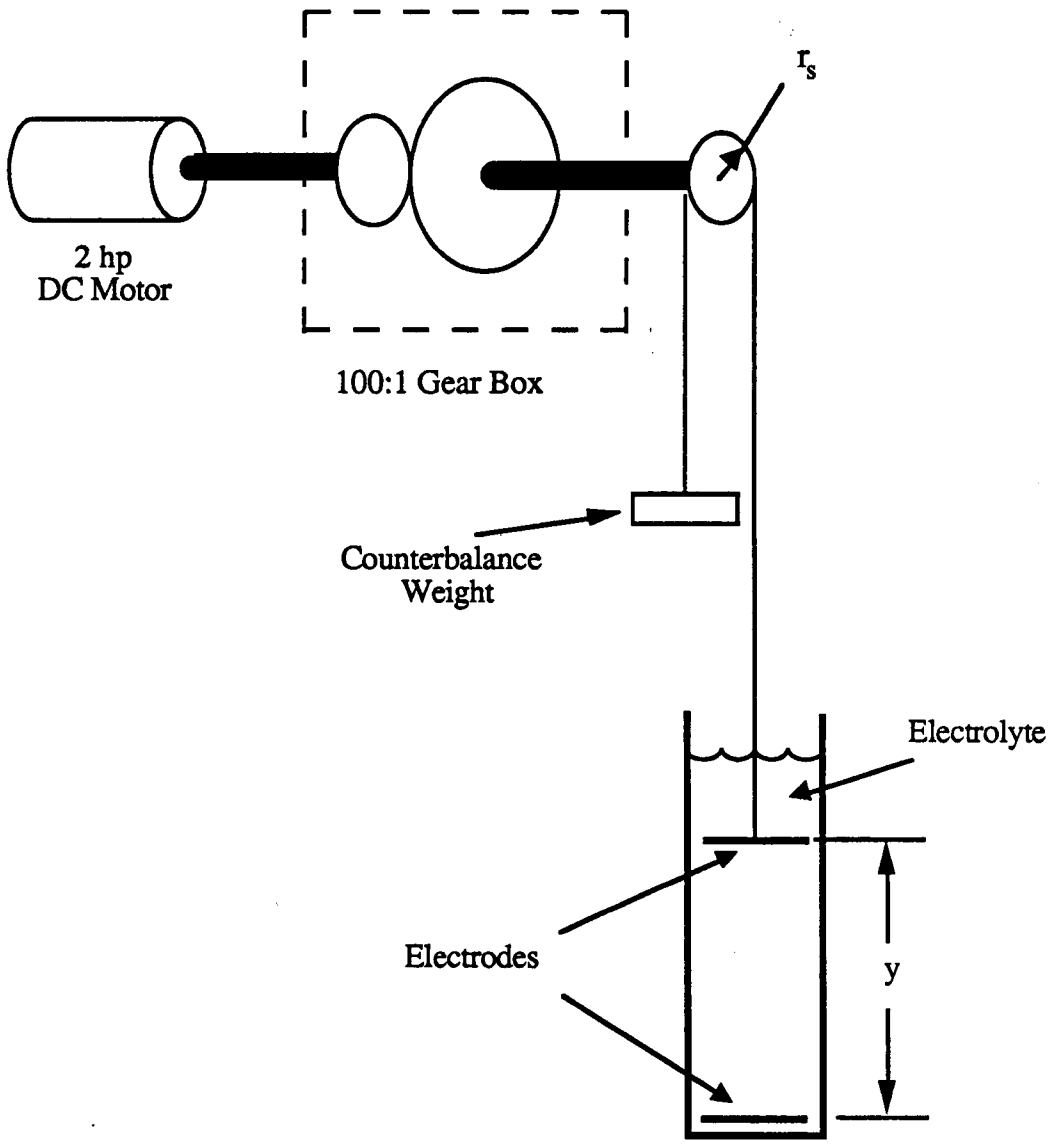



Figure 2-2. Liquid Rheostat Mechanical Schematic

$$R = \frac{r_e y}{.85 A_e} . \qquad (2\text{-}21)$$

where $A_e$ is the area of the electrode and $r_e$ is the electrolyte solution resistivity. The constant 0.85 in the denominator of Eq. (2-21) depends on the geometry of the electrode. The resistivity of the electrolyte is a function of the electrolyte temperature as shown in Figure 2-3.

The electrolyte is cooled by circulating the electrolyte solution through a water to water heat exchanger. During normal operation of the induction motors, the temperature of the electrolyte solution is maintained between 50°C and 80°C.

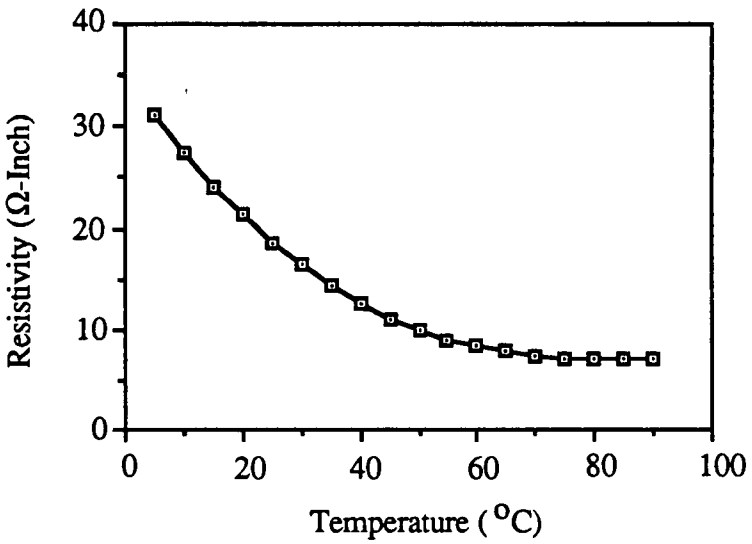



Figure 2-3. Change in Electrolyte Resistance With Temperature.

To verify the model, the performance of the liquid rheostat was observed while the liquid rheostat was raised and lowered. The time for the rheostat electrode to achieve a steady state velocity and to reach the end of its travel were observed and recorded. The time for the electrode to reach a steady state velocity from a dead stop averaged approximately 3 seconds in response to a step input of 125 Volts DC to the Rototrol field. The time for the rheostat electrode to travel from the upper limit of 78 inches to the lower limit of 3/8 inches averaged approximately 31 seconds when the rheostat control switch was held in the lower position for approximately 30 seconds. The performance of the system was also observed to be similar when going from the lower limit of electrode travel to the upper limit of travel.

The values used for the rheostat positioning system constants were obtained from manufacturer's information on the equipment [Westinghouse Main Drive Operators Manual, Section K] and are listed in Table 2-1. Since the electrolyte resistivity varies from 10.0 to 7.0 Ω-inches over the operating temperature (50°C to 80°C) of the system, the value used for the electrolyte resistivity, 8.5 Ω-in, is the average of these two extremes.

From equation (2-6), the time constant of the Rototrol is

$$\tau_r = \frac{L_f}{R_{feq}}. \tag{2-22}$$

Using values from Table 2-1 gives

$$\tau_r = \frac{20.0\ \text{H}}{20.0\ \Omega + 2.0\ \Omega} \times \frac{1\Omega\text{-sec}}{\text{H}} = 0.91\ \text{sec}. \tag{2-23}$$

Table 2-1. Liquid Rheostat Positioning System Values.

| Element | Symbol | Units | Value |
|---|---|---|---|
| Electrode area | $A_e$ | $in^2$ | 1017.9 |
| Rototrol gain | $K_a$ | Volt/Amp | 12.0 |
| DC motor back emf constant | $K_b$ | Volt-rad/sec | 1.91 |
| Current balance regulator gain | $K_s$ | - | 3.5 |
| DC motor torque constant | $K_T$ | ft-lb/Amp | 1.0 |
| Gearbox gear ratio | GR | - | 100.0 |
| DC motor moment of inertia | $J_r$ | ft-lb-$sec^2$ | 0.06 |
| Rototrol control field inductance | $L_f$ | H | 20.0 |
| DC motor armature resistance | $R_a$ | Ω | 0.2 |
| Rototrol control field resistance | $R_f$ | Ω | 2.0 |
| Electrolyte resistivity | $r_e$ | Ω-in | 8.5 |
| Rheostat driveshaft sprocket radius | $r_s$ | in | 4.0 |
| Rototrol external field resistance | $R_1$ | Ω | 20.0 |
| DC motor armature external resistance | $R_2$ | Ω | 1.0 |
| Maximum rheostat travel | $x_{max}$ | in | 78.0 |
| Minimum rheostat travel | $x_{min}$ | in | 0.375 |

From equation (2-17) the time constant of the DC motor is

$$\tau_m = \frac{J_r R_{eq}}{K_T K_b}. \tag{2-24}$$

Using values from Table 2-1,

$$\tau_m = \frac{0.06\text{ft-lb-sec}^2 \times (1.0 + 0.2)\Omega}{1.0\text{ft-lb/Amp} \times 1.91\text{Volt-rad/sec}} \times \frac{1\text{ Volt/Amp}}{\Omega} = 0.038\text{ sec.} \tag{2-25}$$

The time constant of 0.91 seconds associated with the Rototrol is much greater than the time constant of the DC motor and therefore can be considered the dominant time constant of the rheostat positioning system.

The performance of the liquid rheostat was simulated using the Advanced Continuous Simulation Language [ACSL, Mitchell and Gauthier]. The manual operation of the liquid rheostat was simulated using Eqs. (2-4), (2-5), (2-13), (2-20), and (2-21) with the values listed in Table 2-1. The results of the ACSL simulation are shown in Figures 2-4 and 2-5. When operated manually, the rheostat is moved down by applying +125 volts DC and moved up by applying -125 volts DC to the Rototrol control field. To duplicate the input applied by the operator during observed operations, a +125V DC input was applied to the Rototrol control field for 30 seconds as shown in Figure 2-4. The time for the electrode to reach the end of its travel is approximately 30 seconds, which agrees with the observed performance.

The time taken for the system to reach a constant velocity is shown in Figure 2-5 to be approximately 4 seconds which is close to the observed system performance. The time constant of a system is considered the time required for the response to rise to 63

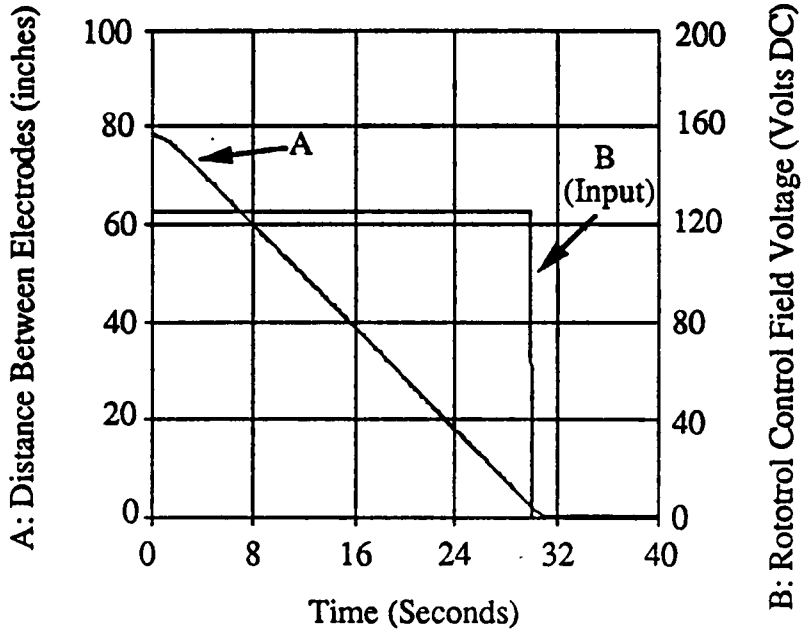



Figure 2-4. Liquid Rheostat Positioning System Simulation Results

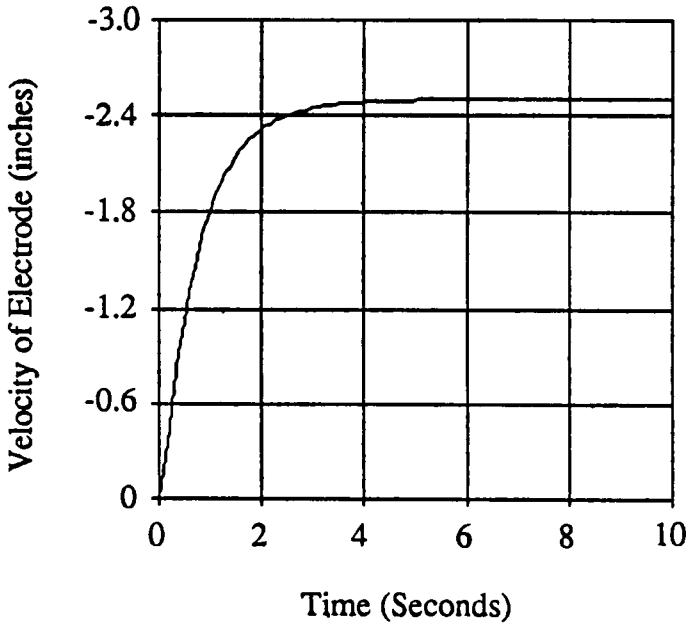



Figure 2-5. Liquid Rheostat Electrode Velocity

percent of its steady state value [Ogata, p. 221]. Using Figure 2-5, this results in a time constant of approximately one second which agrees with equation (2-23). This simulation assumes that the frictional loads and the DC motor armature inductance are negligible. Since the gain of the Rototrol, $K_a$, was not known, this value was adjusted in the ACSL simulation until the performance of the system agreed with the observed performance. This resulted in a Rototrol gain of 12 Volt/Amp.

One or two motor operation of Main Drive during subsynchronous operation is dependent on the operating conditions in the tunnel. When both motors are used, one of the motors is operated as the "master" motor and the other as the "slave" motor. A regulating circuit is used to match the rotor current of the slave motor to the rotor current of the master motor through adjustment of the liquid rheostat. This is shown in the schematic of the system in Figure 1-2 (page 5). The current balance regulator amplifies the difference between the rotor current of the master motor and the rotor current of the slave motor. This amplified signal is input into the control field of the slave motor Rototrol. By doing this the load is shared equally by the two motors. Because the gain of the current balance regulator was not known, it was determined by trial and error in the ACSL simulation program. The gain was adjusted until the performance of the liquid rheostat for the slave motor agreed with the observed performance. The observed time for the slave rheostat electrode to reach a constant velocity from a dead stop was approximately 5 seconds, when the master rheostat was operated as in Figure 2-4. The simulated performance of the system for master/slave operation of the liquid rheostats is shown in Figure 2-6. Since the system is a type one system as shown by Eq. (2-18), the error between the position of the two rheostats approaches zero.

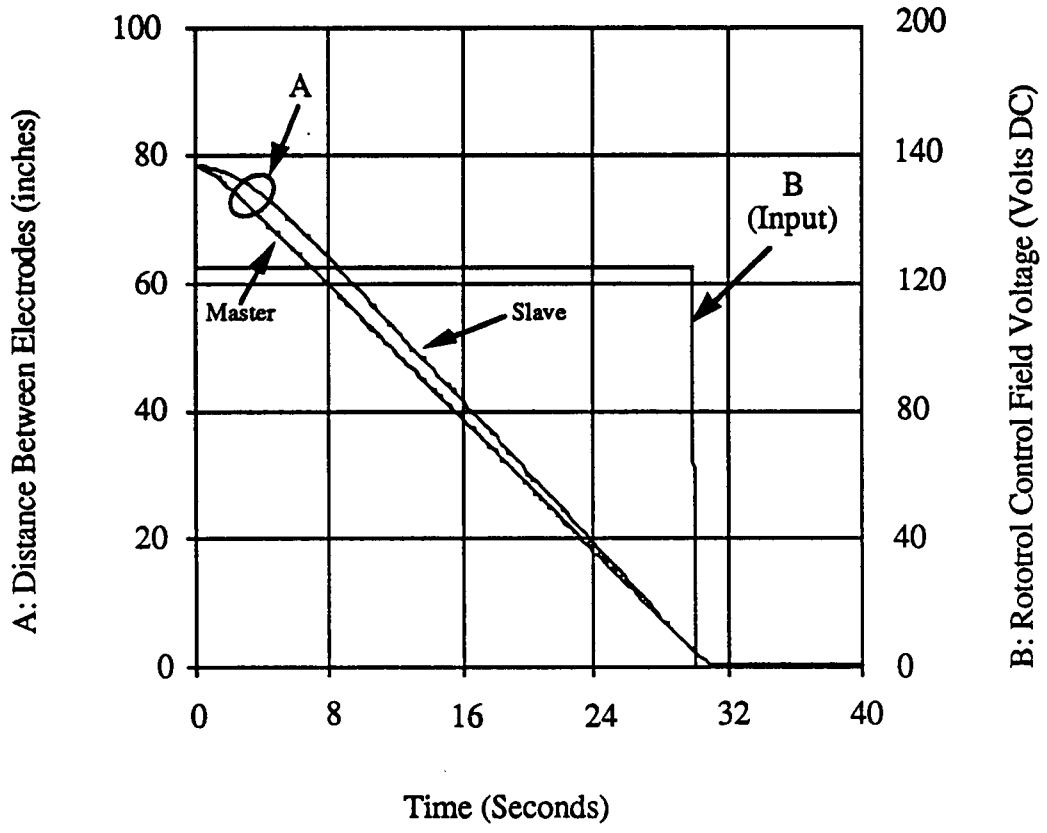



Figure 2-6. Liquid Rheostat Positioning System Simulation Results for Master/Slave Operation

## Induction Motors

During subsynchronous operation of 16T the compressor is driven using one or both wound rotor induction motors depending on the tunnel operating conditions. Both motors have been upgraded to 35,000 hp. The speed of the motor is controlled by the liquid rheostat in the rotor circuit. By lowering the liquid rheostat electrodes and thereby decreasing resistance in the rotor circuit, the speed of the motor is increased. An equivalent circuit of the induction motor for one phase is shown in Figure 2-7. The average power developed by the motor for all three phases is [Del Toro, p. 534]

$$P_m = 3\, I_r^2 \frac{r_2'}{slip}(1 - slip). \qquad (2\text{-}26)$$

The equivalent circuit of the induction motor in Figure 2-7 is obtained by referring the resistances and reactance in the rotor to the stator. The resistance $R'$ is the liquid rheostat resistance referred to the stator by the turns ratio of the induction motor, $\alpha$ ,

$$R' = \alpha^2 R\ . \qquad (2\text{-}27)$$

The resistance $r_2'$ is the induction motor rotor resistance referred to the stator by turns ratio of the induction motor,

$$r_2' = \alpha^2 r_2\ . \qquad (2\text{-}28)$$

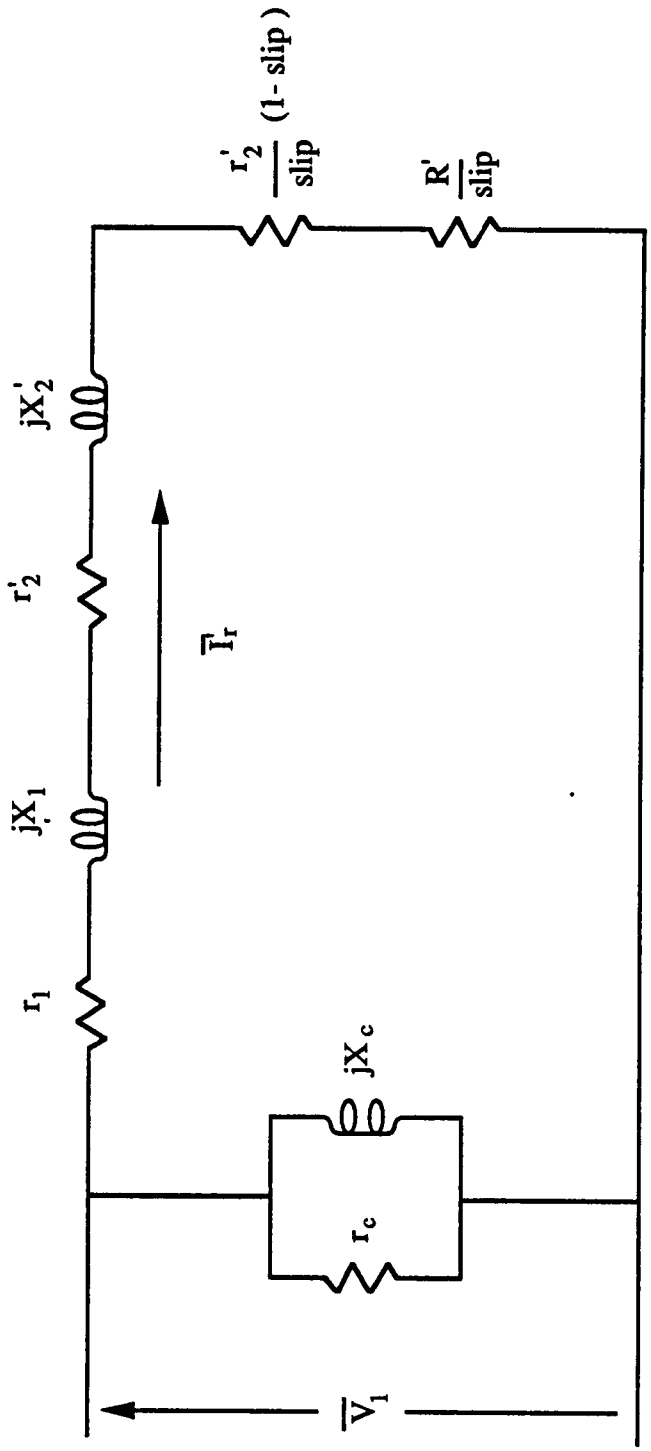



Figure 2-7. Induction Motor Equivalent Circuit for One Phase

The reactance of the rotor circuit referred to the stator, $X_2'$ , is

$$X_2' = \alpha^2 X_2 . \tag{2-29}$$

The stator phasor voltage, $\overline{V}_1$, is found by summing voltages around the circuit in Figure 2-7,

$$\overline{V}_1 = \left( r_1 + \frac{r_2' + R'}{slip} + j(X_1 + X_2') \right) \overline{I}_r . \tag{2-30}$$

Solving Eq. (2-30) for $\overline{I}_r$ gives

$$\overline{I}_r = \frac{\overline{V}_1}{r_1 + \frac{r_2' + R'}{slip} + j(X_1 + X_2')} . \tag{2-31}$$

The power developed by the motor in Eq. (2-26) is dependent on the magnitude of the rotor current ,

$$I_r = \frac{V_1}{\sqrt{\left( r_1 + \frac{r_2' + R'}{slip} \right)^2 + (X_1 + X_2')^2}} . \tag{2-32}$$

The stator resistance $r_1$ is much smaller than the resistance in the rotor referred to the stator, $r_2' + R'$. Neglecting $r_1$, Eq. (2-32) simplifies to

$$I_r = \frac{V_1}{\sqrt{\left(\frac{r_2' + R'}{slip}\right)^2 + (X_1 + X_2')^2}}. \qquad (2\text{-}33)$$

The slip is the ratio of the difference in speed between the synchrounous speed, $\omega_s$, and rotor speed, $\omega_m$, to the synchronous speed [Del Toro,p. 529],

$$slip = \frac{\omega_s - \omega_m}{\omega_s}. \qquad (2\text{-}34)$$

The torque developed by the motor is related to the shaft speed and the developed power by

$$T_m = \frac{0.7376 P_m}{\omega_m}. \qquad (2\text{-}35)$$

The constant 0.7376 in Eq. (2-35) is to convert the units from watt-sec to ft-lb. By combining Eqs. (2-26), (2-33), (2-34) and (2-35) the torque developed by the motor as a function of liquid rheostat resistance and shaft speed is

$$T_m = \frac{(0.7376)3V_1^2 r_2'(\omega_s - \omega_m)}{\omega_s^2(r_2' + R')^2 + (\omega_s - \omega_m)^2(X_1 + X_2')^2}. \qquad (2\text{-}36)$$

The torque developed by the motor is a nonlinear function of both the liquid rheostat resistance and the shaft speed of the motor. In deriving the output torque of the induction motor in this manner, the dynamics of the induction motor have been

neglected. The derivation justifying this assumption is given in Appendix A. Depending on the the speed of the motor and the liquid rheostat resistance, the time constant ranges from $3.228 \times 10^{-4}$ to $1.885 \times 10^{-3}$ seconds. As will be shown in Chapter III, this turns out to be very small when compared to the time constant associated with accelerating the compressor and motors. Table 2-2 lists the induction motor parameters used for the model [Westinghouse Main Drive Operators Manual-Section K].

Table 2-2. Induction Motor Values

| Element | Symbol | Units | Value |
|---|---|---|---|
| Stator resistance per phase | $r_1$ | Ω | 0.00734 |
| Rotor resistance per phase referred to the stator | $r_2'$ | Ω | 0.26 |
| Turns ratio | $\alpha$ | - | 1.75 |
| Stator voltage per phase | $V_1$ | Volt | 3810.5 |
| Stator reactance per phase | $X_1$ | Ω | 0.1351 |
| Rotor reactance per phase referred to the stator | $X_2'$ | Ω | 0.1506 |
| Synchronous speed of motor | $\omega_s$ | rad/sec | 75.4 |

## 16T Compressor

The model of the 16T compressor is based on data taken during an evaluation test conducted to determine the capabilities of 16T when operated in the subsynchronous mode [Nesbitt, p. 17]. The compressor used in the 16T wind tunnel is a three stage axial flow machine. For Mach numbers above 0.6, the compressor is operated at a constant speed of 600 rpm with the flow requirements being obtained by the stator blade angle setting. For operation in the subsynchronous range when the compressor is driven only by the induction motors, the stator blade angle is held constant and the compressor speed is varied to maintain the Mach number. Figure 2-8 shows the stator blade angle setting verses Mach number for operation in the subsynchronous mode. The subsynchronous operating limits for 16T for one and two motor operation are shown in Figure 2-9. Both motors are used for operation above Mach 0.5 regardless of tunnel pressure.

The power required to drive the compressor, $P_c$, is a function of the mass flow of air through the compressor, $\dot{m}_c$, the compressor pressure ratio, $\lambda_c$, the compressor inlet total temperature, $TT_c$, and the compressor efficiency, $\eta_c$ [Pindzola pp. 34],

$$P_c = \frac{C_p \dot{m}_c TT_c (\lambda_c^{\frac{\gamma-1}{\gamma}} - 1)}{\eta_c}, \qquad (2\text{-}37)$$

where $C_p$ is the specific heat at constant pressure for air and $\gamma$ is the specific heat ratio for air.

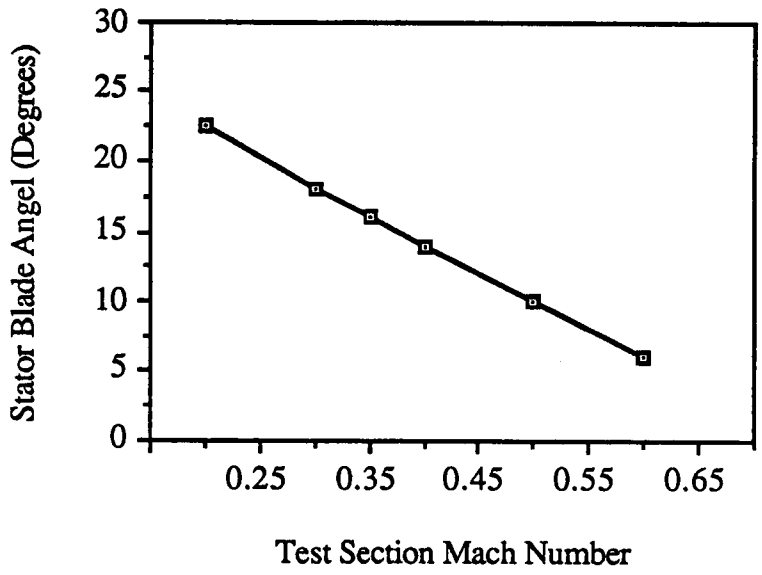



Figure 2-8. Variation of Compressor Stator Blade Angle with Test Section Mach Number.

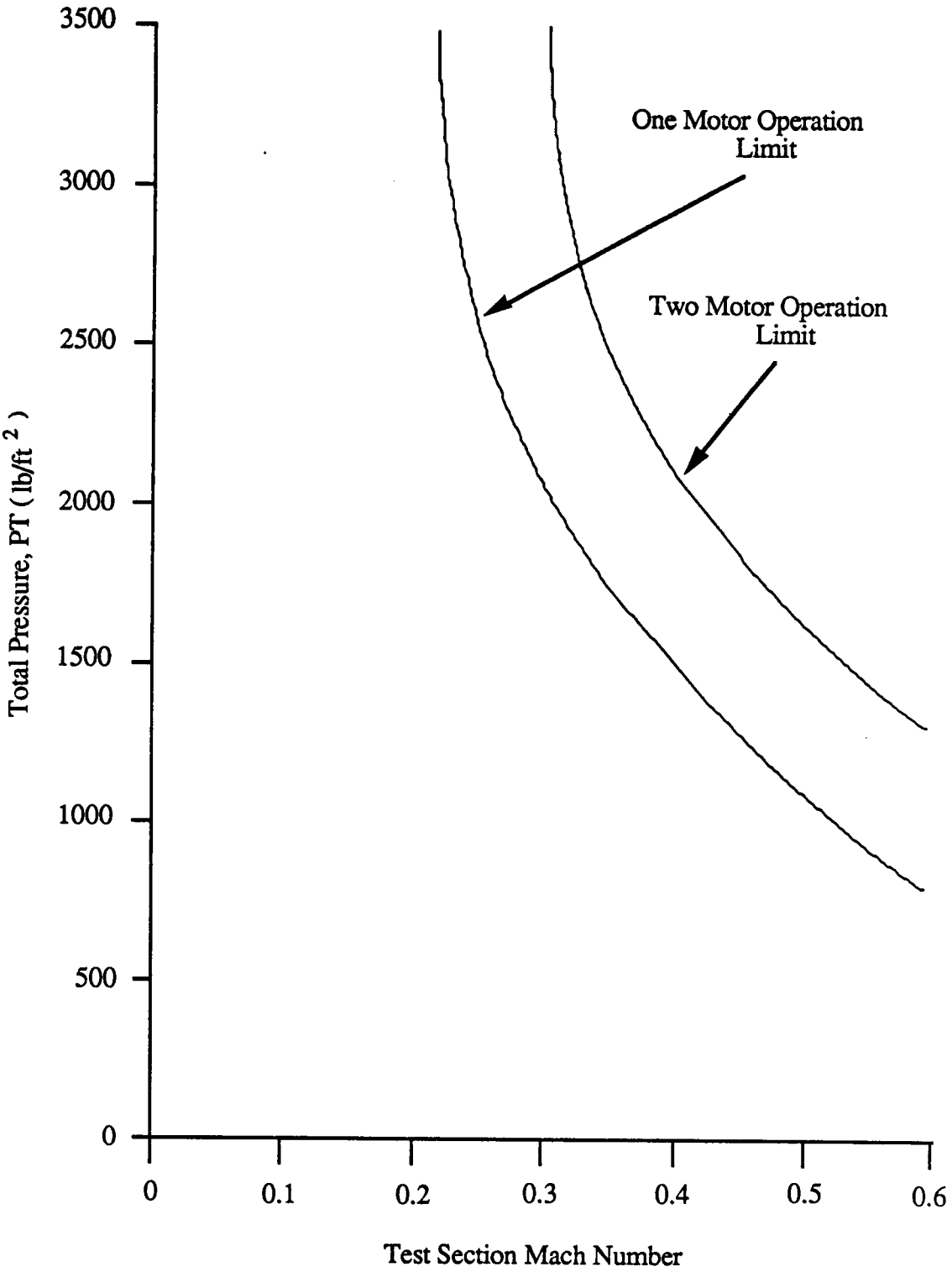



Figure 2-9. 16T Subsynchronous Operating Limits.

Since the mass flow of air is the same throughout the tunnel circuit, the mass flow at the compressor inlet, $\dot{m}_c$, is the same as the mass flow in the test section, $\dot{m}_T$ [Pindzola, p. 31],

$$\dot{m}_c = \dot{m}_T = \rho A_T v_T. \tag{2-38}$$

The density of the air, $\rho$, is a function of the tunnel static pressure, $P_T$ and the static temperature, $T_T$ [Pindzola, p. 9],

$$\rho = \frac{P_T}{R_c T_T}. \tag{2-39}$$

The velocity of the air in the test section, $v_T$, is related to the test section Mach number, M, and the speed of sound, c [Pindzola, p. 10],

$$v_T = cM. \tag{2-40}$$

The speed of sound is given as [Stich, p.27]

$$c = \sqrt{\gamma R_c T_T}, \tag{2-41}$$

where $\gamma$ is the specific heat ratio for air, $R_c$ the gas constant for air, and $T_T$ the static temperature of the air.

Combining Eqs. (2-38) through (2-41) gives the mass flow at the compressor inlet as a function of the test section variables,

$$\dot{m}_c = P_T A_T M \sqrt{\frac{\gamma}{R T_T}}. \tag{2-42}$$

The test section total temperature, $TT_T$, is related to the test section static temperature, $T_T$, by [Pindzola, p. 10]

$$TT_T = T_T\left[1 + \frac{\gamma - 1}{2} M^2\right]. \tag{2-43}$$

The test section total pressure, $PT_T$, is related to the static pressure by [Pindzola, p. 10]

$$PT_T = P_T\left[1 + \frac{\gamma - 1}{2} M^2\right]^{\frac{\gamma}{\gamma-1}}. \tag{2-44}$$

Combining Eqs. (2-42) through (2-44) gives the mass flow in terms of total pressure and total temperature,

$$\dot{m}_c = \sqrt{\frac{\gamma}{R_c TT_T}}\, PT_T A_T M\left[1 + \frac{\gamma - 1}{2} M^2\right]^{\frac{-(\gamma+1)}{2(\gamma-1)}}. \tag{2-45}$$

Substituting the expression for mass flow in Eq. (2-45) into the expression for compressor power in Eq. (2-37) and assuming the total temperature at the compressor inlet, $TT_c$, is the same as the test section total temperature, $TT_T$, gives

$$P_c = \sqrt{\frac{\gamma TT_T}{R_c}}\, \frac{C_p PT_T A_T \left(\lambda_c^{\frac{\gamma-1}{\gamma}} - 1\right)}{\eta_c} M\left[1 + \frac{\gamma - 1}{2} M^2\right]^{\frac{-(\gamma+1)}{2(\gamma-1)}}. \tag{2-46}$$

The Mach number, M, can be expressed as a function of the compressor shaft speed. This relationship using data from a subsynchronous evaluation test on 16T [Nesbitt, p. 17] is shown in Figure 2-10. The solid line in Figure 2-10 is a second order curve fit for the data given by

$$M = 6.582\text{x}10^{-4} + 0.005\,\omega_m + 1.309\text{x}10^{-4}\,\omega_m^2 . \qquad (2\text{-}47)$$

The compressor pressure ratio, $\lambda_c$, is also a function of Mach number as shown in Figure 2-11. A second order curve fit for the data of Figure 2-11 as given by the solid line is

$$\lambda_c = 1.0 + 0.0467M + 0.3M^2. \qquad (2\text{-}48)$$

The compressor efficiency, $\eta_c$, as a function of Mach number is shown in Figure 2-12. A second order approximation to the data as given by the solid line in Figure 2-12 is

$$\eta_c = 0.18 + 2.321M - 2.226M^2. \qquad (2\text{-}49)$$

Since the compressor pressure ratio and compressor efficiency used in Eq. (2-46) are a function of Mach number, the power required to drive the compressor can be expressed as

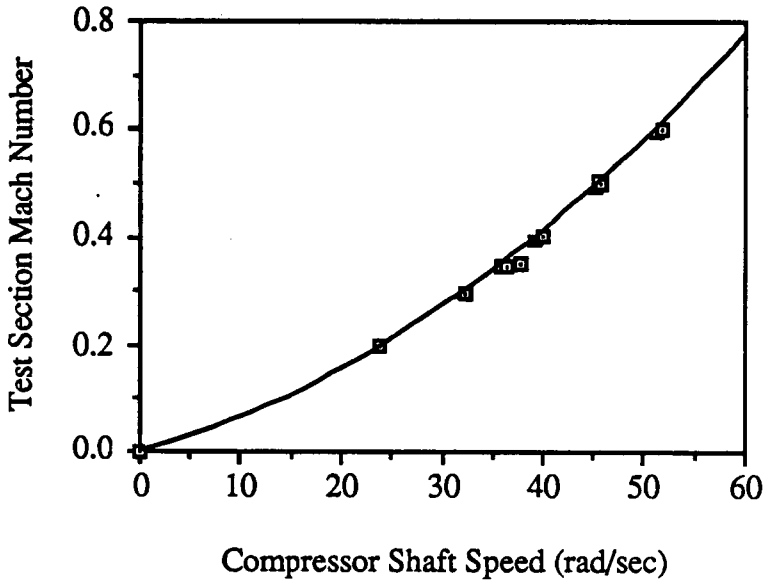



Figure 2-10. Test Section Mach Number as a Function of Compressor Shaft Speed.

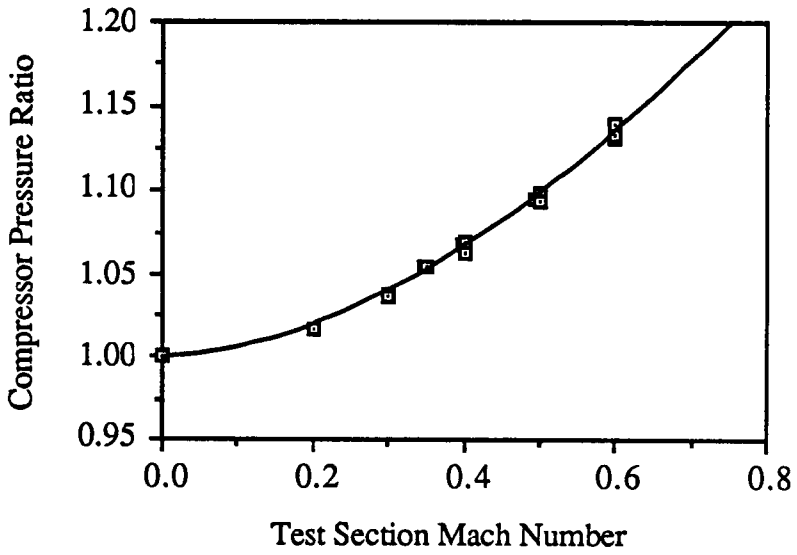



Figure 2-11. Compressor Pressure Ratio as a Function of Test Section Mach Number.

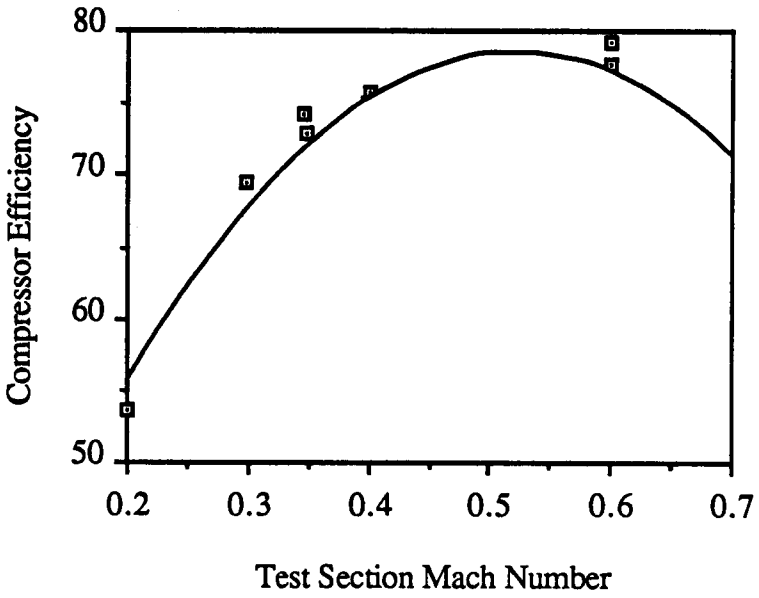



Figure 2-12. Compressor Efficiency as a Function of Test Section Mach Number.

$$P_c = \sqrt{\frac{\gamma T T_T}{R_c}} C_p P T_T A_T F(M), \tag{2-50}$$

where F(M) is a dimensionless function of Mach number,

$$F(M) = \frac{(\lambda_c(M)^{\frac{\gamma-1}{\gamma}} - 1)}{\eta_c(M)} M\left[1 + \frac{\gamma-1}{2} M^2\right]^{\frac{-(\gamma+1)}{2(\gamma-1)}}. \tag{2-51}$$

The torque required to drive the compressor is

$$T_c = \frac{P_c}{\omega_m}. \tag{2-52}$$

Substituting the expression for compressor power in Eq. (2-50) into Eq. (2-52) gives

$$T_c = \sqrt{\frac{\gamma I T_T}{R_c}} C_p P T_T A_T \frac{F(M)}{\omega_m}, \tag{2-53}$$

or

$$T_c = \sqrt{\frac{\gamma I T_T}{R_c}} C_p P T_T A_T \; f(\omega_m), \tag{2-54}$$

where

$$f(\omega_m) = \frac{F(M)}{\omega_m}. \tag{2-55}$$

Since the Mach number is a function of the compressor shaft speed as shown in Eq. (2-47), the function $f(\omega_m)$ in Eq. (2-55) can be written as

$$f(\omega_m) = \frac{F(M(\omega_m))}{\omega_m}. \tag{2-56}$$

Combining Eqs. (2-51) and (2-56) gives

$$f(\omega_m) = \frac{\left[\lambda_c \left(M(\omega_m)\right)^{\frac{\gamma-1}{\gamma}} - 1\right]}{\omega_m \eta_c(M(\omega_m))} M(\omega_m) \left[1 + \frac{\gamma-1}{2} M(\omega_m)^2\right]^{\frac{-(\gamma+1)}{2(\gamma-1)}}. \tag{2-57}$$

Using the expressions for M, $\lambda_c$, and $\eta_c$ given in Eqs. (2-47), (2-48), and (2-49), the relationship between $f(\omega_m)$ and the compressor shaft speed is shown in Figure 2-13. A second order curve fit to the data in Figure 2-13 as given by the solid line is

$$f(\omega_m) = 3.208\text{x}10^{-6} - 3.447\text{x}10^{-6}\omega_m + 2.364\text{x}10^{-7}\omega_m^2 . \qquad (2\text{-}58)$$

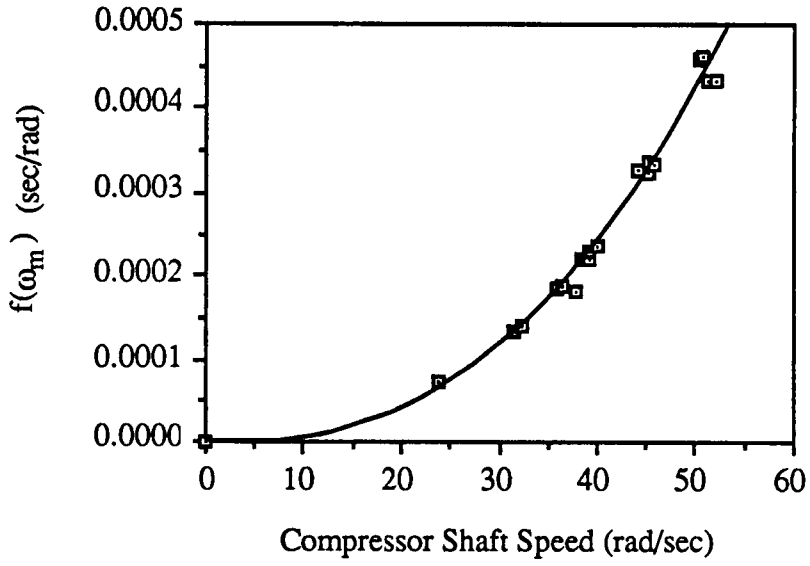



Figure 2-13. $f(\omega_m)$ as a Function of Compressor Shaft Speed.

For mechanical rotational systems, Newton's law relating the acceleration of the motor shaft to the torque necessary to drive the compressor is [Ogata, p. 74]

$$J_c \frac{d\omega_m}{dt} = T_m - T_c. \tag{2-59}$$

Rearranging Eq. (2-59) and solving for shaft speed gives

$$\frac{d\omega_m}{dt} = \frac{T_m - T_c}{J_c}. \tag{2-60}$$

The moment of inertia, $J_c$, in Eq. (2-60) is the combined moment of inertia of the compressor, both induction motors, both synchronous motors, and the brake,

$$J_c = J_{comp} + 2J_{ind} + 2J_{syn} + J_{brake}. \tag{2-61}$$

Values used for the compressor model are summarized in Table 2-3. Using the moment of inertia of the components on the shaft listed in Table 2-3 in Eq. (2-61) gives a total moment of inertia of

$$\begin{aligned} J_c &= (381{,}250 + 2 \times 12{,}420 + 2 \times 46{,}670 + 4670) \text{ ft-lb-sec}^2 \\ &= 504{,}100 \text{ ft-lb-sec}^2. \end{aligned} \tag{2-62}$$

During subsynchronous operation, the total temperature, $TT_T$, ranges from 530 $^{\circ}$R to 550$^{\circ}$R [Nesbitt, p.17]. The torque required to drive the compressor is directly proportional to the square root of the total temperature as shown in Eq. (2-54). Over the range of total temperature, the square root of the total temperature varies as

Table 2-3. Compressor Values

| Element | Symbol | Units | Value |
|---|---|---|---|
| Test section area | $A_T$ | $ft^2$ | 256.0 |
| Specific heat at constant pressure | $C_p$ | $\frac{ft\text{-}lb}{slug\text{-}{}^{o}R}$ | 6006.0 |
| Specific heat ratio for air | $\gamma$ | - | 1.4 |
| Brake moment of inertia | $J_{brake}$ | $ft\text{-}lb\text{-}sec^2$ | 4670 |
| Compressor moment of inertia | $J_{comp}$ | $ft\text{-}lb\text{-}sec^2$ | 381,250 |
| Induction motor moment of inertia | $J_{ind}$ | $ft\text{-}lb\text{-}sec^2$ | 12,420 |
| Synchronous motor moment of inertia | $J_{syn}$ | $ft\text{-}lb\text{-}sec^2$ | 46,670 |
| Gas constant | $R_c$ | $\frac{ft\text{-}lb}{slug\text{-}{}^{o}R}$ | 1716.0 |
| Test section total temperature | $TT_T$ | $^{o}R$ | 540.0 |

$$23.45 > \sqrt{TT_T} > 23.022. \qquad (2\text{-}62)$$

Since $\sqrt{TT_T}$ varies less than 2% over the range of operating temperatures, an average total temperature of 540 $^{o}$R was assumed.

Using the models of the liquid rheostat positioning system, the induction motors, and the 16T compressor derived in this chapter, the open loop performance of the system was simulated using an ACSL program. A flow diagram for this program is shown in Figure 2-14. A step input voltage was applied to the Rototrol control field for approximately 15 seconds in duration. This simulated the operator lowering the liquid rheostat to a position approximately half of its total travel. Figure 2-15 shows the output for two motor operation at a total pressure of 2000 lb/ft$^2$. The second input is a step input of 5 second duration which shows the effect of lowering the rheostat electrode after the output has reached steady state. Appendix C gives similar simulation results for both one and two motor operation over the range of operating total pressures.

In deriving the compressor model, the effects of accelerating the air in the tunnel circuit have been neglected. This is justified through the derivation and simulation results given in Appendix B. The results show the effect of the inertia of the air to a 10% step increase in compressor shaft speed. The time constant associated with the mass of the air varies depending on the operating point. As the Mach number operating point is increased, the time required for the system to reach a steady state decreases. The time constant associated with the mass of the air ranged from approximately 3.5

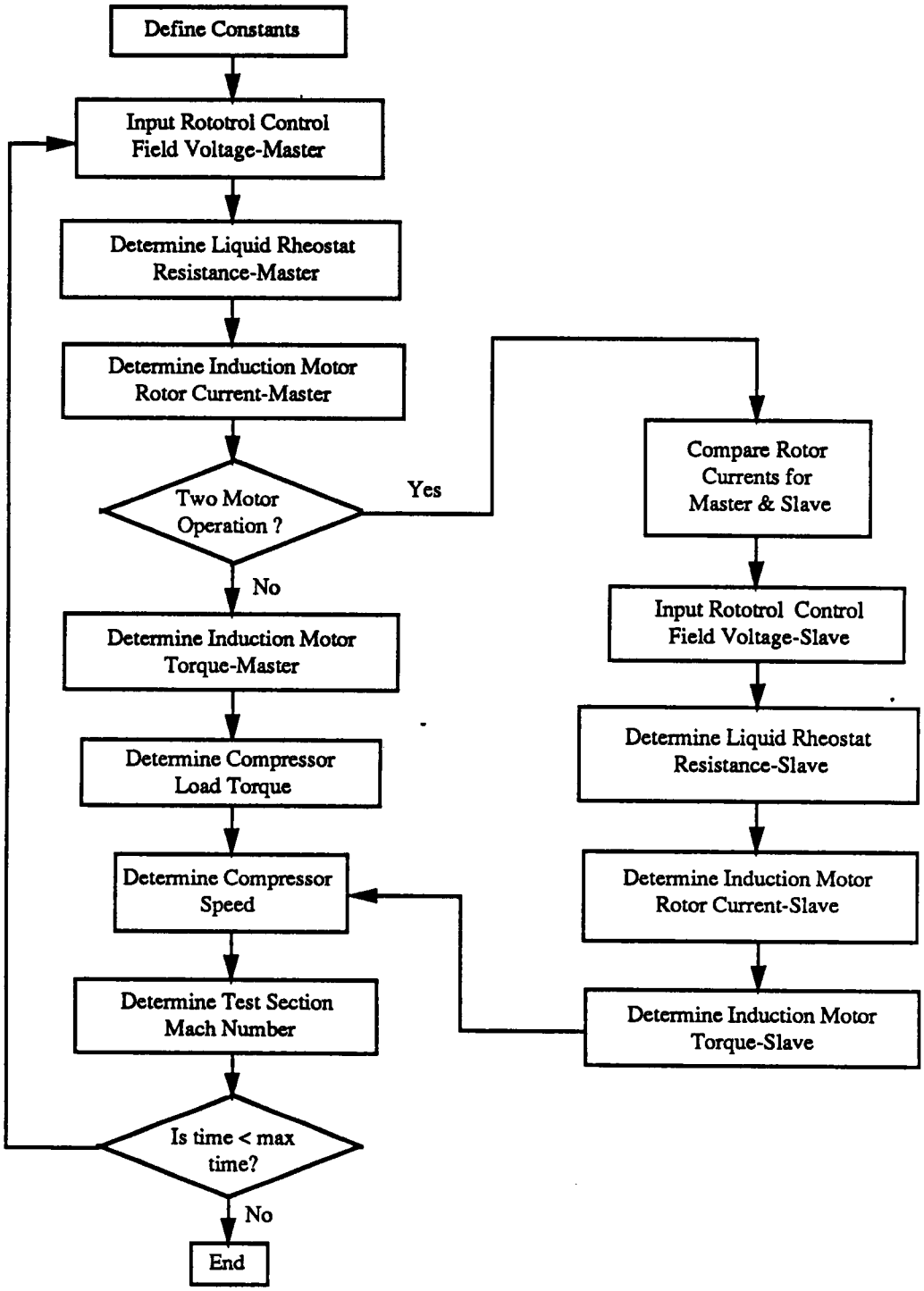



Figure 2-14. Open Loop Simulation Flow Diagram

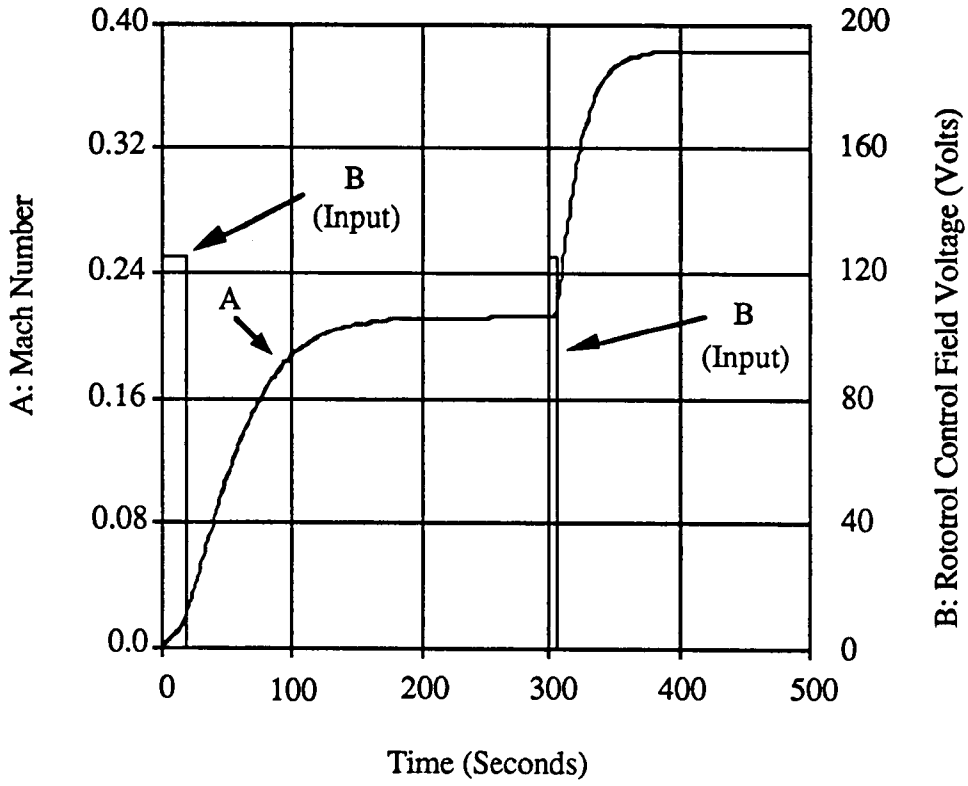



Figure 2-15. Open Loop Response to a Step Input for Two Motor Operation and $PT_T$=2000 lb/ft$^2$

seconds at a Mach number operating point of 0.2 to a time constant of approximately 0.5 seconds at a Mach number operating point of 0.6. This time constant is negligible when compared to the time of approximately 100 seconds necessary to accelerate the compressor and motor rotors as shown in the simulation results given in Figure 2-15 and in Appendix C.

# CHAPTER III

# CONTROLLER DEVELOPMENT

The approach taken to control the system is by means of closed loop feedback. The primary objective in providing closed loop control is that the system maintain the Mach number to within ± 3 percent of its setpoint. This is the tolerance presently allowed in order to maintain test conditions and continue data taking. Failure to stay within this tolerance means that data taking in the test section must be suspended until the Mach number is brought back to within the tolerance range. This results in additional testing time and higher operating costs.

The expressions derived in Chapter II for the torque developed by the induction motor and the torque required to drive the compressor are nonlinear. This presents a problem in analyzing the system using transforms since use of classical design techniques requires a linear model. However, by linearizing the model about different operating points, the parameters of the controller can be designed to provide the desired system performance for particular operating conditions.

## Linearization of Model

Any nonlinear relation

$$y = f(x) \tag{3-1}$$

can be expanded in a Taylor series about an operating condition $\bar{x}$, $\bar{y}$, as [Ogata, p. 82]

$$y = f(\bar{x}) + \left[\frac{df}{dx}\right]_{x=\bar{x}} (x - \bar{x}) + \frac{1}{2!}\left[\frac{d^2f}{dx^2}\right]_{x=\bar{x}} (x - \bar{x})^2 + \ldots \qquad (3\text{-}2)$$

If variations in x are small, the higher order terms in Eq. (3-2) can be neglected and Eq. (3-2) written as

$$y = f(\bar{x}) + \left[\frac{df}{dx}\right]_{x=\bar{x}} (x - \bar{x}), \qquad (3\text{-}3)$$

so

$$y = \bar{y} + \left[\frac{df}{dx}\right]_{x=\bar{x}} (x - \bar{x}). \qquad (3\text{-}4)$$

When $y$ is a function of two inputs, Eq.(3-3) becomes

$$y = f(\bar{x}_1, \bar{x}_2) + \left[\frac{\partial f}{\partial x}\right]_{\bar{x}_1\bar{x}_2} (x_1 - \bar{x}_1) + \left[\frac{\partial f}{\partial x}\right]_{\bar{x}_1,\bar{x}_2} (x_2 - \bar{x}_2). \qquad (3\text{-}5)$$

Linearization in this manner can be used to find an expression for the torque developed by the induction motor in terms of the liquid rheostat resistance and the shaft speed. The torque developed by the induction motors can be expressed by modifying Eq. (2-36) to account for either one or two motor operation,

$$T_m = \frac{2.213BV_1^2\, r_2'(\omega_s - \omega_m)}{\omega_s^2\left(r_2' + R'\right)^2 + (\omega_s - \omega_m)^2(X_1 + X_2')^2}. \qquad (3\text{-}6)$$

The B term in Eq. (3-6) is dependent on the number of induction motors being used. For single motor operation B is one; when using both induction motors, B is two. In simplifying the torque developed by the induction motors in this manner, the time constant associated with the current balance regulator circuitry used during two motor operation is neglected. This time constant was shown in Figure 2-6 to be approximately 3 seconds which is small compared to the time necessary to accelerate the compressor as shown in Figure 2-15 (p. 40).

Linearization of Eq. (3-6) gives

$$\Delta T_m = T_m - \bar{T}_m = \left[\frac{\partial \bar{T}_m}{\partial \omega_m}\right]_{\bar{\omega}_m, \bar{R}'} \Delta\omega_m + \left[\frac{\partial \bar{T}_m}{\partial R'}\right]_{\bar{\omega}_m, \bar{R}'} \Delta R', \tag{3-7}$$

where

$$\Delta\omega_m = \omega_m - \bar{\omega}_m, \tag{3-8}$$

$$\Delta R' = R' - \bar{R}', \tag{3-9}$$

$$\left[\frac{\partial \bar{T}_m}{\partial \omega_m}\right]_{\bar{\omega}_m, \bar{R}'} = -\bar{T}_m \frac{1}{\omega_s - \bar{\omega}_m} + \bar{T}_m^2 \left(\frac{2X_{eq}^2}{2.213BV_1^2 r_2'}\right), \tag{3-10}$$

$$X_{eq}^2 = (X_1 + X_2')^2, \tag{3-11}$$

and

$$\left[\frac{\partial \bar{T}_m}{\partial R'}\right]_{\bar{\omega}_m,\,\bar{R}'} = -\bar{T}_m^2\left[\frac{2\omega_s^2\left(r_2' + \bar{R}'\right)}{2.213BV_1^2\, r_2'(\omega_s - \bar{\omega}_m)}\right]. \tag{3-12}$$

Combining Eqs. (3-7) and (3-10) through (3-12) gives

$$\Delta T_m = \left[-\bar{T}_m\frac{1}{\omega_s - \bar{\omega}_m} + \bar{T}_m^2\left(\frac{2X_{eq}^2}{2.213BV_1^2\, r_2'}\right)\right]\Delta\omega_m$$

$$-\bar{T}_m^2\left[\frac{2\omega_s^2\left(r_2' + \bar{R}'\right)}{2.213BV_1^2\, r_2'(\omega_s - \bar{\omega}_m)}\right]\Delta R'. \tag{3-13}$$

Linearizing Eq. (2-54) with respect to the compressor shaft speed, the torque required to drive the compressor is

$$\Delta T_c = T_c - \bar{T}_c = \left[\frac{\partial T_c}{\partial \omega_m}\right]_{\bar{\omega}_m}\Delta\omega_m, \tag{3-14}$$

where

$$\left[\frac{\partial T_c}{\partial \omega_m}\right]_{\bar{\omega}_m} = \sqrt{\frac{\gamma T T_T}{R_c}}C_p P T_T A_T\left[\frac{\partial f(\omega_m)}{\partial \omega_m}\right]_{\bar{\omega}_m}, \tag{3-15}$$

or

$$\left[\frac{\partial T_c}{\partial \omega_m}\right]_{\bar{\omega}_m} = \frac{\bar{T}_c}{f(\bar{\omega}_m)}\left[\frac{\partial f(\omega_m)}{\partial \omega_m}\right]_{\bar{\omega}_m}. \tag{3-16}$$

From Eq. (2-58)

$$f(\omega_m) = C_1 + C_2\,\omega_m + C_3\,\omega_m^2, \tag{3-17}$$

where

$$C_1 = 3.208\text{x}10^{-6}, \tag{3-18}$$

$$C_2 = -3.447\text{x}10^{-6}, \tag{3-19}$$

and

$$C_3 = 2.364\text{x}10^{-7}. \tag{3-20}$$

Taking the derivative of Eq. (3-17) with respect to $\omega_m$ gives

$$\left[\frac{\partial f(\omega_m)}{\partial \omega_m}\right]_{\bar{\omega}_m} = C_2 + 2C_3\,\bar{\omega}_m. \tag{3-21}$$

Combining Eqs. (3-14), (3-16), and (3-21) gives

$$\Delta T_c = \frac{\bar{T}_c}{f(\bar{\omega}_m)}(C_2 + 2C_3\,\bar{\omega}_m)\,\Delta\omega_m. \tag{3-22}$$

The operating point torque of the motor in Eq. (3-13), $\bar{T}_m$, and the operating point torque of the compressor in Eq. (3-22), $\bar{T}_c$, are the same,

$$\bar{T}_m = \bar{T}_c = \bar{T} . \tag{3-23}$$

The motor torque and the compressor torque are related by Eq. (2-59) as

$$J_c \frac{d\omega_m}{dt} = \Sigma T = T_m - T_c , \tag{3-24}$$

so we also have

$$J_c \frac{d\Delta\omega_m}{dt} = \Delta T_m - \Delta T_c . \tag{3-25}$$

Combining Eqs. (3-13), (3-22), and (3-25) yields

$$J_c \frac{d\Delta\omega_m}{dt} = -\bar{T}\left[ \frac{1}{\omega_s - \bar{\omega}_m} - \bar{T}\left(\frac{2X_{eq}^2}{2.213BV_1^2 r_2'}\right) + \frac{(C_2 + 2C_3\,\bar{\omega}_m)}{f(\bar{\omega}_m)} \right]\Delta\omega_m$$

$$-\bar{T}^2\left[\frac{2\omega_s^2\left(r_2' + \bar{R}'\right)}{2.213BV_1^2 r_2'(\omega_s - \bar{\omega}_m)}\right]\Delta R' \tag{3-26}$$

Equation (3-26) can be simplified by introducing a constant $K_1$ which is dependent on the opearating point conditions,

$$K_1 = \bar{T}\left[ \frac{1}{\omega_s - \bar{\omega}_m} - \bar{T}\left(\frac{2X_{eq}^2}{2.213BV_1^2 r_2'}\right) + \frac{(C_2 + 2C_3\,\bar{\omega}_m)}{f(\bar{\omega}_m)} \right] \tag{3-27}$$

or

$$K_1 = K_1(\bar{\omega}_m, \bar{T}). \tag{3-28}$$

Equation (3-26) then becomes

$$J_c \frac{d\Delta\omega_m}{dt} = -K_1\Delta\omega_m - \bar{T}^2 \left[ \frac{2\omega_s^2 \left(r_2' + \bar{R}'\right)}{2.213BV_1^2 r_2'(\omega_s - \bar{\omega}_m)} \right] \Delta R' . \tag{3-29}$$

Taking the Laplace transform of Eq. (3-29) and rearranging yields

$$\Delta\omega_m(s) = - \frac{K_2}{\frac{J_c}{K_1} s + 1} \Delta R'(s) . \tag{3-30}$$

The constant $K_2$ is introduced for simplification of Eq. (3-30) and is dependent on the operating point conditions,

$$K_2 = \frac{\bar{T}^2 \left[ \frac{2\omega_s^2 \left(r_2' + \bar{R}'\right)}{2.213BV_1^2 r_2'(\omega_s - \bar{\omega}_m)} \right]}{K_1} . \tag{3-31}$$

The liquid rheostat resistance at the operating point, $\bar{R}'$, is determined by setting the torque developed by the motor(s) from Eq. (3-6) to the torque required to drive the compressor as given in Eq. (3-23) and solving for the resistance. This gives

$$\bar{R}' = \frac{1}{\omega_s} \sqrt{\frac{2.213BV_1^2 r_2'(\omega_s - \bar{\omega}_m)}{\sqrt{\frac{\gamma TT_T}{R_c}} C_p P T_T A_T f(\bar{\omega}_m)} - (\omega_s - \bar{\omega}_m)^2 X_{eq}^2} - r_2' . \quad (3\text{-}32)$$

The time constant associated with the acceleration of the compressor and motor(s) from Eq. (3-30) is

$$\tau_c = \frac{J_c}{K_1}, \quad (3\text{-}33)$$

or

$$\tau_c = \frac{J_c}{\bar{T}\left[\frac{1}{\omega_s - \bar{\omega}_m} - \bar{T}\left(\frac{2X_{eq}^2}{2.213BV_1^2 r_2'}\right) + \frac{(C_2 + 2C_3 \bar{\omega}_m)}{f(\bar{\omega}_m)}\right]} . \quad (3\text{-}34)$$

As Eq. (3-34) shows, the time constant is a function of the operating point torque, $\bar{T}$, and the shaft speed, $\bar{\omega}_m$ . The operating torque was shown in Chapter II to be directly proportional to the tunnel total pressure and compressor shaft speed. Figure 3-1 shows the effects of total pressure on the time constant $\tau_c$ for Mach 0.4 and two motor operation. The relationship between total pressure and the time constant $\tau_c$ for other operating conditions and motor configurations is similar to Figure 3-1. For a constant tunnel total pressure, the time constant $\tau_c$ also decreases with increasing compressor shaft speed. This is shown in Figure 3-2 for a total pressure of 1000 lb/ft$^2$ and two

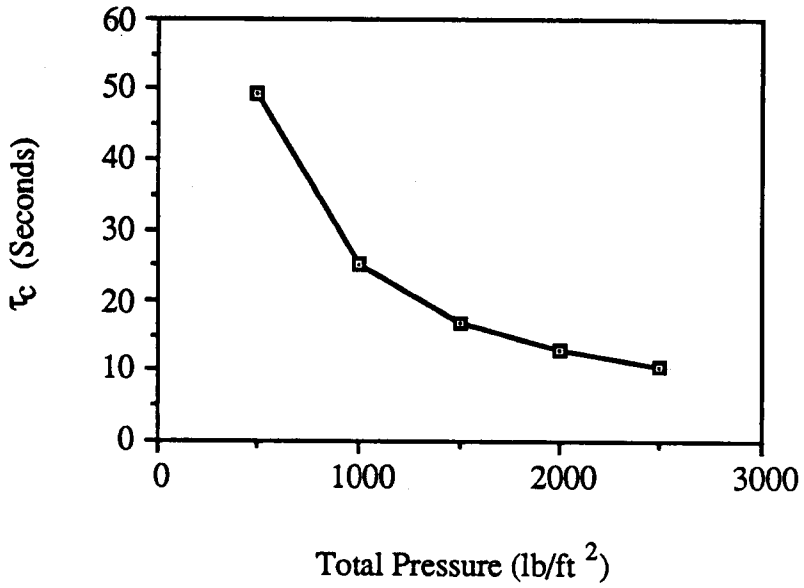



Figure 3-1. Variation of Time Constant $\tau_c$ with Total Pressure for Mach 0.4, Two Motor Operation.

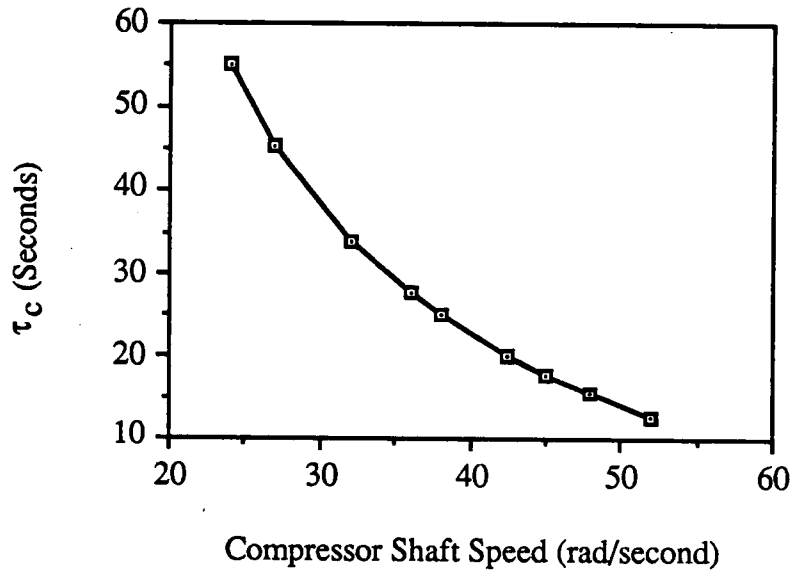



Figure 3-2. Variation of Time Constant $\tau_c$ with Compressor Shaft Speed for a Total Pressure of 1000 lb/ft$^2$, Two Motor Operation.

motor operation. This relationship is similar for other operating conditions and motor configurations.

The relationship between the test section Mach number and the compressor shaft speed as given in Eq. (2-47) can be expressed by

$$M = C_4 + C_5\,\omega_m + C_6\,\omega_m^2 \tag{3-35}$$

where

$$C_4 = 6.582\text{x}10^{-4}, \tag{3-36}$$

$$C_5 = 0.005\,, \tag{3-37}$$

and

$$C_6 = 1.309\text{x}10^{-4}. \tag{3-38}$$

Linearizing Eq. (3-35) gives

$$\Delta M = M - \bar{M} = \left[\frac{\partial M}{\partial \omega_m}\right]_{\bar{\omega}_m} \Delta\omega_m\,, \tag{3-39}$$

where

$$\left[\frac{\partial M}{\partial \omega_m}\right] = C_5 + C_6\,\omega_m\,. \tag{3-40}$$

Taking the Laplace transform of Eq. (3-39) gives

$$\Delta M(s) = \left[\frac{\partial M}{\partial \omega_m}\right]_{\bar{\omega}_m} \Delta\omega_m(s)\,. \tag{3-41}$$

The transfer function derived in Chapter II, Eq. (2-18), relating the angle of the DC motor to the Rototrol control field voltage is

$$\frac{\Theta(s)}{E_f(s)} = \frac{\dfrac{K_a}{K_b R_{feq}}}{s\left(\tau_r s + 1\right)\left(\tau_m s + 1\right)}. \tag{3-42}$$

As shown in Eqs. (2-23) and (2-25), the time constants $\tau_r$ and $\tau_m$ in Eq. (3-42) are very small (0.91 seconds and 0.038 seconds respectively) when compared to the time required to accelerate the compressor, $\tau_c$ as shown in Figure 3-1. Neglecting these time constants, Eq. (3-42) can be reduced to

$$\frac{\Theta(s)}{E_f(s)} = \frac{\dfrac{K_a}{K_b R_{feq}}}{s}. \tag{3-43}$$

Combining Eqs. (2-21) and (2-27) the relationship between the liquid rheostat resistance referred to the induction motor stator and the electrode position is

$$\frac{R'(s)}{y(s)} = \frac{r_e \alpha^2}{.85 A_e}. \tag{3-44}$$

Taking the Laplace transform of Eq. (3-9)

$$\Delta R'(s) = R'(s) - \bar{R}'(s). \tag{3-45}$$

Combining Eqs. (2-20), (3-44), and (3-45) gives

$$\Delta R'(s) = \frac{r_e \alpha^2}{.85 A_e} y(s) - \bar{R}'(s). \tag{3-46}$$

Combining Eqs. (3-30), (3-40), and (3-46) gives

$$\Delta M(s) = \frac{-K_2(C_5 + C_6\,\bar{\omega}_m)\dfrac{r_e\alpha^2}{0.85A_e}}{\left[\dfrac{J_c}{K_1}s + 1\right]} x_{max}(s) + \frac{K_2(C_5 + C_6\,\bar{\omega}_m)}{\left[\dfrac{J_c}{K_1}s + 1\right]}\bar{R}'(s) -$$

$$+ \frac{\dfrac{K_a r_s r_e \alpha^2 K_2(C_5 + C_6\,\bar{\omega}_m)}{K_b R_{feq} GR(0.85A_e)}}{s\left[\dfrac{J_c}{K_1}s + 1\right]} E_f(s). \qquad (3\text{-}47)$$

Simplifying Eq. (3-47) gives

$$\Delta M(s) = \frac{-K_2K_3K_4}{\left[\dfrac{J_c}{K_1}s + 1\right]} x_{max}(s) + \frac{K_2K_3}{\left[\dfrac{J_c}{K_1}s + 1\right]}\bar{R}'(s)$$

$$+ \frac{K_2K_3K_4K_5}{s\left[\dfrac{J_c}{K_1}s + 1\right]} E_f(s). \qquad (3\text{-}48)$$

where

$$K_3 = C_5 + C_6\,\bar{\omega}_m, \qquad (3\text{-}49)$$

$$K_4 = \frac{r_e\alpha^2}{0.85A_e}, \qquad (3\text{-}50)$$

and

$$K_5 = \frac{K_a r_s}{K_b R_{feq} GR}. \qquad (3\text{-}51)$$

The Mach number from Eq. (3-39) is

$$M(s) = \bar{M}(s) + \Delta M(s) \qquad (3\text{-}52)$$

The block diagram of the linearized system from Eqs. (3-48) through (3-52) is shown in Figure 3-3. The input to the system in Eq. (3-48) is the Rototrol control field voltage, $E_f(s)$, and the output is the change in Mach number, $\Delta M(s)$. Using this linear expression, classical control system analysis techniques can be used to develop a control algorithm.

## Development of Control Algorithm

One of the primary objectives in the closed loop control of this system is to maintain the setpoint Mach number with a steady state error of zero. Because this is a type one system (due to the integrator in the rheostat positioning system), the closed loop system will have a steady state error of zero in response to a step input. Thus due to the inherent qualities of the system, the steady state error requirements of the system are already met. What remains is to decide what kind system performance is desirable and develop a controller to achieve this performance. Because the performance of the system depends on the total pressure and the Mach number, a controller is needed which takes into consideration these variables. The objective of the controller then becomes one of consistently maintaining the desired system performance.

As decribed in Chapter I, the induction motors are brought up to operating speed automatically. This controller would not be used to bring the motors up to speed, but

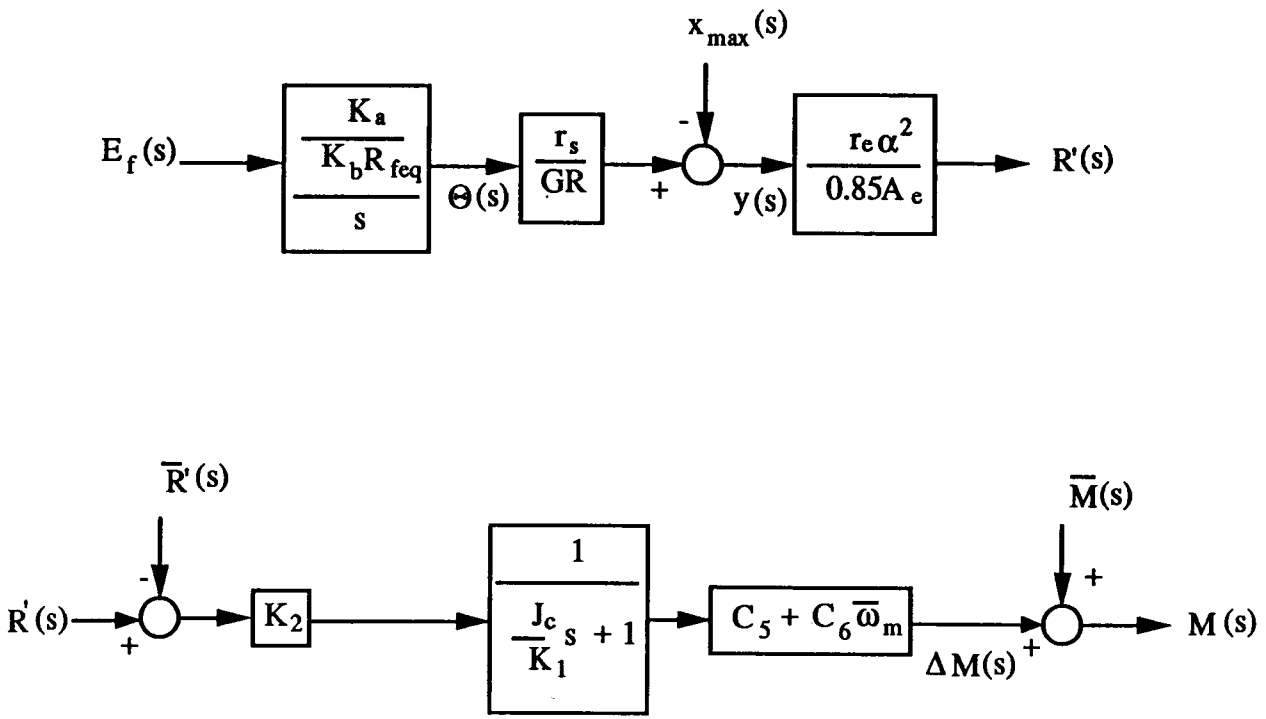



Figure 3-3. Block Diagram of Linearized Model

only to maintain the setpoint Mach number once the motors are brought up to speed. Instead of switching to manual once the compressor is brought up to speed, the operator would switch control of the liquid rheostat to the controller. The most feasible manner in which to incorporate this adaptive controller within the system is through the use of a digital controller. A block diagram of the closed loop system with the controller implemented is shown in Figure 3-4.

For closed loop control as shown in Figure 3-4, the sampled transfer function of the controller is

$$G_c(z) = \frac{E_f(z)}{E(z)}, \tag{3-53}$$

where $E_f(z)$ is the Rototrol input voltage and the error, E(z), is

$$E(z) = \left[\hat{M}(z) - M(z)\right]. \tag{3-54}$$

Using a zero order hold, the Z-transform of Eq. (3-48) becomes

$$\Delta M(z) = Z\left\{ \frac{-K_2K_3K_4}{\left[\frac{J_c}{K_1}s + 1\right]} x_{max}(s) + \frac{K_2K_3}{\left[\frac{J_c}{K_1}s + 1\right]} \bar{R}'(s) \right\}$$

$$+ Z\left\{ \frac{K_2K_3K_4K_5}{s^2\left[\frac{J_c}{K_1}s + 1\right]} \right\} \frac{(z-1)}{z} E_f(z). \tag{3-55}$$

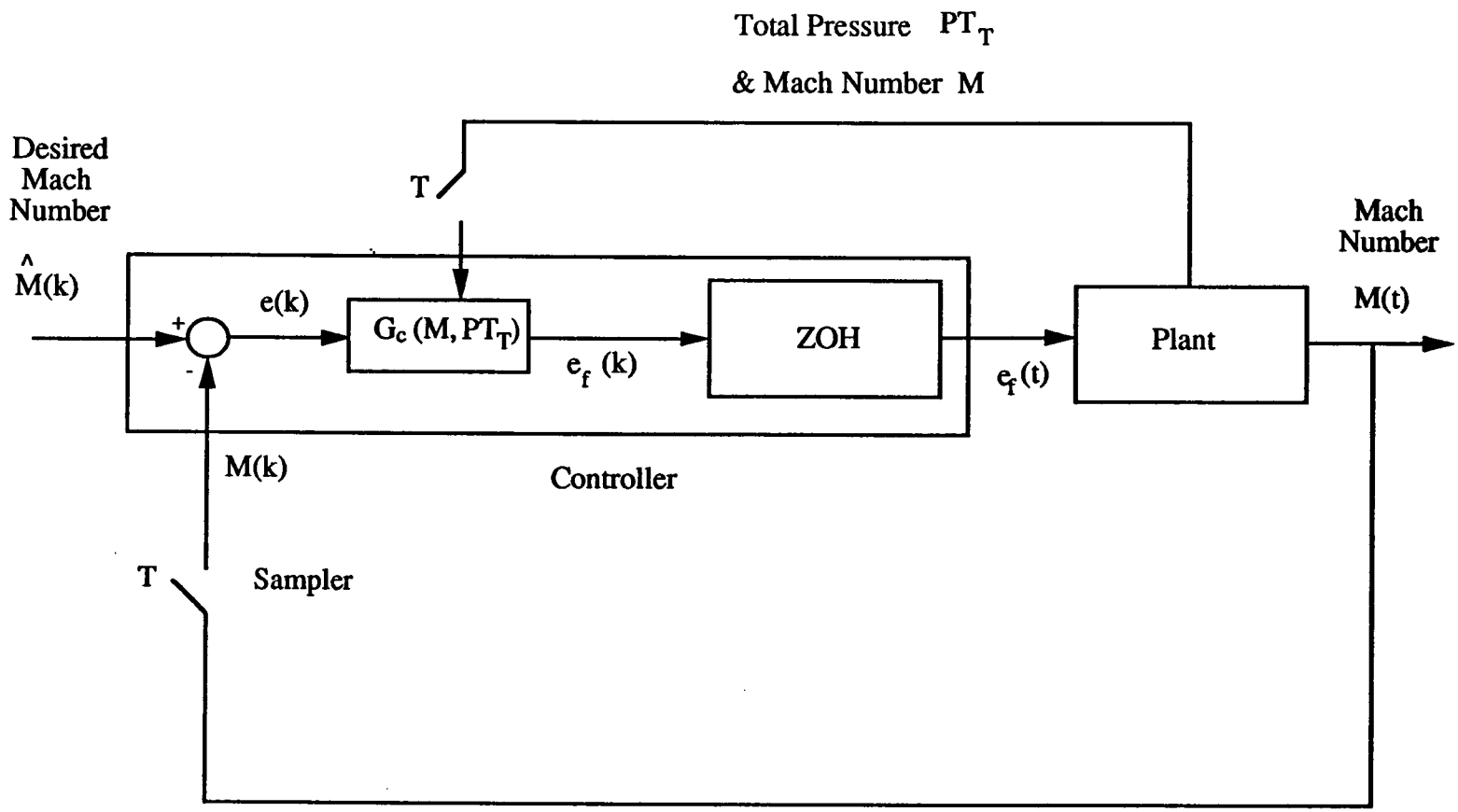



Figure 3-4. Block Diagram for Closed Loop Control of Mach Number

Combining Eqs. (3-53) through (3-55) gives

$$\Delta M(z) = Z\left\{ \frac{-K_2K_3K_4}{\left[\frac{J_c}{K_1}s + 1\right]} x_{max}(s) + \frac{K_2K_3}{\left[\frac{J_c}{K_1}s + 1\right]} \bar{R}'(s) \right\}$$

$$+ Z\left\{ \frac{K_2K_3K_4K_5}{s^2\left[\frac{J_c}{K_1}s + 1\right]} \right\} \frac{(z-1)}{z} G_c(z) \left[\hat{M}(z) - M(z)\right]. \quad (3\text{-}56)$$

From Eq. (3-56), the characteristic equation of the system is

$$1 + G_c(z) \frac{(z-1)}{z} Z\left\{ \frac{K_2K_3K_4K_5}{s^2\left[\frac{J_c}{K_1}s + 1\right]} \right\} = 0. \quad (3\text{-}57)$$

Taking the Z-transform of the term in the brackets in Eq. (3-57) gives

$$1 + G_c(z)K_2K_3K_4K_5 \frac{z(e^{-aT} + aT - 1) + 1 - e^{-aT}(1 + aT)}{a(z-1)(z-e^{-aT})} = 0, \quad (3\text{-}58)$$

where T is the sampling period and

$$a = \frac{K_1}{J_c}. \quad (3\text{-}59)$$

Equation (3-58) can be expressed as

$$1 + G_1(z), \quad (3\text{-}60)$$

where

$$G_1(z) = G_c(z)K_2K_3K_4K_5\frac{z(e^{-aT} + aT - 1) + 1 - e^{-aT}(1 + aT)}{a(z-1)(z-e^{-aT})}. \qquad (3\text{-}61)$$

By mapping $G_1(z)$ into the w-plane, frequency domain techniques (Bode Plots) can be used to analyze the function. Mapping $G_1(z)$ into the w-plane is done through the use of the bilinear transformation [Phillips, p. 194],

$$z = \frac{1 + \frac{T}{2}w}{1 - \frac{T}{2}w}. \qquad (3\text{-}62)$$

As seen in Eq. (3-62), the transformation is dependent on the sampling period T. In selecting a sampling period, it is important that the period be small compared to the smallest time constant of the system. A sampling period of 0.1 seconds was chosen to accommodate the time constant of 0.91 seconds associated with the Rototrol as given by Eq. (2-23). A Fortran program was written to perform the transformation of $G_1(z)$ into the w-plane and output the phase and gain of the function [Phillips, p. 522]. Since $G_1(z)$ depends on the Mach number and total pressure, the program was run for several different operating points with $G_c(z) = 1.0$. For Mach number operating points of 0.2 through 0.6 in increments of 0.1, the program was run for several different total pressures for both one motor and two motor operation. An example Bode plot for an operating point of Mach 0.4 and a total pressure of 2000 $lb/ft^2$ with two motors is shown in Figure 3-5.

From this point, the approach taken in controlling the system was to make the system damped such that it exhibits little or no overshoot to a step change in input. This

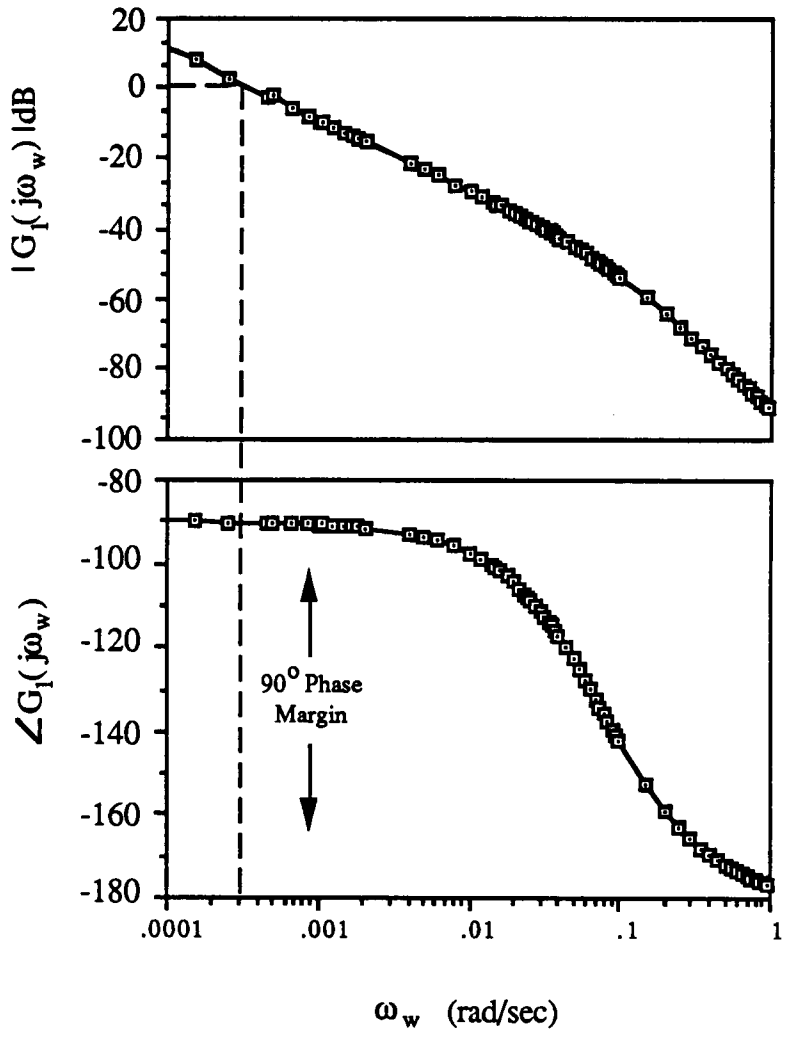



Figure 3-5. w-Plane Bode Plot for Mach 0.4 and a Total Pressure of 2000 lb/ft$^2$ with Two Motors.

system as described by $G_1(z)$ is a second order system with a pole at the origin and a pole at $J_c/K_1$. For a second order system, the damping ratio, $\zeta$, is directly related to the phase margin as shown in Figure 3-6. By designing the controller so that this damping ratio is maintained, the overshoot of the system in response to a step change in input can also be maintained. For a second order system, the overshoot in percent is related to the damping ratio by [Ogata, p. 435]

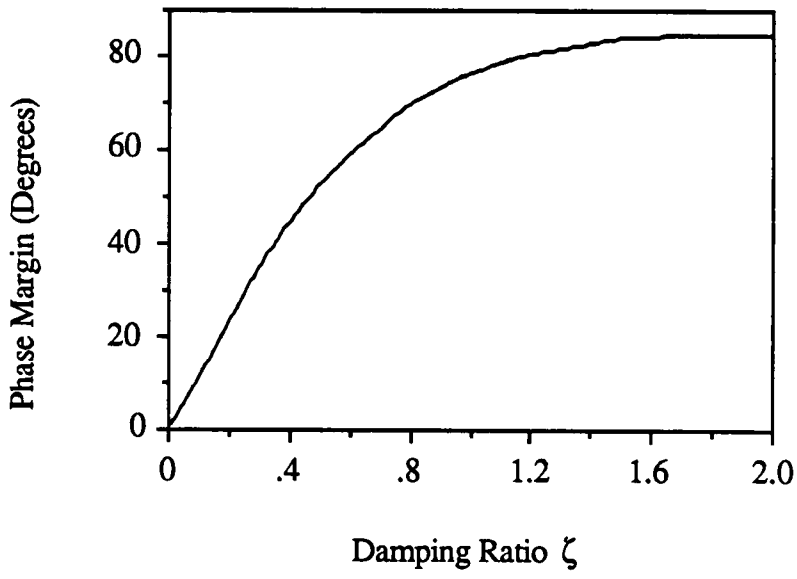
$$M_p = 100\exp\left[\frac{-\zeta\pi}{\sqrt{1 - \zeta^2}}\right]. \tag{3-63}$$

It is desirable that the system be damped to minimize overshoot and oscillations to prevent exercising the system more than necessary. In general, second order systems with a damping ratio $\zeta$ of between 0.5 and 0.8 gets close to the final value more rapidly than a critically damped or over damped system [Ogata, p. 232]. By choosing the more heavily damped ratio in this range, $\zeta = 0.8$, this gives a good compromise between overshoot and speed of response. A damping ratio of 0.8 gives an overshoot of 1.5 percent in response to a step change in input, allowing the system to reach its final value in a reasonable time with a minimum of oscillation.

From Figure 3-6 [Ogata, p. 437], a damping ratio of 0.8 requires a phase margin of approximately 70°. This phase margin can be attained by adding a proportional gain to the system which raises the gain curve thus providing the desired phase margin at the gain crossover frequency. The phase margin is expressed as

$$PM = 180^\circ + \angle G_1(\omega_w). \tag{3-64}$$

For a phase margin of 70°,




[Ogata, p.437]

Figure 3-6. Damping Ratio versus Phase Margin for a Second Order System.

$$\angle G_1(\omega_w) = 70^\circ - 180^\circ = -110^\circ. \tag{3-65}$$

From Figure 3-5, it is necessary to shift the gain curve upward such that the gain crossover occurs where the phase is -110°. This occurs at $\omega_w = 0.03$. The gain at this frequency is -38.8 dB. The amount of proportional gain necessary to shift the gain curve up is

$$20\log K_p = 38.8. \tag{3-66}$$

Solving for $K_p$ gives

$$K_p = 87.1. \tag{3-67}$$

The controller $G_c(z)$ becomes

$$G_c(z) = K_p \tag{3-68}$$

The w-plane frequency response of the system with the gain as determined in Eq. (3-67) is shown in Figure 3-7. The system now has a phase margin of 70°. This procedure was followed for several different total pressures at Mach 0.4 with two motor operation to obtain the value of $K_p$ necessary to give the system a phase margin of 70°. Figure 3-8 shows the variation of $K_p$ with total pressure for two motor operation at Mach 0.4. The gain $K_p$ for Mach 0.2 through 0.6 for both one and two motor operation was obtained in a similar manner. By applying a second order curve fit to the plot in Figure 3-8, the gain $K_p$ can be expressed as a function of the total pressure, $PT_T$, as

$$K_p = 29.2 + 0.0378\ PT_T - 4.629\text{x}10^{-6}\ PT_T^2\ . \tag{3-69}$$

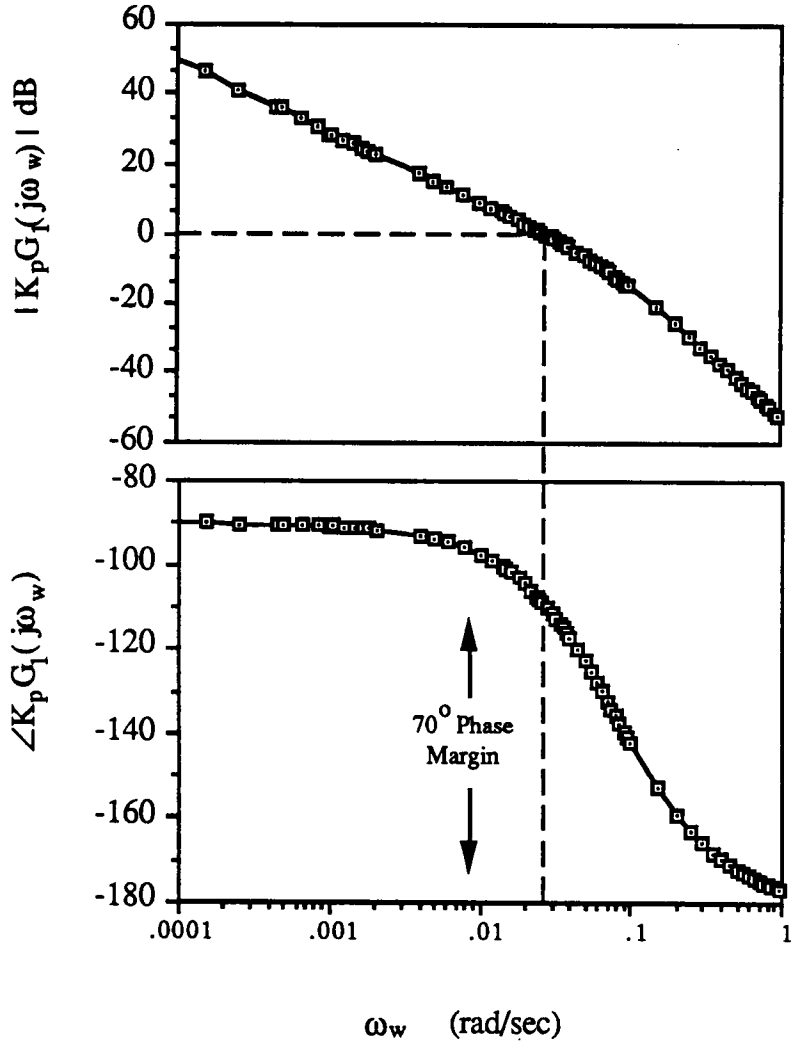



Figure 3-7. w-Plane Bode Plot with Proportional Gain $K_p$ for Mach 0.4 and a Total Pressure of 2000 lb/ft$^2$ with Two Motors.

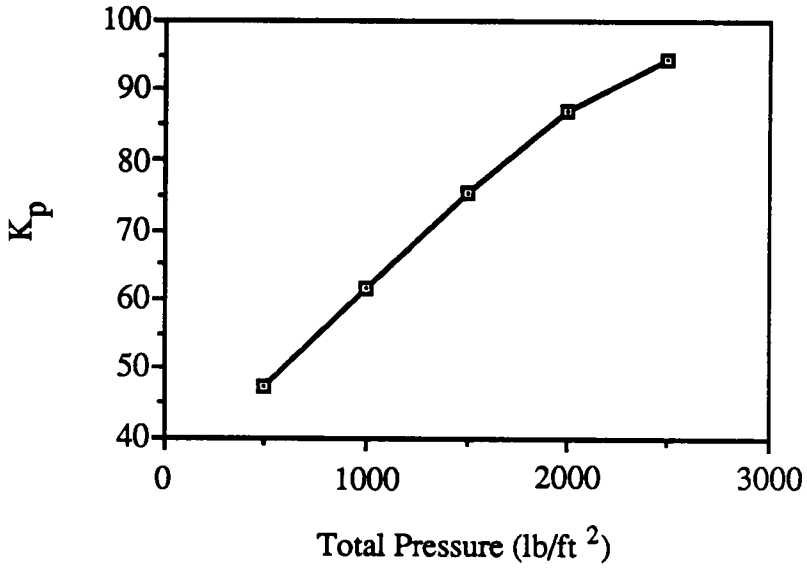



Figure 3-8. Change in Controller Gain $K_p$ for Mach 0.4 and a Total Pressure of 2000 lb/ft$^2$ with Two Motors.

Similar expressions for $K_p$ can be obtained for Mach 0.2 through 0.6 for both motor configurations. The approach taken in designing the algorithm is to choose the expression for $K_p$ depending on the operating point Mach number range and the number of motors used to drive the compressor. For the operating condition of Mach 0.4, when the Mach number is greater than Mach 0.35 and less than or equal to Mach 0.45 with two motor operation, the gain $K_p$ will be calculated using the expression in Eq. (3-69). The control algorithm first determines what the Mach number range is and then which expression to use for $K_p$ depending on whether one or two motors are used to drive the compressor. For Mach 0.5 and above, both induction motors are used, thus choosing one or two motor operation is not necessary. Figure 3-9 shows the flow diagram of the control algorithm.

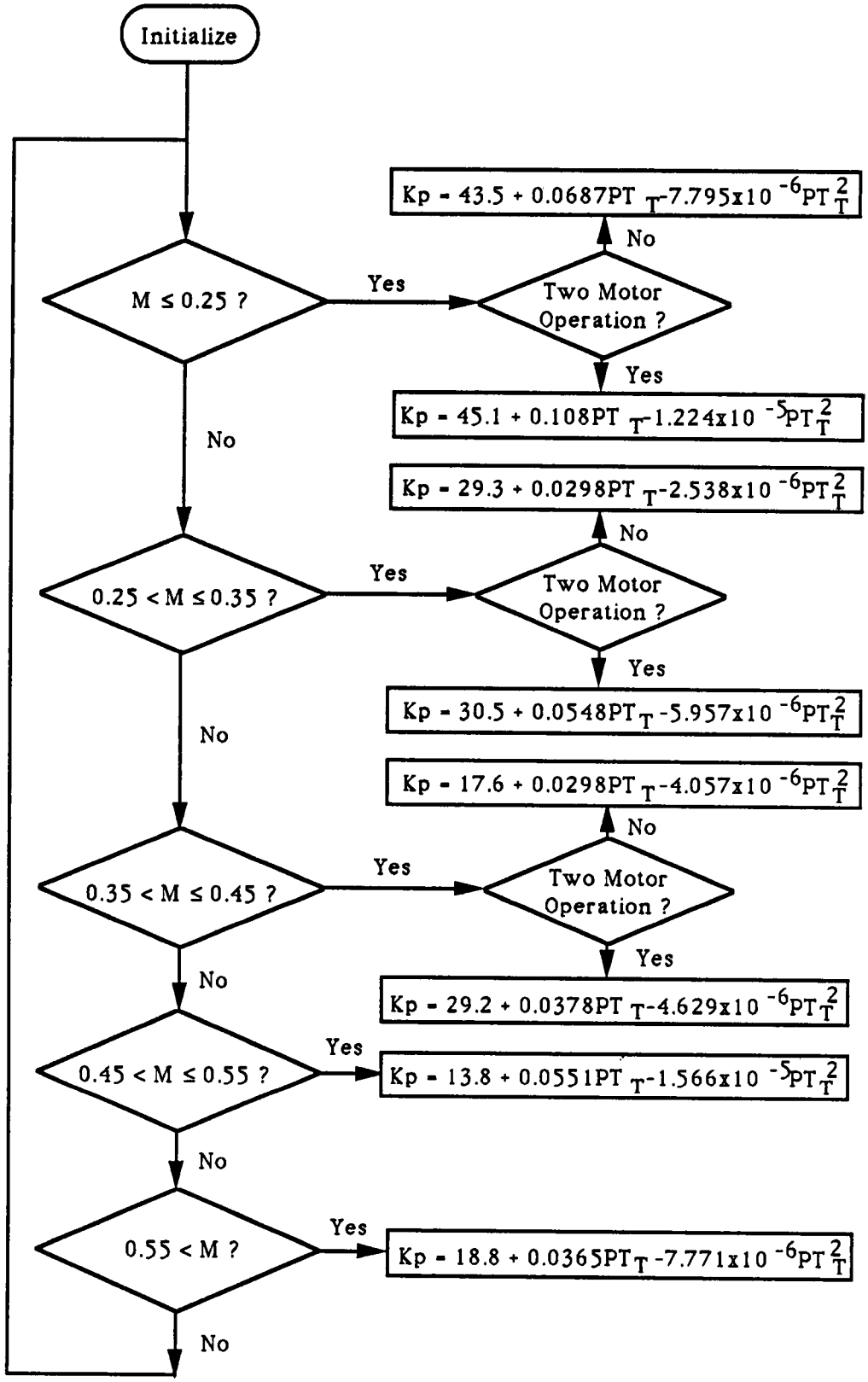



Figure 3-9. Control Algorithm Flow Diagram.

# CHAPTER IV

## RESULTS

To evaluate the ability of the control algorithm to carry out its purpose, the closed loop performance of the system was simulated over the range of operating conditions for which it was designed. In testing the performance of the system with the controller implemented, the system was brought up to the operating point Mach number and a step change in input of 10 percent was made. This was done for several different tunnel total pressures. Although in actual operation changes in the set point are unlikely once test conditions are reached, this was a reasonable manner in which to determine controller performance. Performance of the system with the control algorithm of Figure 3-9 was simulated using ACSL. The flow diagram of the program is shown in Figure 4-1.

To demonstrate the capabilities of the controller it was exercised in the simulation over the range of operating conditions. At the lower end of the operating envelope, Figure 4-2 shows the response of the system to a 10 percent increase in operating point Mach number at Mach 0.2, 1000 $lb/ft^2$ , and one motor operation. The straight line in the figure is the setpoint and the sloped line is the response. Towards the midrange of the subsynchronous operating envelope, Figure 4-3 shows the response for Mach 0.4, 2000 $lb/ft^2$ , and two motor operation. At the upper end of the envelope, Figure 4-4 shows the response of the system for Mach 0.6, 1000 $lb/ft^2$ , and two motor operation. Results for similar changes in the operating point are given in Appendix C over a wide range of operating conditions. In all cases the system reaches its final value with a steady state error of zero.The design objective in Chapter III was a damping ratio of

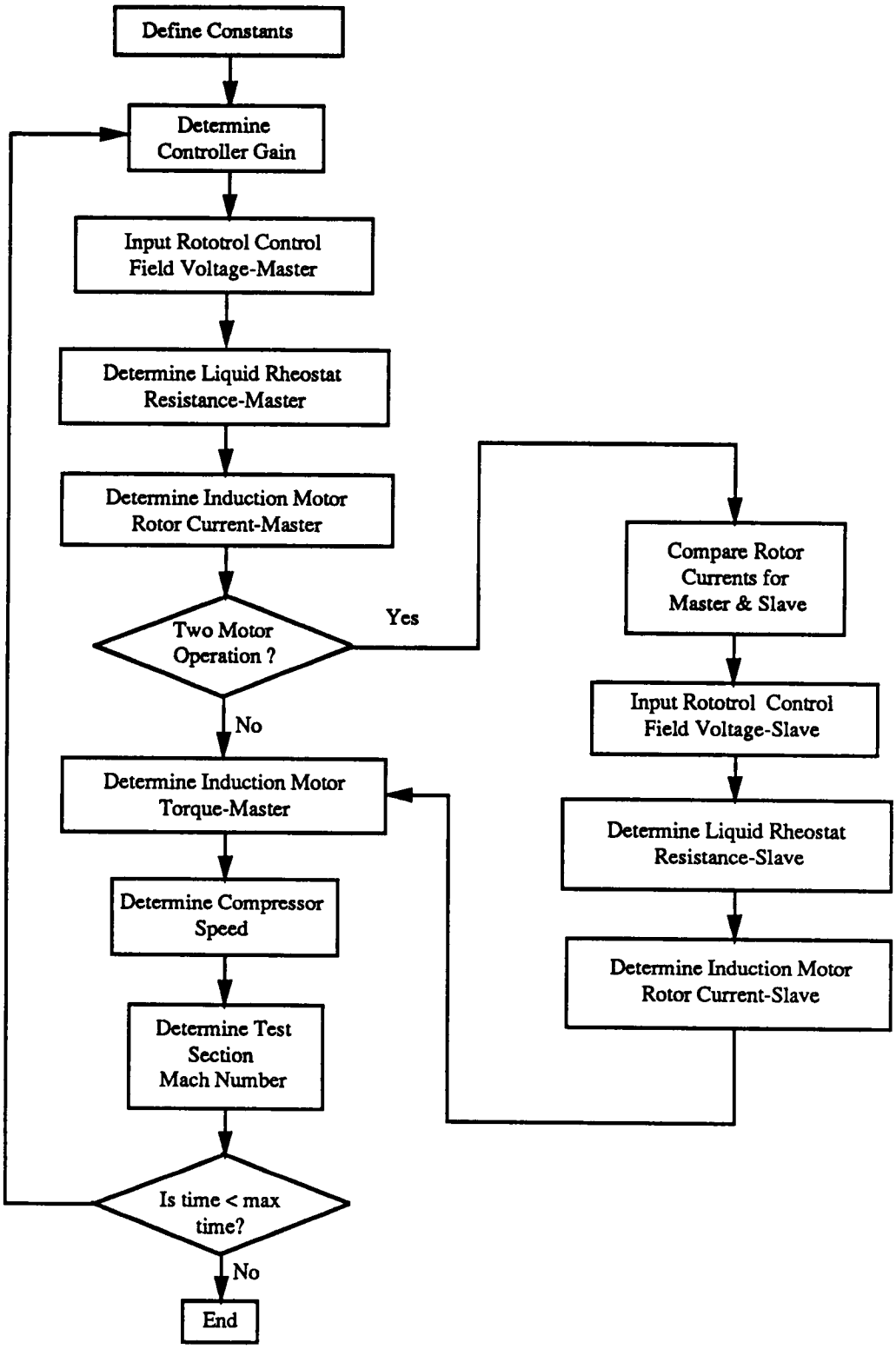



Figure 4-1. Closed Loop Simulation Flow Diagram

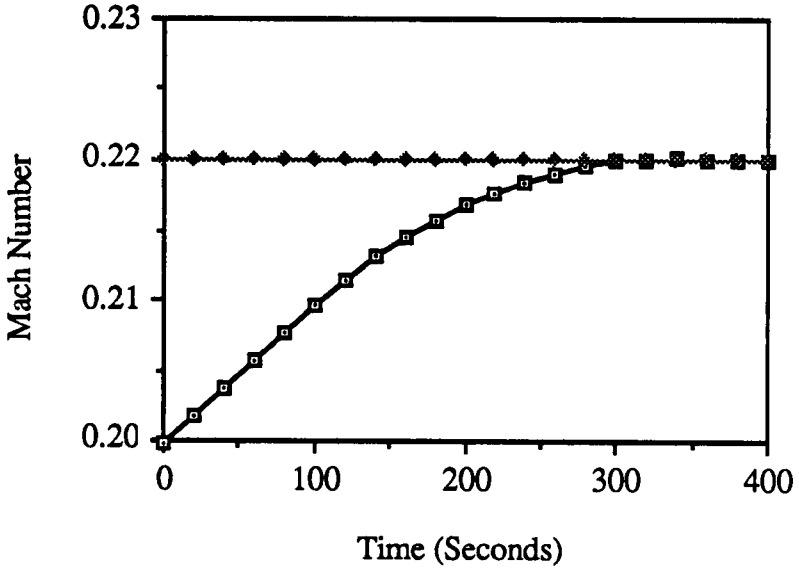



Figure 4-2. Simulation Results for a Total Pressure of 1000 lb/ft$^2$ at Mach 0.2 and One Motor Operation.

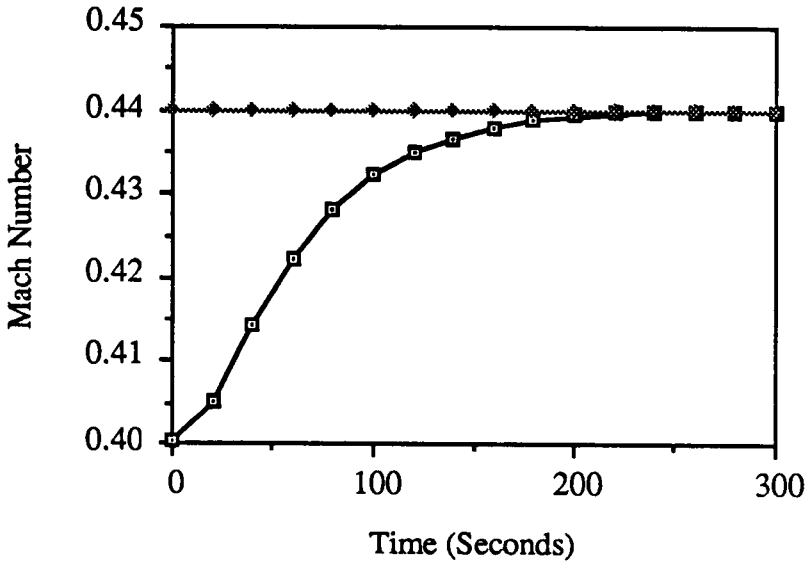



Figure 4-3. Simulation Results for a Total Pressure of 2000 lb/ft$^2$ at Mach 0.4 and Two Motor Operation.

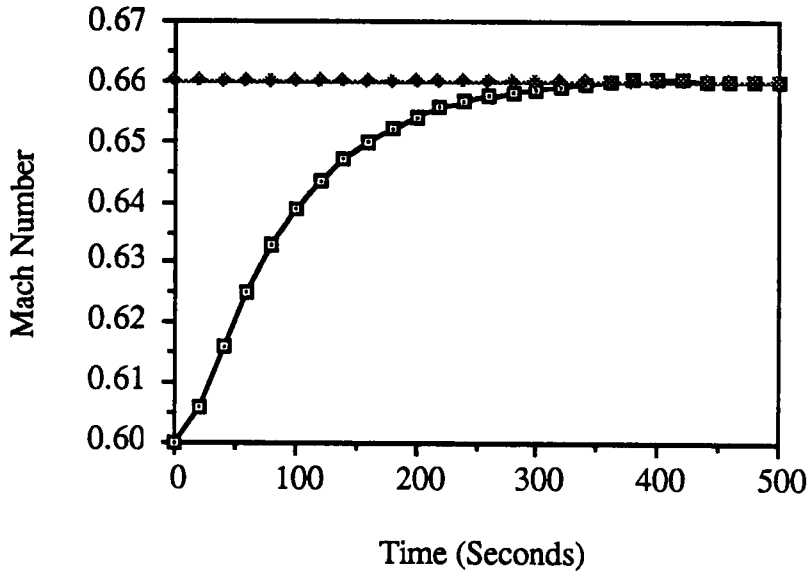



Figure 4-4. Simulation Results for a Total Pressure of 1000 lb/ft$^2$ at Mach 0.6 and Two Motor Operation.

0.8, or an overshoot of approximately 1.5 percent. The results of the ACSL simulation reveals the overshoot in response to a 10 percent change in Mach number set point is minimal (less than approximately two percent) for the operating range of the system. This overshoot is somewhat evident in Figures 4-2 and 4-4.

For any given Mach number, the system takes longer to respond at lower total pressures. This is because the dominant time constant $\tau_c$, which is associated with accelerating the compressor, is higher at lower total pressures for a constant Mach number as was shown in Chapter III, Figure 3-1 (page 50). For example, at Mach 0.4 for two motor operation and a total pressure of 1000 $lb/ft^2$ (Figure C-18, Appendix C), the system takes approximately 400 seconds to reach its final value for a 10 percent change in set point. At a total pressure of 3000 $lb/ft^2$ (Figure C-19, Appendix C), the system takes approximately 175 seconds. When the total pressure increases, the time constant $\tau_c$ is smaller which results in a faster system.

To simulate the behavior of the system when subjected to a disturbance, a 10 percent step increase in the torque required to drive the compressor was introduced. For Mach 0.4, 2000 $lb/ft^2$ , and two motor operation, the disturbance was introduced for 20 seconds while the system was running at steady state. This simulated a disturbance caused by the pitching of the model in the test section, restricting the air passing through the section. Figure 4-5 shows the response of the system when the disturbance in Figure 4-6 is applied. As the figure shows, the system stays within 3 percent of the setpoint after some oscillation.

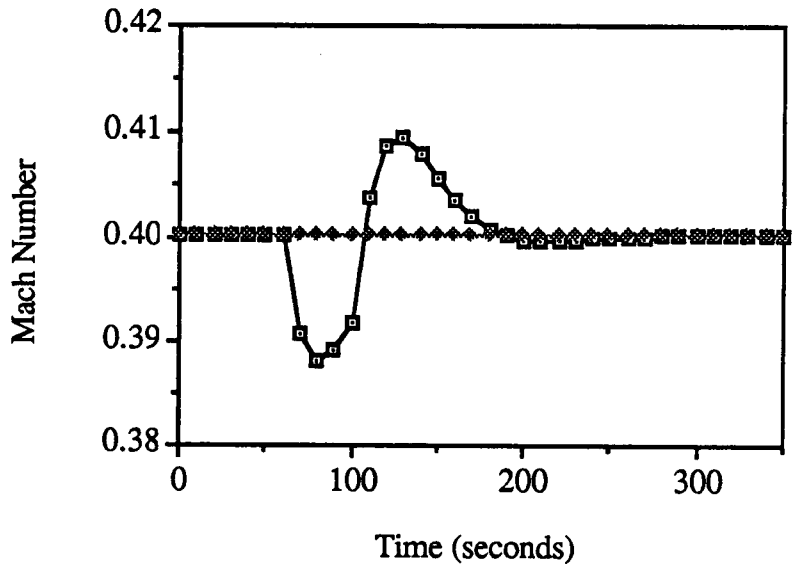



Figure 4-5. Simulation Results for a 10% Disturbance in Compressor Load at 2000 lb/ft$^2$, Mach 0.4, and Two Motor Operation.

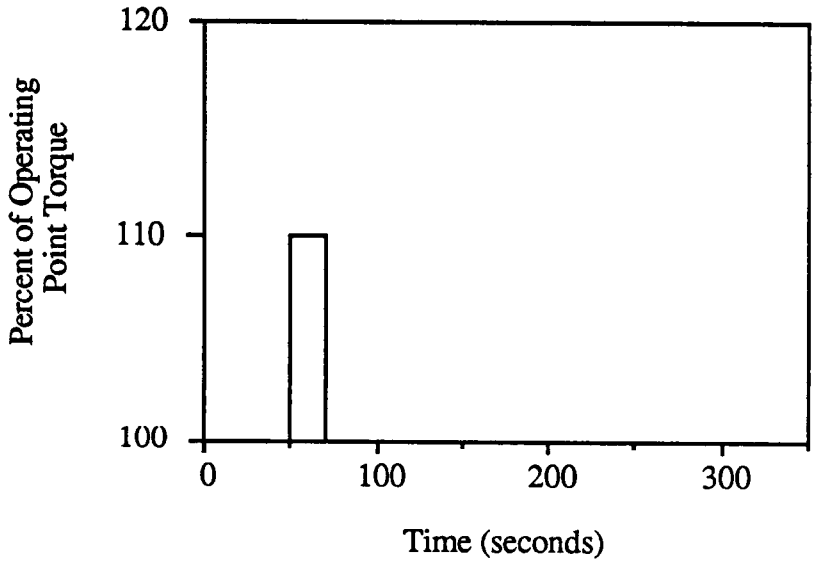



Figure 4-6. Compressor Load Disturbance

# CHAPTER V

## CONCLUSIONS AND RECOMMENDATIONS

The purpose of this study was to develop a control algorithm for the AEDC-PWT Main Drive induction motors during subsynchronous operation. This controller must maintain the test section Mach number to within 3 percent of the setpoint by controlling the speed of the PWT Main Drive induction motors. This controller would be used to control the speed of the motors after the motors have been brought up to speed. The characteristics of the rheostat positioning system used to control the speed of the motors make it a type one system. A type one system with unity feedback will maintain a steady state error of zero in response to a step input. Due to this inherent property of the system, the objective of attaining the error requirements was met. Developing the control algorithm then focused on designing a controller which would maintain consistent performance over the range of operating conditions.

Since the performance of the system varies with tunnel total pressure, test section Mach number, and the number of motors used to drive the compressor, an algorithm was developed which would take these variables into consideration when determining the controller parameters. A proportional control algorithm was developed which would adjust its gain depending on the tunnel total pressure, Mach number, and the number of motors used. This controller was designed to maintain a damping ratio of approximately 0.8, and thus an overshoot of less than 2 percent in response to a 10 percent step change in input .

The most involved aspects of this study was the development of the model of the liquid rheostat positioning system, the induction motors, and the 16T compressor.

When possible, measured parameters, observed performance, and manufacturers' data were used in developing the model. Expressions derived for the model of the induction motor and the 16T compressor were nonlinear. By using linearization techniques, a simplified second order model was obtained. The control algorithm was developed by analyzing this simplified model about several different operating points. Using an ACSL simulation program, the performance of the model with the controller was tested. The results of the simulations revealed that the control algorithm met the steady state error and system damping design objectives.

Although it is beyond the scope of this study to produce a detailed design, a possible means of controller implementation will be discussed. Discussions with personnel familiar with the 16T plant data acquisition system indicate that analog signals for both the tunnel total pressure and Mach number can be obtained from the existing facility data acquisition system. These analog signals can be used as controller inputs, allowing the sampling of these signals to be performed by the controller. Since the tunnel total pressure does not change very rapidly or often, it would not be necessary to sample it as frequently as the Mach number.

Development and debugging of the algorithms shown in Figure 3-9 (p. 67) and Figure 4-1 (p.69) could be done using a personal computer such as an IBM-compatible system. This type of system would be feasible due to the availability of interface boards and software. Another advantage with this type of system would be the ability to easily change or adjust the algorithm. This control system would consist of a personal computer, an analog input/output board with a minimum capability of accepting two analog inputs and providing one analog output, and a power amplifier. The power amplifier rated for approximately 500 watts is necessary to drive the control field of the Rototrol for the liquid rheostat positioning system. A block diagram of this system is

shown in Figure 5-1. Once the algorithm is developed, a dedicated controller could be used for permanent implementation. This could take the form of a small programmable controller which has the capability to make calculations using more than one variable.

In conclusion, this study has shown that closed loop control of the Main Drive induction motors during subsynchronous operation is possible using a controller with scheduled gain. Improvement and verification of the model derived in this study would require a dedicated test of the AEDC-PWT 16T tunnel during subsynchronous operation. This would involve studying the response of the system to a step input and disturbance for different operating conditions and comparing this response to the response obtained through computer simulation.

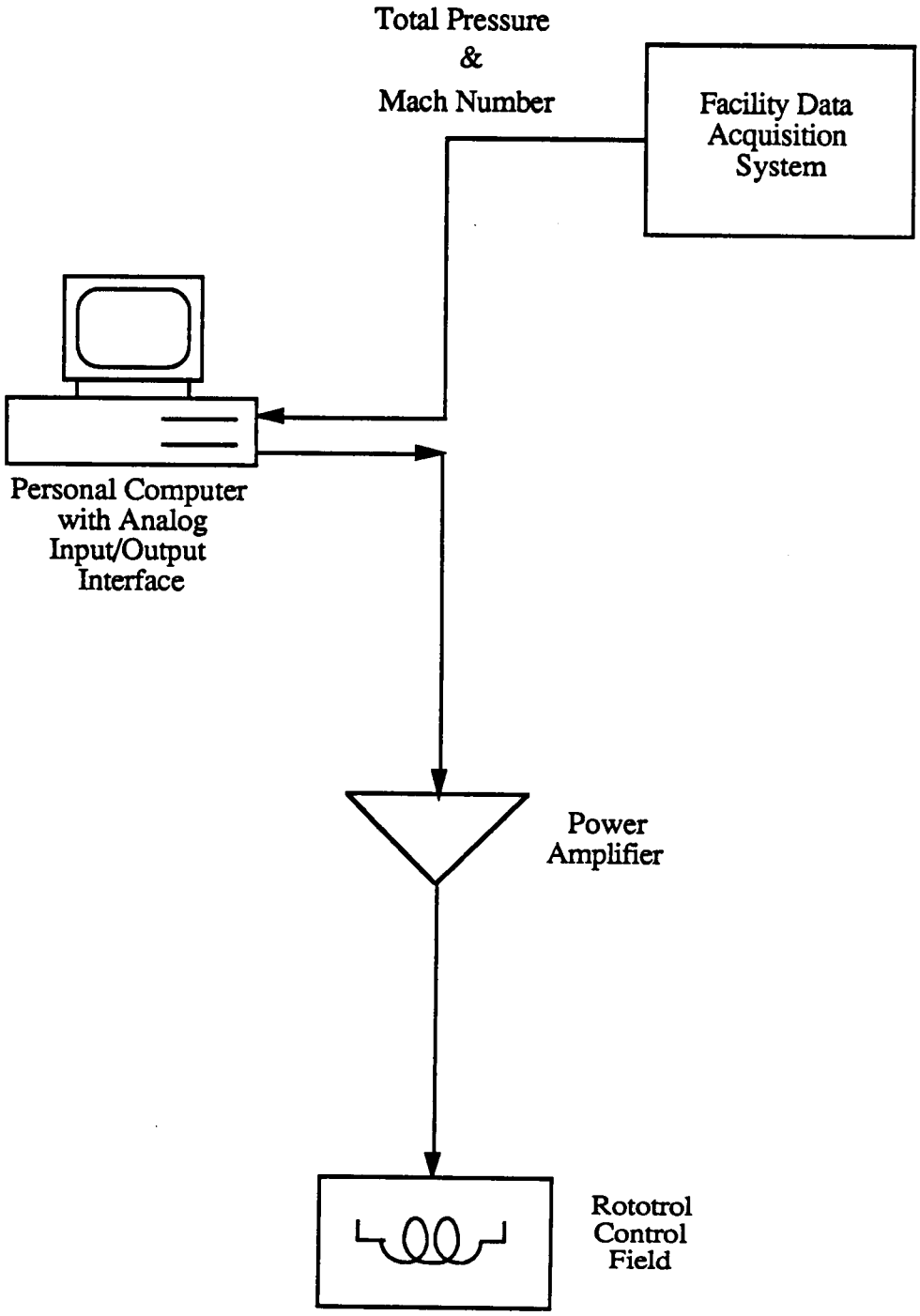



Figure 5-1. Control System Implementation.

# BIBLIOGRAPHY

# BIBLIOGRAPHY


Del Toro, Vincent. " Electrical Engineering Fundamentals." Englewood Cliffs, NJ: Prentice-Hall Inc., 1972.

Estabrooks, B. B. , and J. R. Milillo. "Aerodynamic Performance of the AEDC-PWT Transonic Circuit Compressor." Arnold Engineering Development Center TR-57-15, Arnold Air Force Station, TN, October 1957.

Heumann, Gerhart W. "Magnetic Control of Industrial Motors." New York: John Wiley & Sons, Inc., 1947.

Kuo, Benjamin C. "Automatic Control Systems." Fifth Edition. Englewood Cliffs NJ: Prentice-Hall Inc., 1987.

Mitchell and Gauthier Associates, "Advanced Continuous Simulation Language." Concord, MA, 1987.

Meriam, J. L., "Engineering Mechanics, Volume 2, Dynamics." New York: John Wiley and Sons, Inc., 1978.

Nesbitt, M. H. "Subsynchronous Operation of PWT Tunnel 16T with the Rerated Main Drive Induction Motor M3." Arnold Engineering Development Center TMR-79-P28, Arnold Air Force Station, TN, September 1979.

Ogata, Katsuhiko. "Modern Control Engineering." Englewood Cliffs, NJ: Prentice-Hall, Inc., 1970.

Parli, C. L. "Aerodynamic Calibration of the AEDC 16-ft Transonic Tunnel Compressor with Fiberglass Rotor Blades." Arnold Engineering Development Center TR-65-242, Arnold Air Force Station, TN, November 1965.

Phillips, Charles L. and H. Troy Nagle, Jr. " Digital Control System Analysis and Design." Englewood Cliffs, NJ: Prentice-Hall, Inc., 1984.

Pindzola, M. "Supersonic Wind Tunnel Design and Performance Equations, Tables and Charts." Arnold Engineering Development Center TM-58-3, Arnold Air Force Station, TN, January 1958.

Stich, Philip B. "Mathematical Modeling of the AEDC-PWT 16-ft Transonic Wind Tunnel." M.S. Thesis, University of Tennessee, Knoxville, TN, March 1984.

Summers, Wilford I. , ed. "American Electricians' Handbook." Tenth Edition. New York: McGraw Hill, Inc. , 1981.

Westinghouse. "Main Drive Operators Manual.", Arnold Engineering Development Center, Arnold Air Force Station, TN, 1952.

# APPENDIXES

# APPENDIX A

# DERIVATION OF INDUCTION

# MOTOR TIME CONSTANT

To determine if the time constant of the induction motor is significant, the following derivation is necessary. A differential equation relating the induction motor stator voltage to the rotor current can be obtained by summing the voltages around the circuit shown in Figure 2-7 (p. 22)

$$\overline{V}_1 = \left( r_1 + \frac{r_2' + R'}{slip} \right) \overline{I}_r + (L_1 + L_2') \frac{d\overline{I}_r}{dt}. \qquad \text{(A-1)}$$

Taking the Laplace transform of Eq. (A-1) gives

$$\overline{V}_1(s) = \overline{I}_r(s) \left[ s(L_1 + L_2') + \left( r_1 + \frac{r_2' + R'}{slip} \right) \right]. \qquad \text{(A-2)}$$

Solving for $\overline{I}_r(s)$ yields

$$\overline{I}_r(s) = \frac{\overline{V}_1(s)}{\left[ (L_1 + L_2')s + \left( r_1 + \frac{r_2' + R'}{slip} \right) \right]}. \qquad \text{(A-3)}$$

The inductance, L, is related to the reactance, X, by

$$L = \frac{X}{\omega}, \qquad \text{(A-4)}$$

where $\omega$ is the frequency of the rotor current, 60 Hz. Using the reactances from Table 2-2 (p. 25), the inductances are

$$L_1 = \frac{0.1351\ \Omega}{377\ \frac{\text{rad}}{\text{sec}}} \times \frac{\text{H}}{\Omega\ \text{sec}} = 3.584 \times 10^{-4}\ \text{H} \qquad \text{(A-5)}$$

$$L_2' = \frac{0.1506\ \Omega}{377\ \frac{\text{rad}}{\text{sec}}} \times \frac{\text{H}}{\Omega\ \text{sec}} = 3.995 \times 10^{-4}\ \text{H}. \qquad \text{(A-6)}$$

The resistance of the liquid rheostat is obtained by combining Eqs. (2-21) and (2-27). This yields

$$R' = \frac{\alpha^2 r_e y}{.85 A_e}. \qquad \text{(A-7)}$$

The maximum liquid rheostat resistance occurs when the liquid rheostat electrodes are the maximum distance apart, 78 inches. Using the values for $r_e$ and $A_e$ from Table 2-1 (p. 16) the maximum liquid rheostat resistance is

$$R'_{max} = \frac{(1.75)^2 \times 8.5\ \Omega\text{-in} \times 78.0\ \text{in}}{0.85 \times 1017.5\ \text{in}^2} = 2.348\ \Omega. \qquad \text{(A-8)}$$

The minimum resistance occurs when the electrodes are the minimum distance apart, 0.375 in. The minimum liquid rheostat resistance is

$$R'_{min} = \frac{(1.75)^2 \times 8.5\ \Omega\text{-in} \times 0.375\ \text{in}}{0.85 \times 1017.5\ \text{in}^2} = 0.0113\ \Omega. \qquad \text{(A-9)}$$

The combined resistance terms in equation (A-3) is a maximum when the slip is a minimum and the liquid rheostat resistance is a maximum. The minimum slip occurs at the maximum shaft speed which for subsynchronous operation is 500 rpm. This gives a minimum slip of

$$\text{slip}_{min} = \frac{720 \text{ rpm} - 500 \text{ rpm}}{720 \text{ rpm}} = 0.3056. \qquad \text{(A-10)}$$

The maximum combined resistance is

$$\left(r_1 + \frac{r_2' + R'_{max}}{\text{slip}_{min}}\right)_{max} = 0.00731\ \Omega + \frac{2.348\ \Omega + 0.26\ \Omega}{0.3056}$$

$$= 8.54\ \Omega. \qquad \text{(A-11)}$$

The minimum combined resistance in (A-3) occurs when the slip is a maximum and the liquid rheostat resistance is a minimum. The maximum slip occurs at the minimum shaft speed which is approximately 225 rpm. This gives a maximum slip of

$$\text{slip}_{max} = \frac{720 \text{ rpm} - 225 \text{ rpm}}{720 \text{ rpm}} = 0.6875. \qquad \text{(A-12)}$$

The minimum combined resistance is

$$\left(r_1 + \frac{r_2' + R'_{min}}{\text{slip}_{max}}\right)_{min} = 0.00731\ \Omega + \frac{0.0113\ \Omega + 0.26\ \Omega}{0.6875}$$

$$= 0.402\ \Omega. \qquad \text{(A-13)}$$

The time constant of the motor is from Eq. (A-3),

$$\tau = \frac{(L_1 + L_2')}{\left(r_1 + \frac{r_2' + R'}{slip}\right)}. \qquad \text{(A-14)}$$

The minimum time constant is

$$\tau_{min} = \frac{(L_1 + L_2')}{\left(r_1 + \frac{r_2' + R'_{max}}{slip_{min}}\right)_{max}} = \frac{(3.584x10^{-4} + 3.995x10^{-4})H}{2.348\ \Omega} x \frac{\Omega\ sec}{H}$$

$$= 3.228x10^{-4}\ sec. \qquad \text{(A-15)}$$

The maximum time constant is

$$\tau_{max} = \frac{(L_1 + L_2')}{\left(r_1 + \frac{r_2' + R'_{min}}{slip_{max}}\right)_{min}} = \frac{(3.584x10^{-4} + 3.995x10^{-4})H}{0.402\ \Omega} x \frac{\Omega\ sec}{H}$$

$$= 1.885x10^{-3}\ sec. \qquad \text{(A-16)}$$

The maximum induction motor time constant is much less than the time constants of the liquid rheostat positioning system and the time constant associated with accelerating the compressor and therefore may be neglected without effecting the performance of the model.

# APPENDIX B

# EFFECTS OF THE MASS

# OF THE AIR IN THE TUNNEL CIRCUIT

To determine if the time constant associated with accelerating the air in the 16T tunnel circuit is significant, the effects of changes in compressor shaft speed on the Mach number must be investigated.

The difference in pressure across the compressor is the pressure rise necessary to overcome the tunnel losses, $\Delta p_L$, and that necessary to accelerate the air in the tunnel circuit, $\Delta p_A$,

$$p_o - p_i = \Delta p_L + \Delta p_A, \tag{B-1}$$

where

$$p_o - p_i = \left[\frac{p_o}{p_i} - 1\right] p_i . \tag{B-2}$$

The ratio of the compressor outlet pressure, $p_o$ , to the compressor inlet pressure, $p_i$ , is the compressor pressure ratio [Pindzola, p.3],

$$\lambda_c = \frac{p_o}{p_i}. \tag{B-3}$$

During transient or steady state conditions, $\lambda_c$ is a function of the compressor shaft speed, $\lambda_c = \lambda_c(\text{rpm})$. Equation (B-2) then becomes

$$p_o - p_i = ( \lambda_c(\text{rpm}) - 1 ) p_i. \tag{B-4}$$

During steady state conditions $\lambda_c = \lambda_{ss}(M)$ and Eq. (B-2) becomes

$$p_o - p_i = \Delta p_L = ( \lambda_{ss}(M) - 1 ) p_i. \quad \text{(B-5)}$$

During transient conditions the mass flow in the tunnel is a function of time as given by

$$\frac{dm}{dt} = \frac{dm(t)}{dt} = \dot{m}\,(t), \quad \text{(B-6)}$$

or in terms of tunnel cross sectional area, A, density, $\rho$, and velocity, $\frac{dx}{dt}$,

$$\frac{dm}{dt} = \rho\, A \frac{dx}{dt}. \quad \text{(B-7)}$$

The area of the tunnel , A, is dependent on the location in the tunnel,

$$A = A(x). \quad \text{(B-8)}$$

The force required to accelerate the air is [Meriam, p. 6]

$$F = ma, \quad \text{(B-9)}$$

or

$$F = m \frac{dv}{dt}. \quad \text{(B-10)}$$

The difference in force across a small section of tunnel, dx, is

$$dF = dm \frac{dv}{dt}, \tag{B-11}$$

where dm is

$$dm = \rho\, A(x)dx\,. \tag{B-12}$$

Combining Eqs. (B-11) and (B-12) gives

$$dF = \rho\, A(x)dx\, \frac{dv}{dt}. \tag{B-13}$$

The change in force can also be expressed as

$$dF = A(x)dp_A. \tag{B-14}$$

Substituting this expression for dF in Eq. (B-13) yields

$$A(x)dp_A = \rho\, A(x)dx\, \frac{dv}{dt}. \tag{B-15}$$

Simplifying Eq. (B-15) gives

$$dp_A = \rho\, dx \frac{dv}{dt}. \tag{B-16}$$

The air velocity, v, is a function of position and time,

$$v = v(x,t) = \frac{dx}{dt}. \tag{B-17}$$

Combining Eqs. (B-16) and (B-17) gives

$$dp_A = \rho\, dx \frac{\delta v(x,t)}{\delta t}. \qquad \text{(B-18)}$$

Integrating Eq. (B-18) over the length of the tunnel gives

$$\Delta p_A = \int_o^L \rho \frac{\delta v(x,t)}{\delta t} dx \ . \qquad \text{(B-19)}$$

The air velocity, v(x,t), is obtained by combining Eqs. (B-7) and (B-17),

$$v(x,t) = \frac{dm}{dt} \frac{1}{\rho\, A(x)}. \qquad \text{(B-20)}$$

Combining Eqs. (B-19) and (B-20) yields

$$\Delta p_A = \int_o^L \rho \frac{d}{dt} \left[ \frac{dm}{dt} \frac{1}{\rho\, A(x)} \right] dx\,, \qquad \text{(B-21)}$$

which reduces to

$$\Delta p_A = \int_o^L \frac{dx}{A(x)} \frac{d}{dt} \left( \frac{dm}{dt} \right), \qquad \text{(B-22)}$$

or

$$\Delta p_A = S \frac{d}{dt}\left(\frac{dm}{dt}\right), \tag{B-23}$$

where

$$S = \int_0^L \frac{dx}{A(x)} . \tag{B-24}$$

Using the dimensions for the tunnel given in Figure B-1 and integrating around the tunnel circuit,

$$S = \int_0^L \frac{dx}{A(x)} = 1.513 . \tag{B-25}$$

Substituting Eqs. (B-4), (B-5), and (B-23) into Eq. (B-1) gives

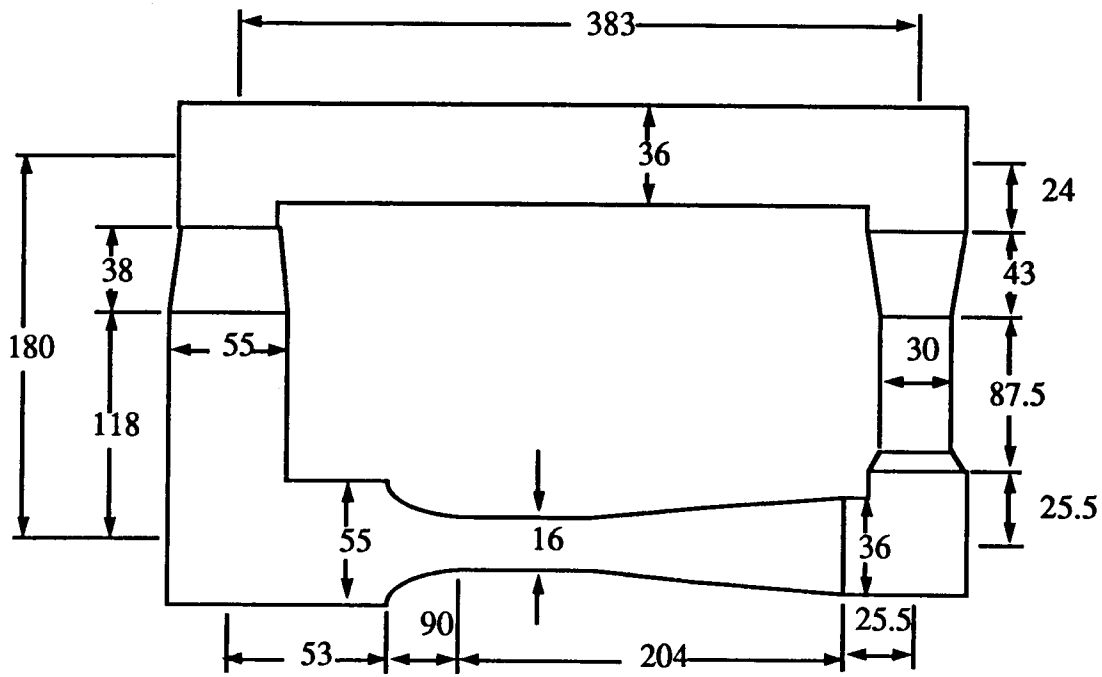
$$[\lambda_c(rpm) - 1]\, p_i = [\lambda_{ss}(M) - 1]\, p_i + S \frac{d}{dt}\left[\frac{dm}{dt}\right], \tag{B-26}$$

or

$$\lambda_c(rpm) = \lambda_{ss}(M) + \frac{S}{p_i} \frac{d}{dt}\left[\frac{dm}{dt}\right] . \tag{B-27}$$

The velocity of the air in the tunnel circuit can be expressed as a function of the Mach number and the speed of sound, c, as [Pindzola, p.10]

$$v = cM, \tag{B-28}$$




All dimensions in feet

Figure B-1. 16T Wind Tunnel Dimensions

where

$$c = \sqrt{\gamma R T_T}\,. \tag{B-29}$$

The density of the air in the tunnel, $\rho$, is related to the static pressure, $P_T$, and static temperature, $T_T$, as

$$\rho = \frac{P_T}{RT_T}\,. \tag{B-30}$$

Combining Eqs. (B-7), (B-28), (B-29), and (B-30) the mass flow can be expressed as

$$\dot{m} = P_T A_T M \sqrt{\frac{\gamma}{RT_T}}\,. \tag{B-31}$$

The static temperature is related to the total temperature by [Pindzola, p.10]

$$T_T = \frac{TT_T}{1 + \frac{\gamma - 1}{2} M^2} \tag{B-32}$$

and the static pressure is related to the total pressure by [Pindzola, p.10]

$$P_T = \frac{PT_T}{\left[1 + \frac{\gamma - 1}{2} M^2\right]^{\frac{\gamma}{\gamma - 1}}}\,. \tag{B-33}$$

Combining Eqs. (B-31) through (B-33) the mass flow is

$$\dot{m} = \frac{PT_T A_T}{\sqrt{RTT_T}} \sqrt{\gamma} M \left[ 1 + \frac{\gamma - 1}{2} M^2 \right]^{\frac{1}{2} - \frac{\gamma}{\gamma - 1}}, \tag{B-34}$$

or

$$\dot{m} = \frac{PT_T A_T}{\sqrt{RTT_T}} f(M), \tag{B-35}$$

where

$$f(M) = \sqrt{\gamma} M \left[ 1 + \frac{\gamma - 1}{2} M^2 \right]^{\frac{1}{2} - \frac{\gamma}{\gamma - 1}}. \tag{B-36}$$

Inserting the expression for mass flow from Eq. (B-35) into Eq. (B-27) yields

$$\lambda_c(\text{rpm}) = \lambda_{ss}(M) + \lambda_T(M)\, S \frac{A_T}{\sqrt{RTT_T}} \frac{d}{dt} f(M), \tag{B-37}$$

where $\lambda_T(M)$ is the tunnel pressure ratio defined as

$$\lambda_T(M) = \frac{p_T}{p_i}. \tag{B-38}$$

Taking the derivative of Eq. (B-36) and substituting the specific heat ratio for air, $\gamma = 1.4$, gives

$$\frac{d}{dt} f(M) = 1.183 \frac{dM}{dt} \frac{(1 - M^2)}{(1 + 0.2M^2)^4} \tag{B-39}$$

Combining Eqs. (B-37) and (B-39) gives a first order differential equation as a function of Mach number,

$$\lambda_c(\text{rpm}) = \lambda_{ss}(M) + \lambda_T(M)\frac{1.183SA_T}{\sqrt{RTT_T}}\frac{(1 - M^2)}{(1 + 0.2M^2)^4}\frac{dM}{dt}. \qquad \text{(B-40)}$$

Figures B-2, B-3, and B-4 show $\lambda_c(\text{rpm})$, $\lambda_{ss}(M)$, and $\lambda_T(M)$ respectively plotted from data obtained from an evaluation test on the subsynchronous operation of Main Drive [Nesbitt, p. 17]. A second order curve fit of Figures B-2, B-3, and B-4 gives

$$\lambda_c(\text{rpm}) = 1.0 - 1.37\text{x}10^{-4}\text{rpm} + 8.39\text{x}10^{-7}\text{rpm}^2, \qquad \text{(B-41)}$$

$$\lambda_{ss}(M) = 1.0 + 0.047M + 0.3M^2, \qquad \text{(B-42)}$$

and

$$\lambda_T(M) = 1.0 + 0.03M + 0.27M^2. \qquad \text{(B-43)}$$

Using an ACSL simulation program, Eqs. (B-40) through (B-43) were utilized to determine the effect of a 10 percent change in the compressor shaft speed on the test section Mach number. This was done for Mach number operating points of 0.2, 0.3, 0.4, 0.5, and 0.6. The results of the simulation are shown in Figures B-5 through B-9. The time constant related to accelerating the air in the tunnel depends on the operating point. As the Mach number operating point increases, the time required for the Mach number to settle in response to the change in shaft speed decreases.

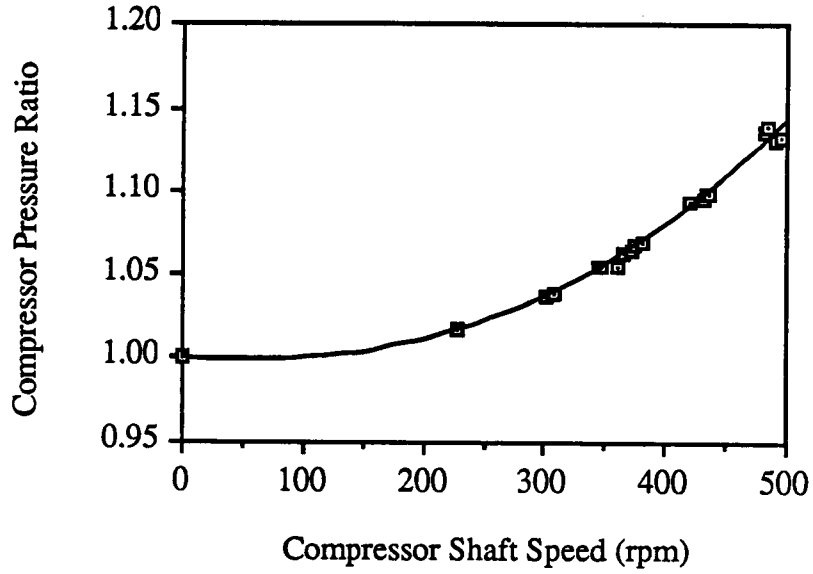



Figure B-2. Compressor Pressure Ratio $\lambda_c$(rpm) as a Function of Compressor Shaft Speed.

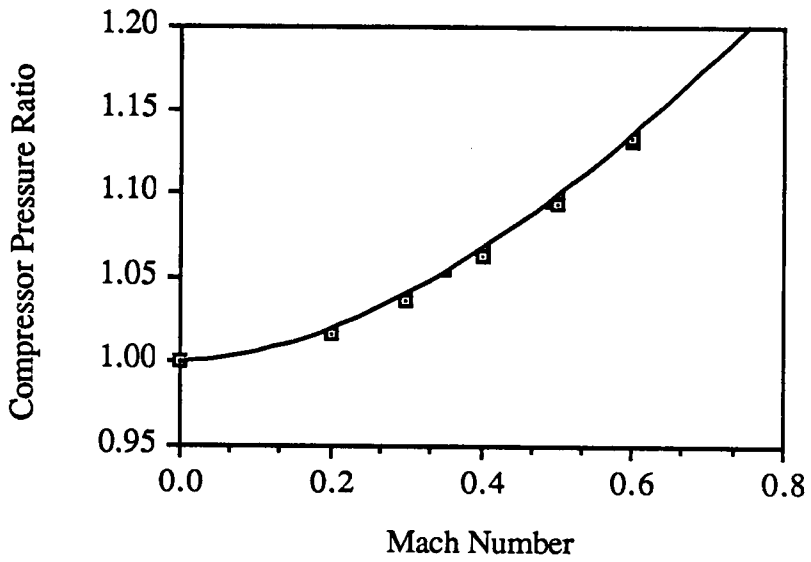



Figure B-3. Steady State Compressor Pressure Ratio $\lambda_{ss}$(M) as a Function of Test Section Mach Number.

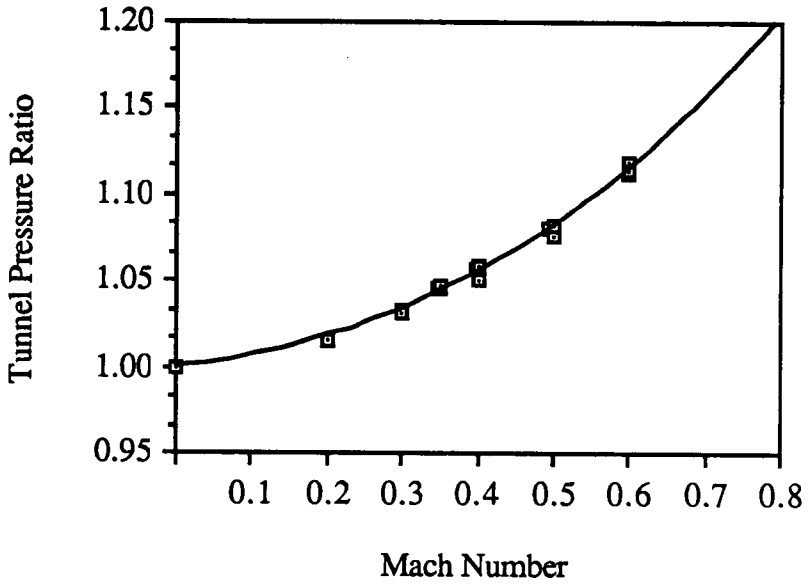



Figure B-4. Tunnel Pressure Ratio $\lambda_T(M)$ as a Function of Test Section Mach Number.

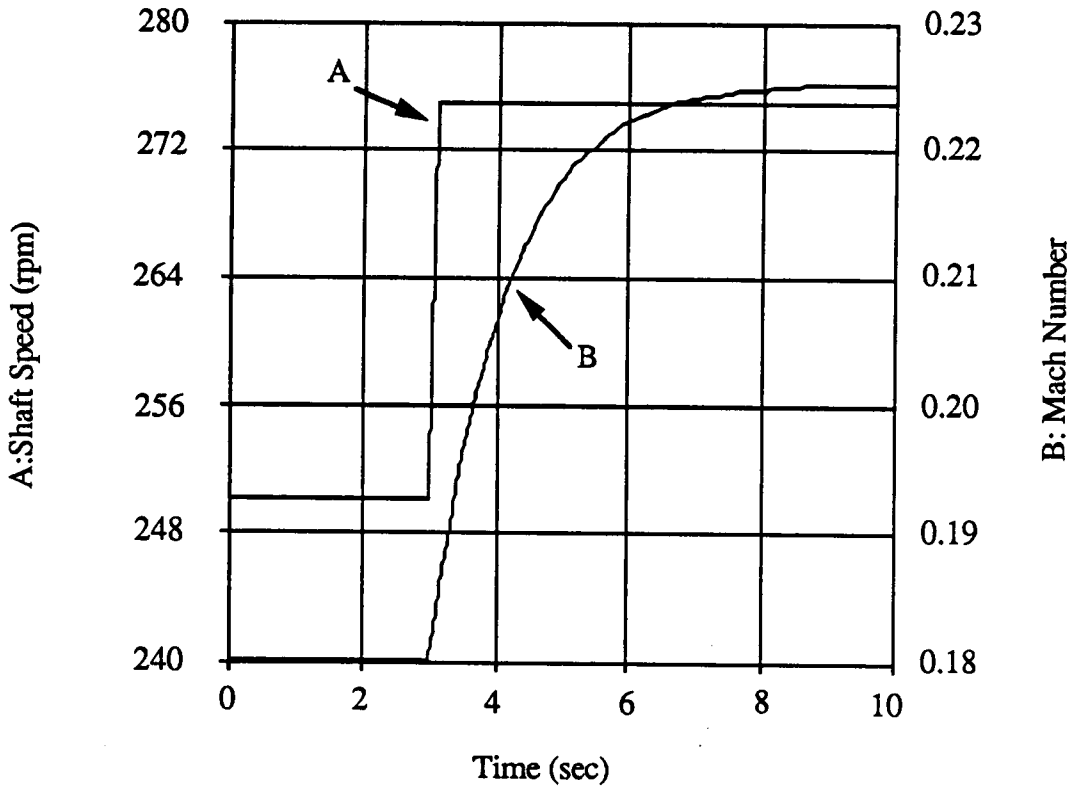



Figure B-5. Effect of a 10 Percent Change in Compressor Shaft Speed for a Mach Number Operating Point of 0.2.

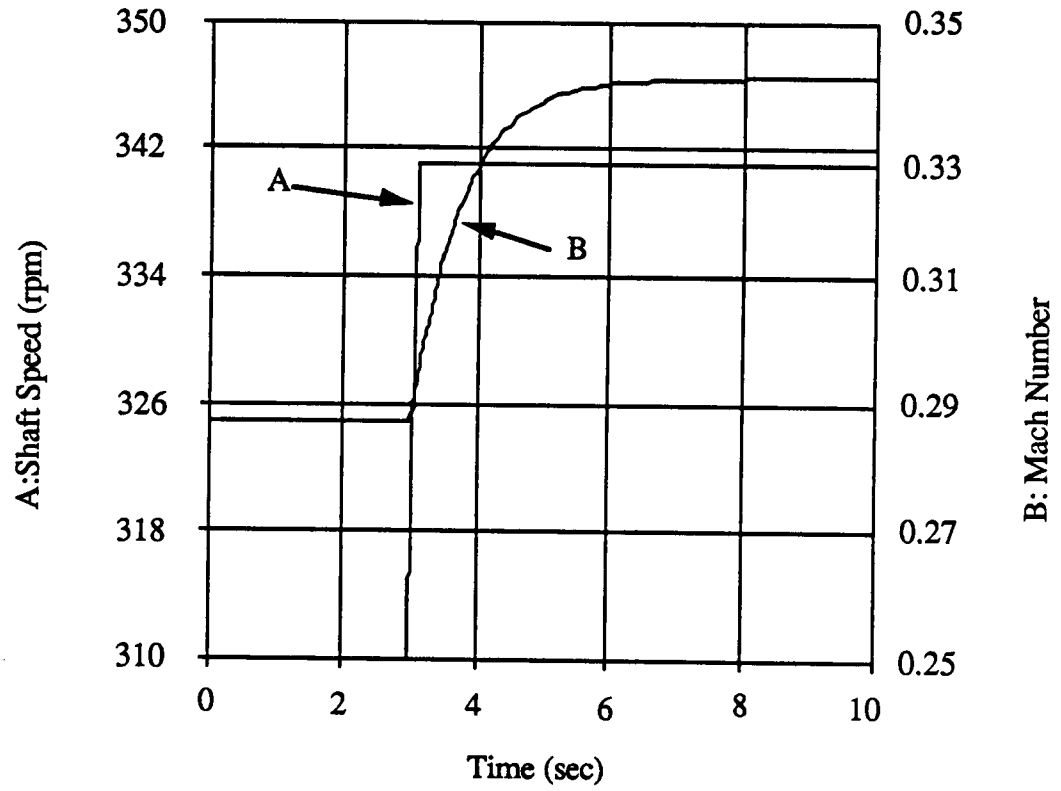



Figure B-6. Effect of a 10 Percent Change in Compressor Shaft Speed for a Mach Number Operating Point of 0.3.

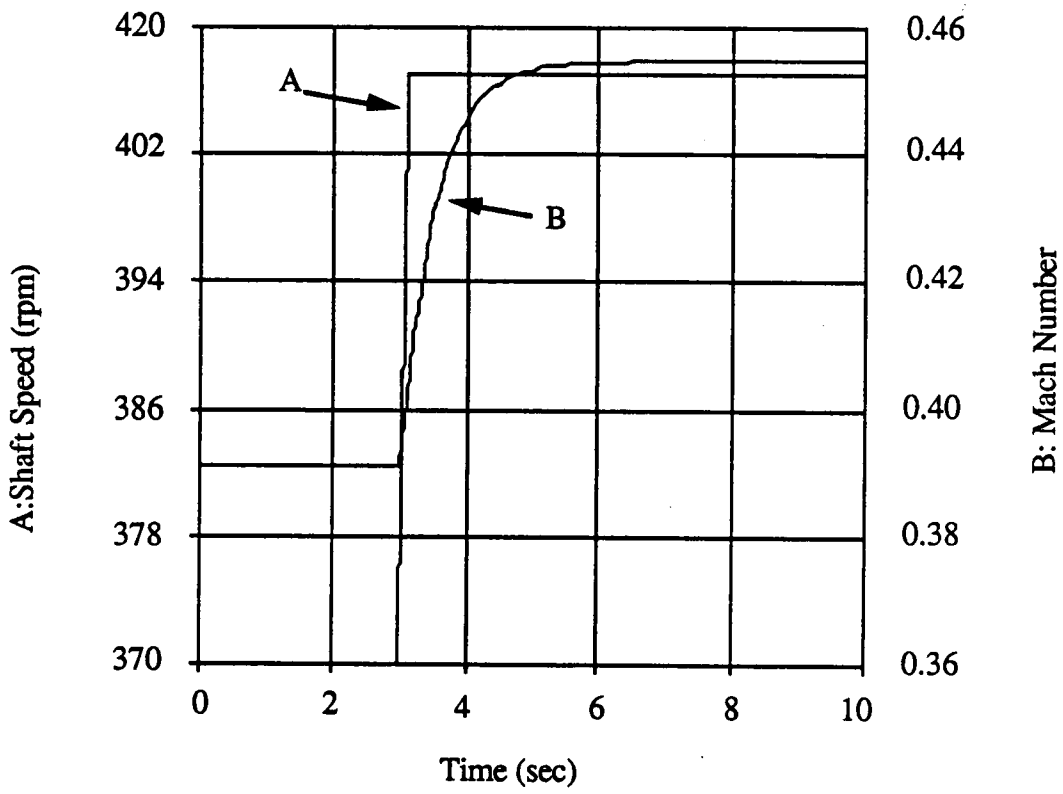



Figure B-7. Effect of a 10 Percent Change in Compressor Shaft Speed for a Mach Number Operating Point of 0.4.

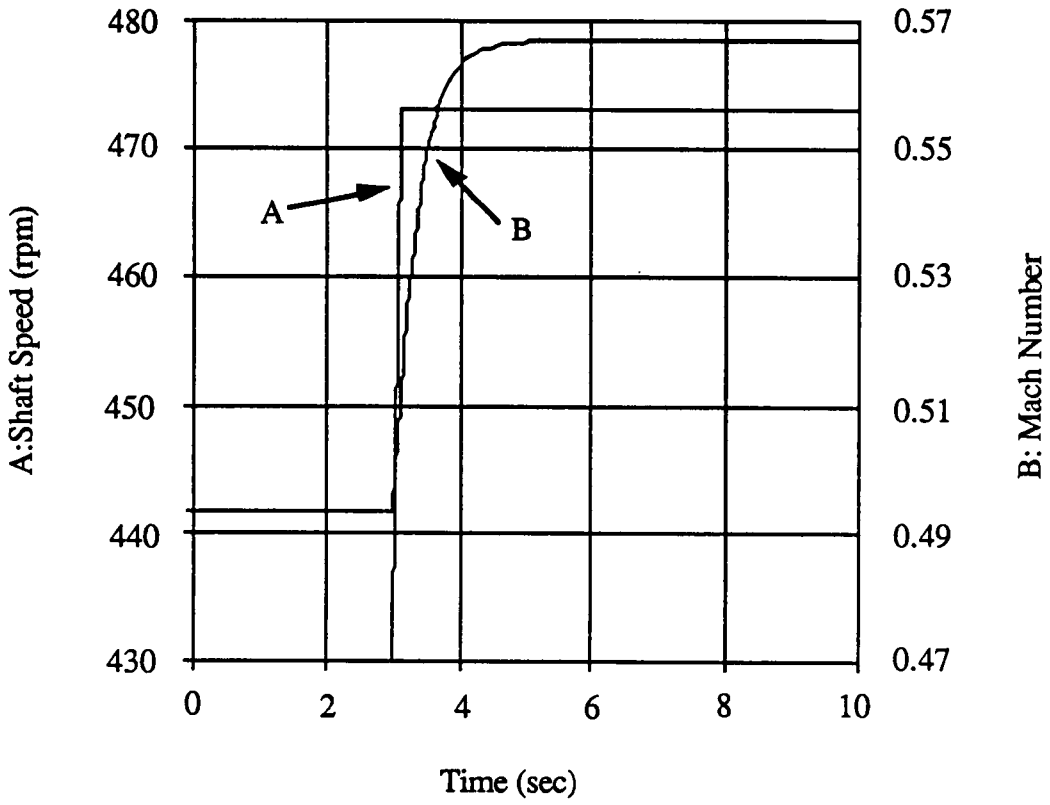



Figure B-8. Effect of a 10 Percent Change in Compressor Shaft Speed for a Mach Number Operating Point of 0.5.

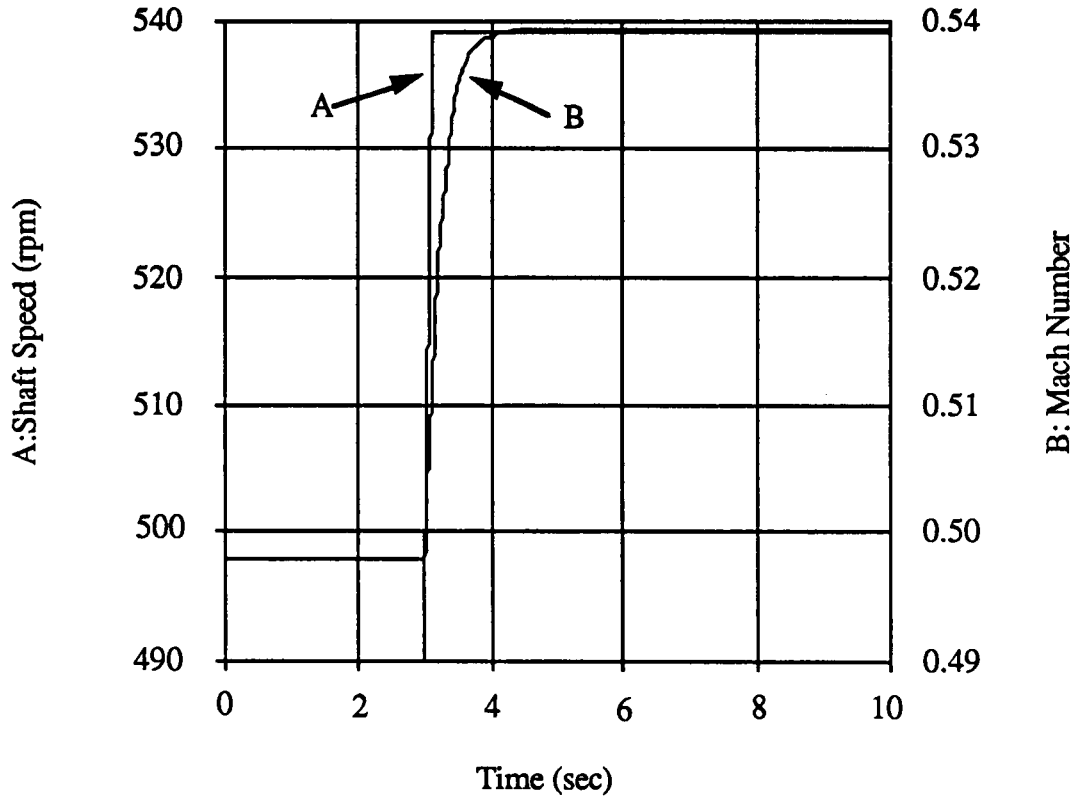



Figure B-9. Effect of a 10 Percent Change in Compressor Shaft Speed for a Mach Number Operating Point of 0.6.

# APPENDIX C

# ADDITIONAL SIMULATION

# RESULTS

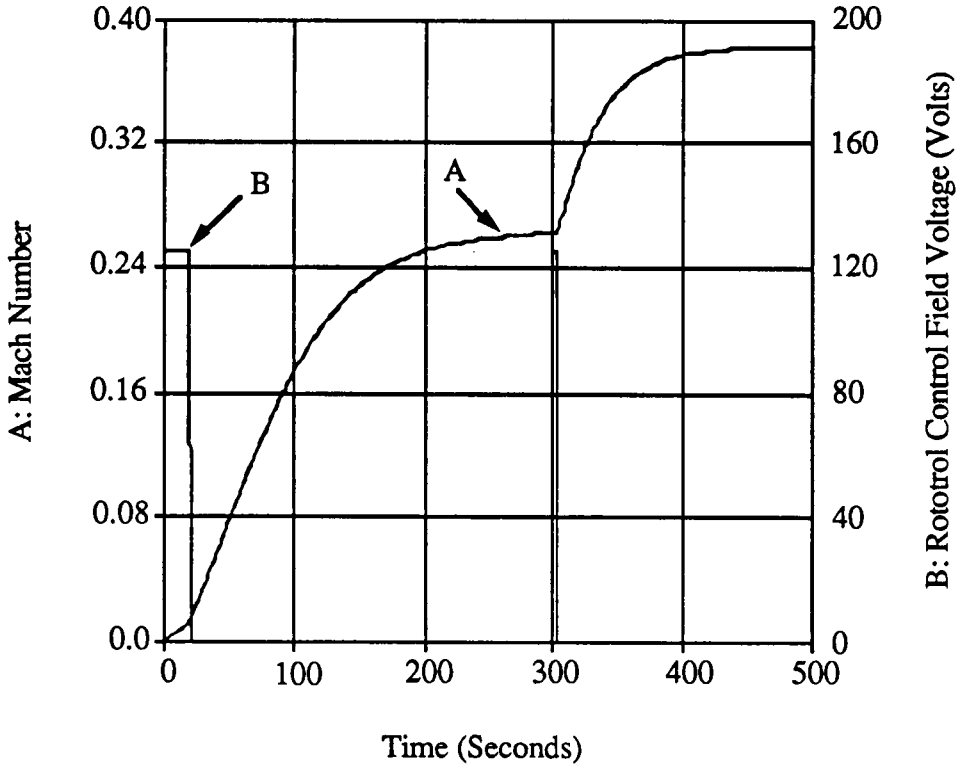



Figure C-1. Open Loop Response to a Step Input for One Motor Operation and $PT_T$=1000 lb/ft$^2$

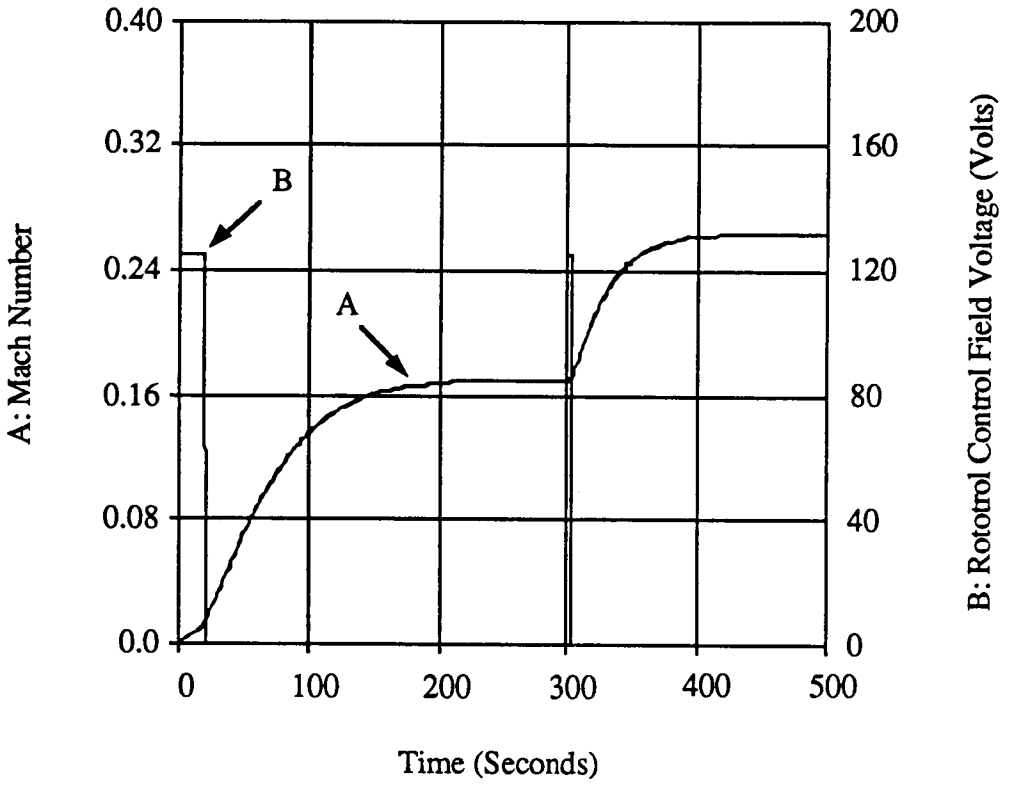



Figure C-2. Open Loop Response to a Step Input for One Motor Operation and $PT_T$=2000 lb/ft$^2$

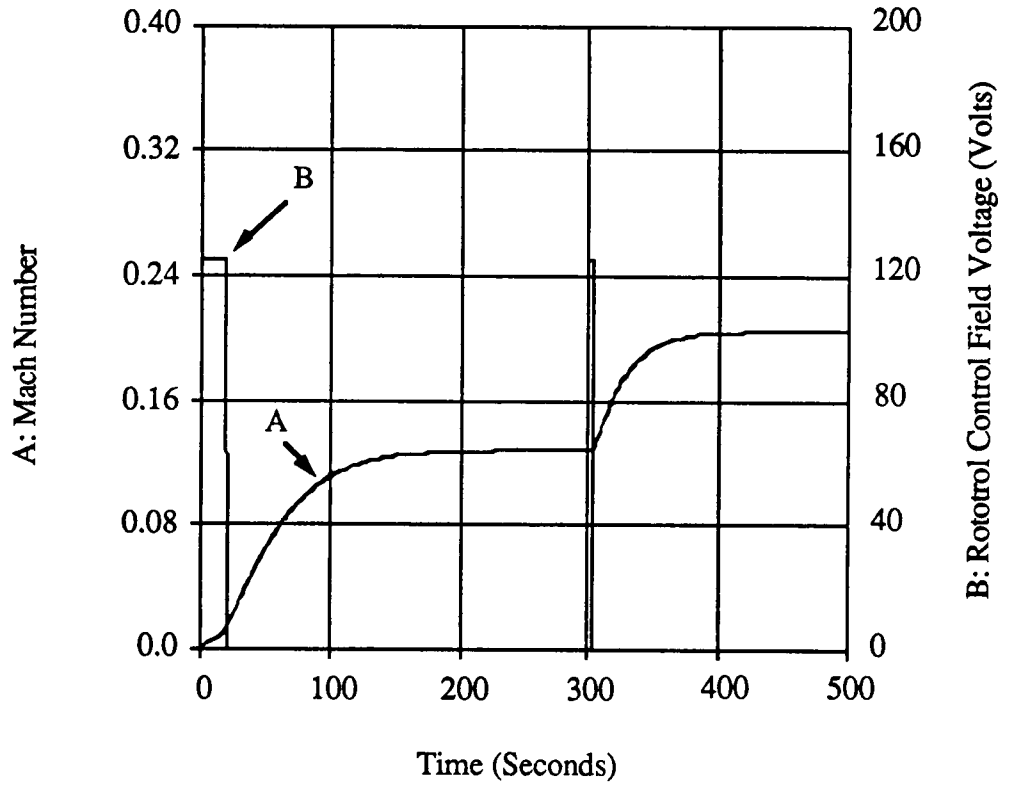



Figure C-3. Open Loop Response to a Step Input for One Motor Operation and $PT_T$=3000 lb/ft$^2$

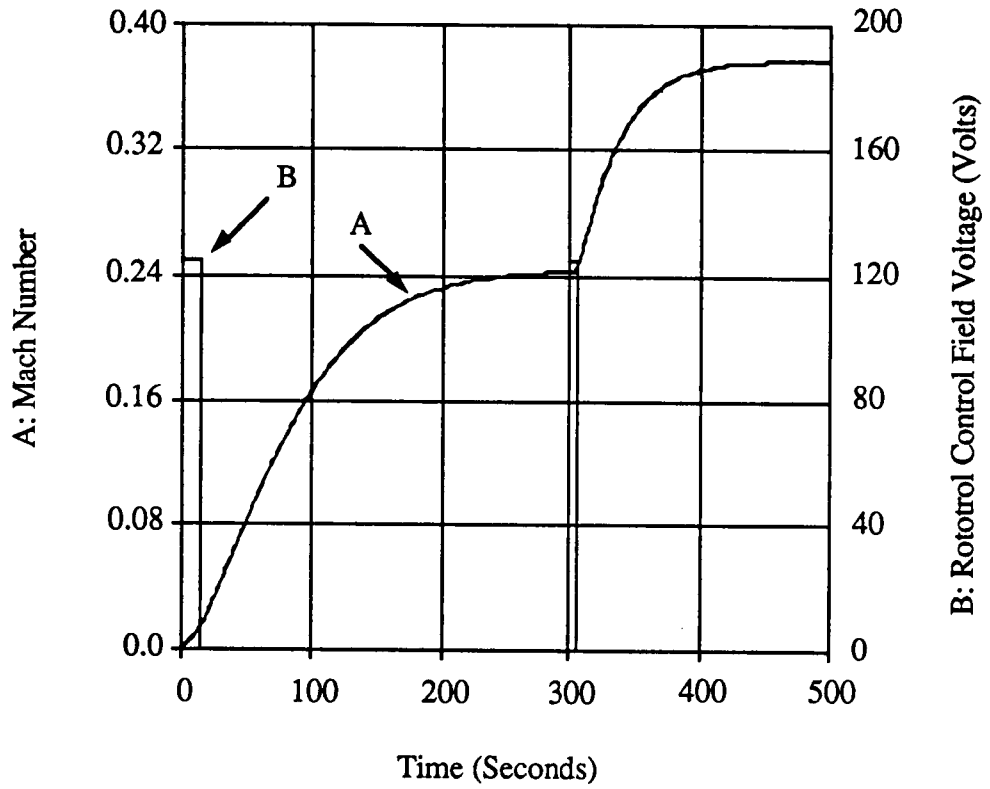



Figure C-4. Open Loop Response to a Step Input for Two Motor Operation and $PT_T$=1000 lb/ft$^2$

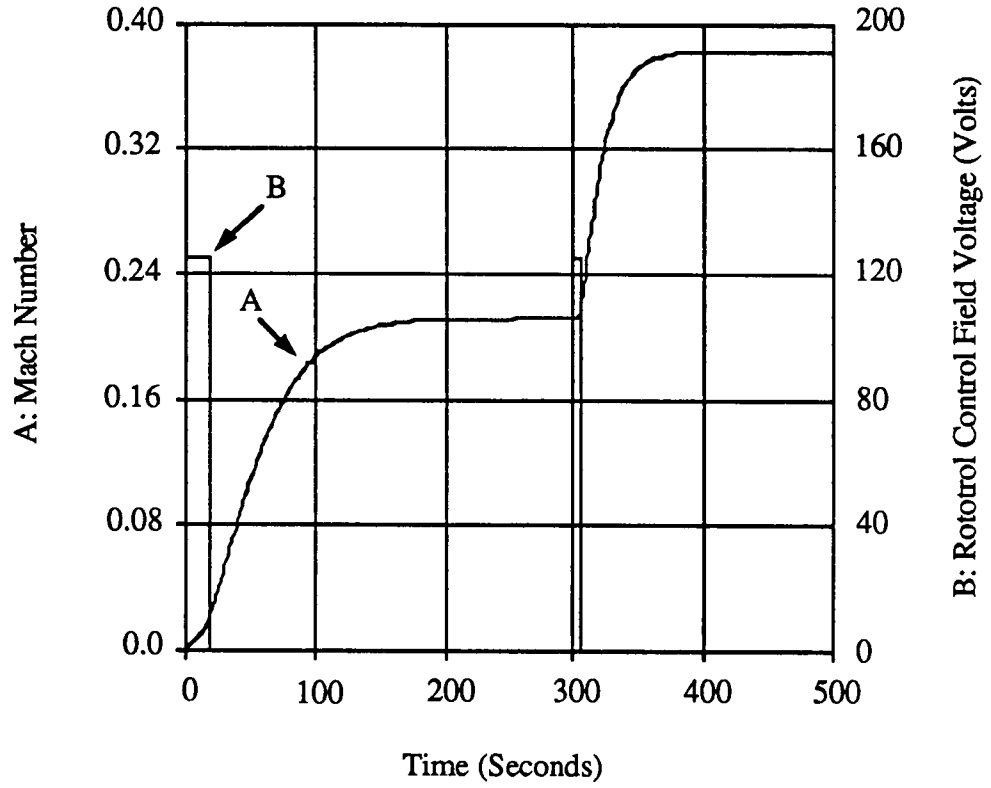



Figure C-5. Open Loop Response to a Step Input for Two Motor Operation and $PT_T$=2000 lb/ft$^2$

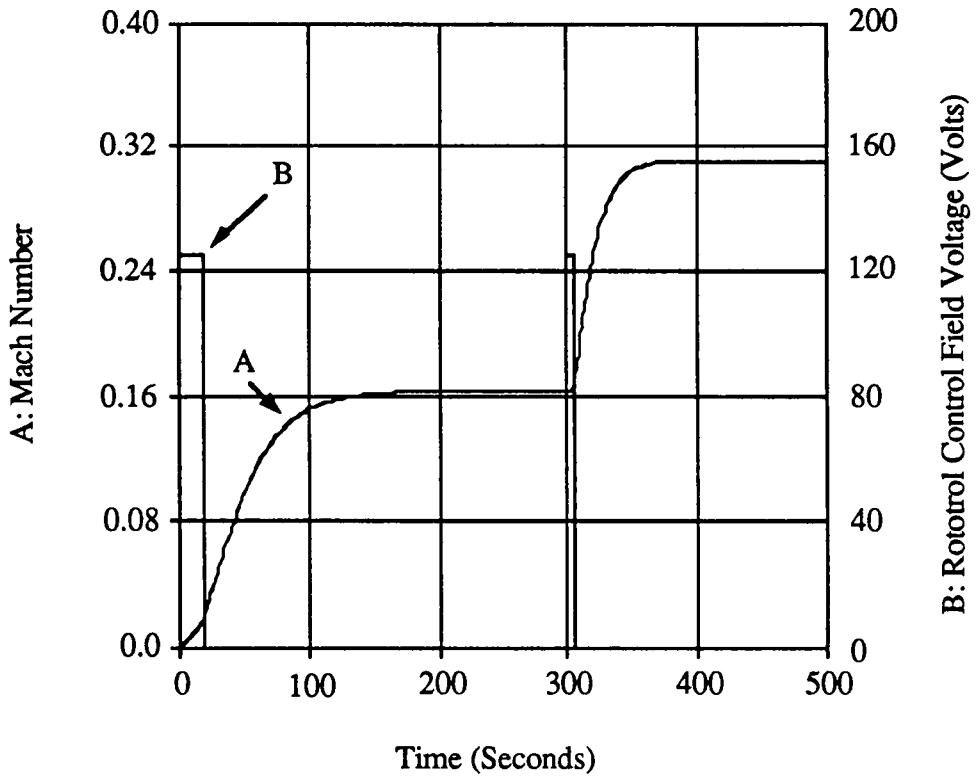



Figure C-6. Open Loop Response to a Step Input for Two Motor Operation and $PT_T$=3000 lb/ft$^2$

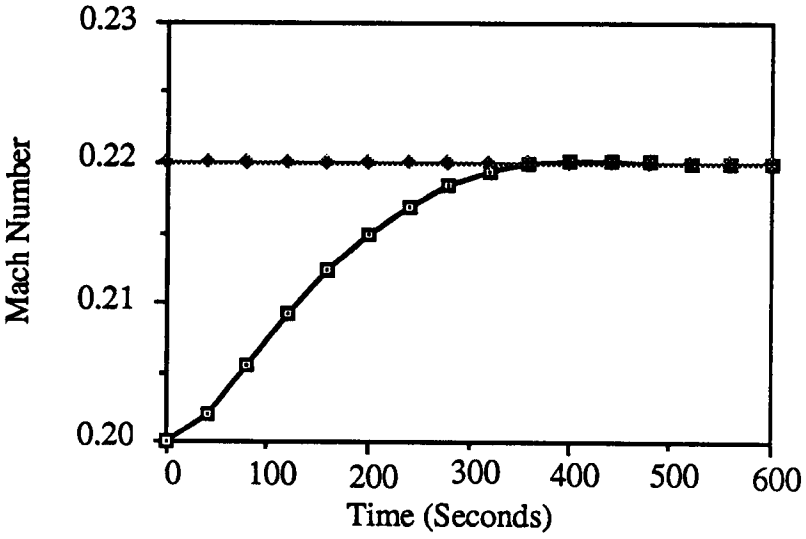



Figure C-7. Simulation Results for a Total Pressure of 2000 lb/ft$^2$ at Mach 0.2 and One Motor Operation.

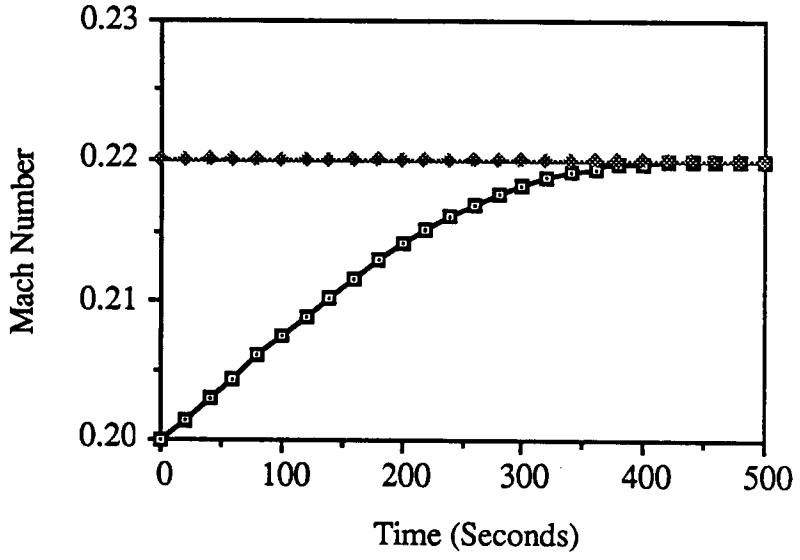



Figure C-8. Simulation Results for a Total Pressure of 1000 lb/ft$^2$ at Mach 0.2 and Two Motor Operation.

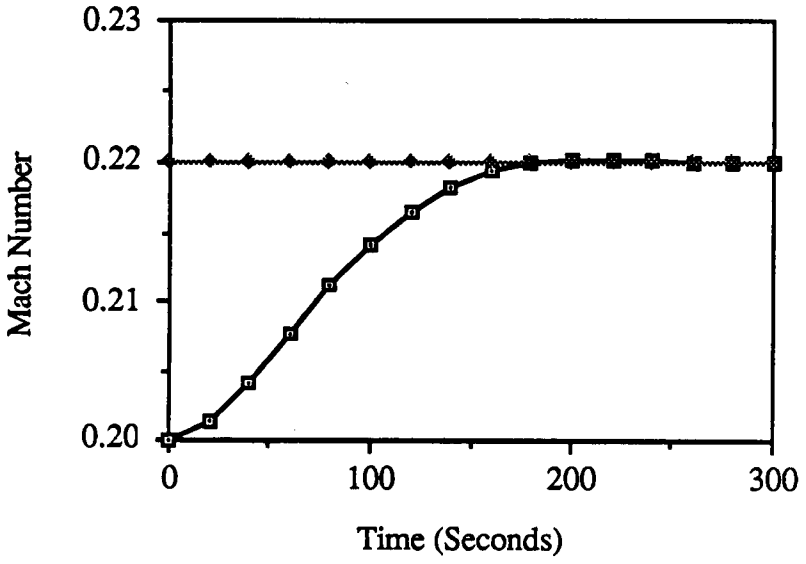



Figure C-9. Simulation Results for a Total Pressure of 2000 lb/ft$^2$ at Mach 0.2 and Two Motor Operation.

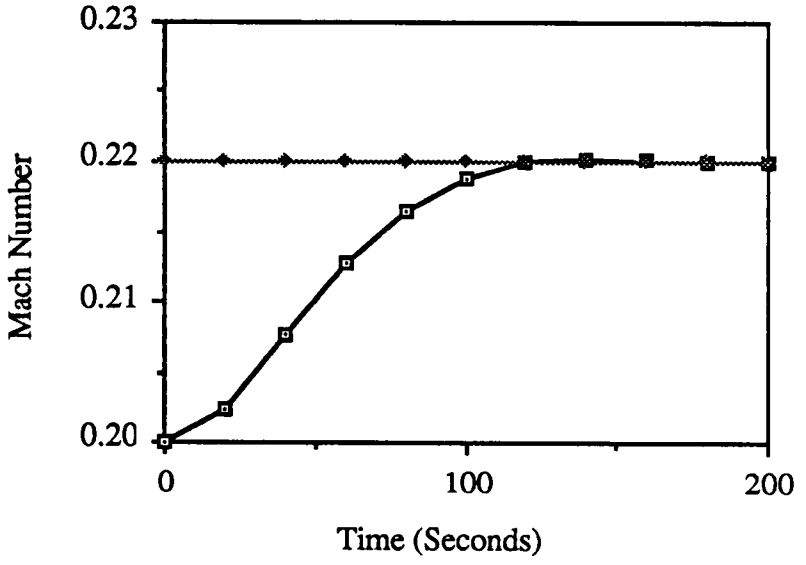



Figure C-10. Simulation Results for a Total Pressure of 3000 lb/ft$^2$ at Mach 0.2 and Two Motor Operation.

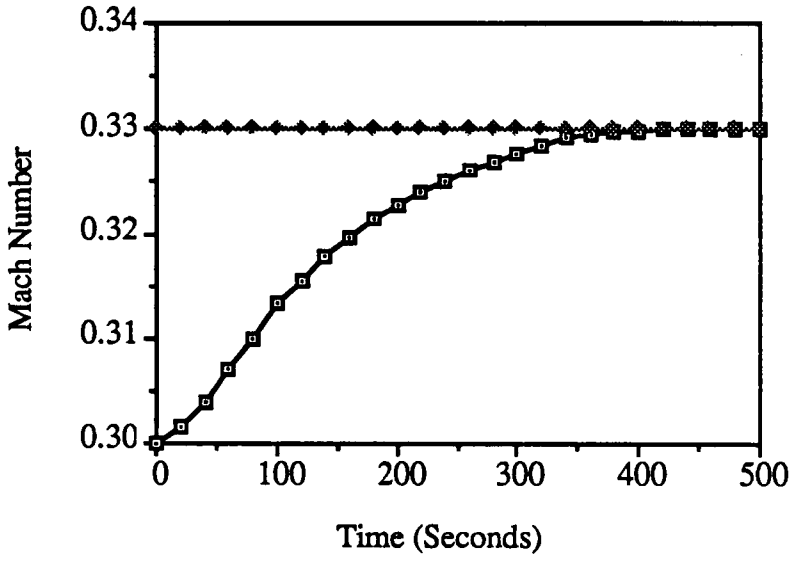



Figure C-11. Simulation Results for a Total Pressure of 1000 lb/ft$^2$ at Mach 0.3 and One Motor Operation.

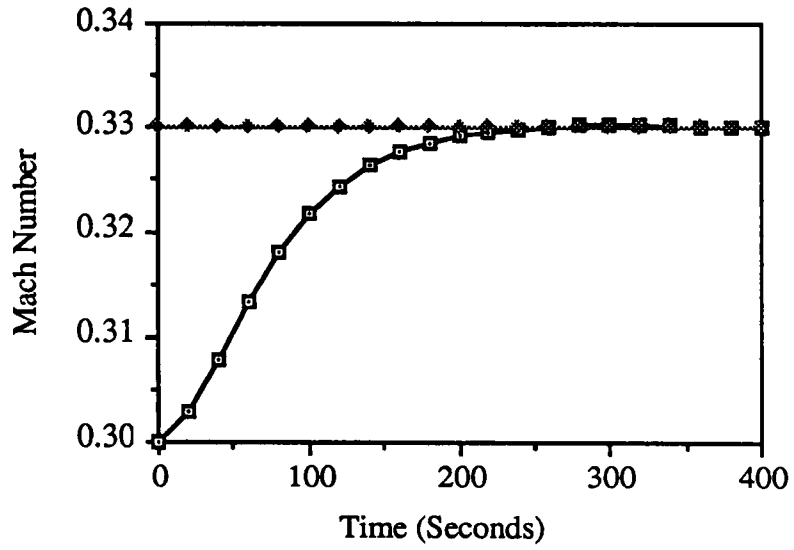



Figure C-12. Simulation Results for a Total Pressure of 2000 lb/ft$^2$ at Mach 0.3 and One Motor Operation.

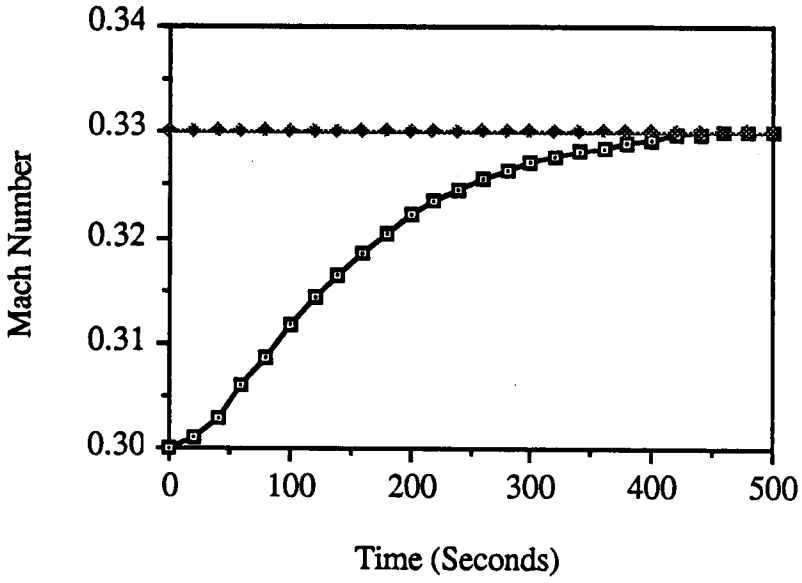



Figure C-13. Simulation Results for a Total Pressure of 1000 lb/ft$^2$ at Mach 0.3 and Two Motor Operation.

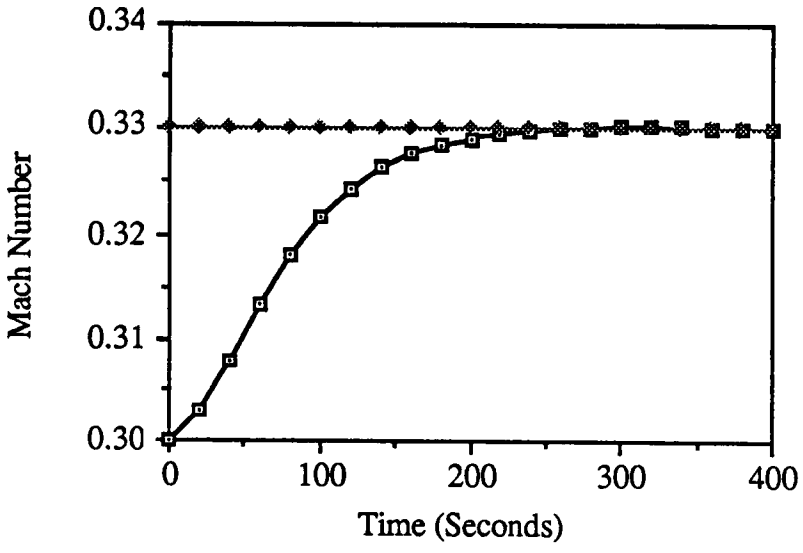



Figure C-14. Simulation Results for a Total Pressure of 2000 lb/ft$^2$ at Mach 0.3 and Two Motor Operation.

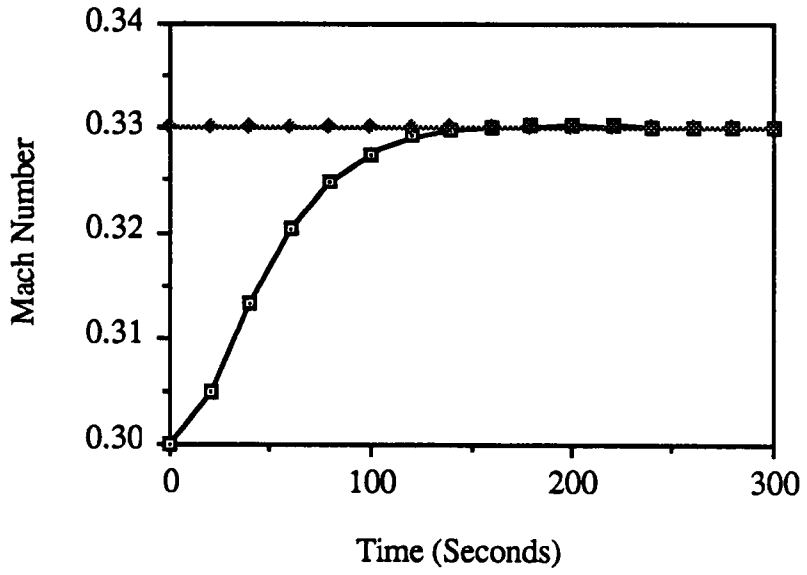



Figure C-15. Simulation Results for a Total Pressure of 3000 lb/ft$^2$ at Mach 0.3 and Two Motor Operation.

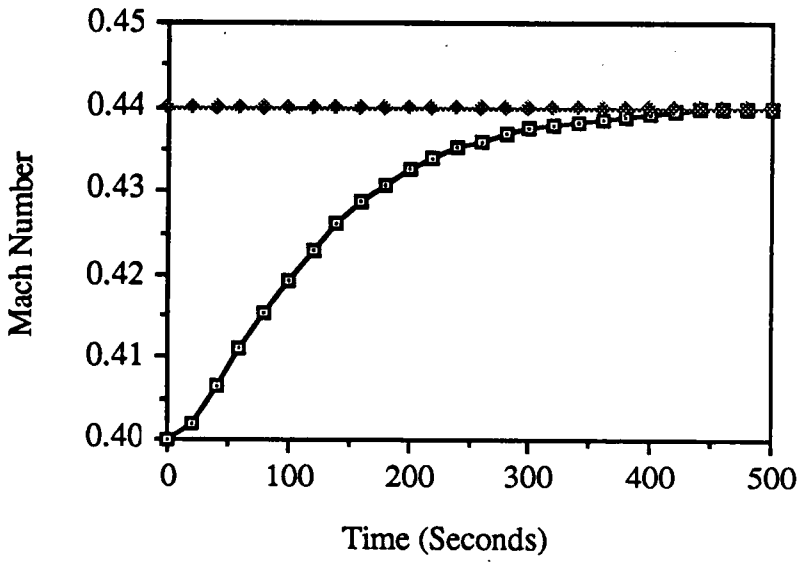



Figure C-16. Simulation Results for a Total Pressure of 1000 lb/ft$^2$ at Mach 0.4 and One Motor Operation.

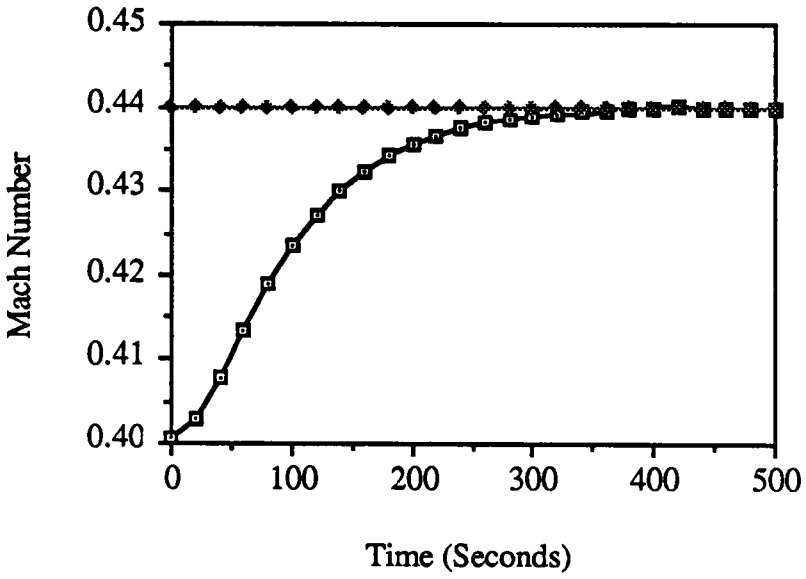



Figure C-17. Simulation Results for a Total Pressure of 1250 lb/ft$^2$ at Mach 0.4 and One Motor Operation.

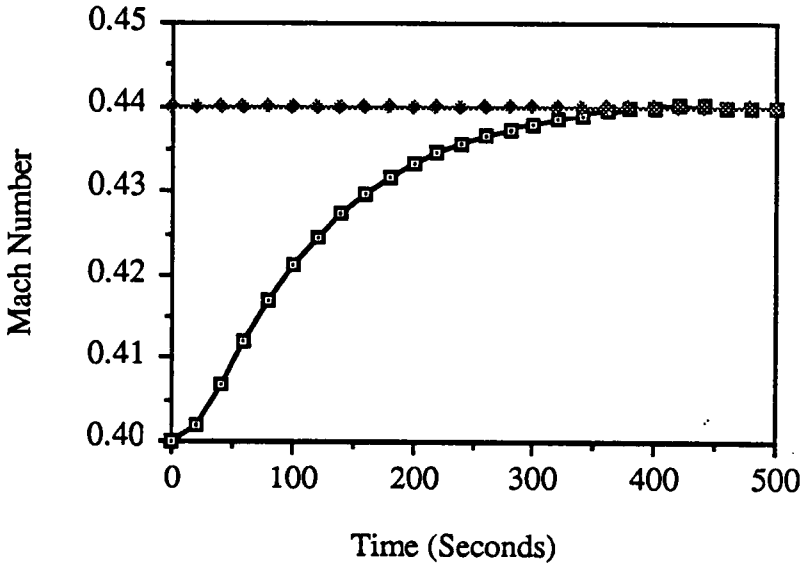



Figure C-18. Simulation Results for a Total Pressure of 1000 lb/ft$^2$ at Mach 0.4 and Two Motor Operation.

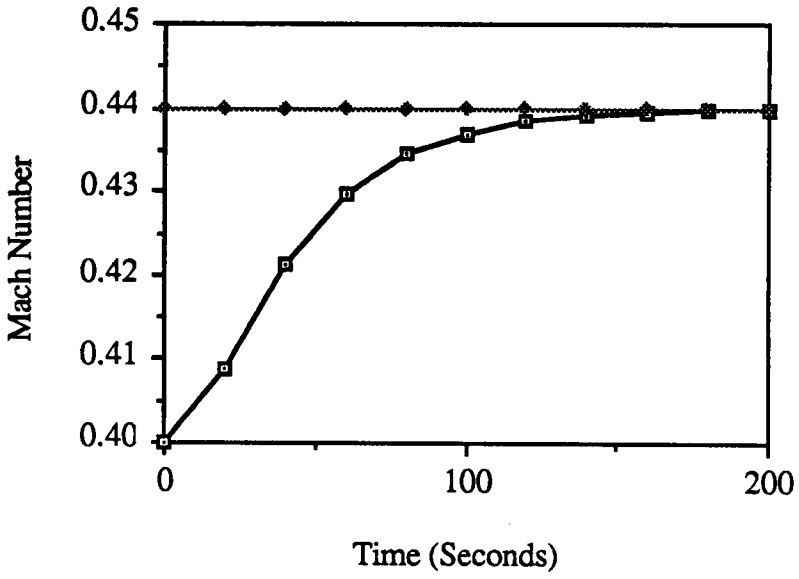



Figure C-19. Simulation Results for a Total Pressure of 3000 lb/ft$^2$ at Mach 0.4 and Two Motor Operation.

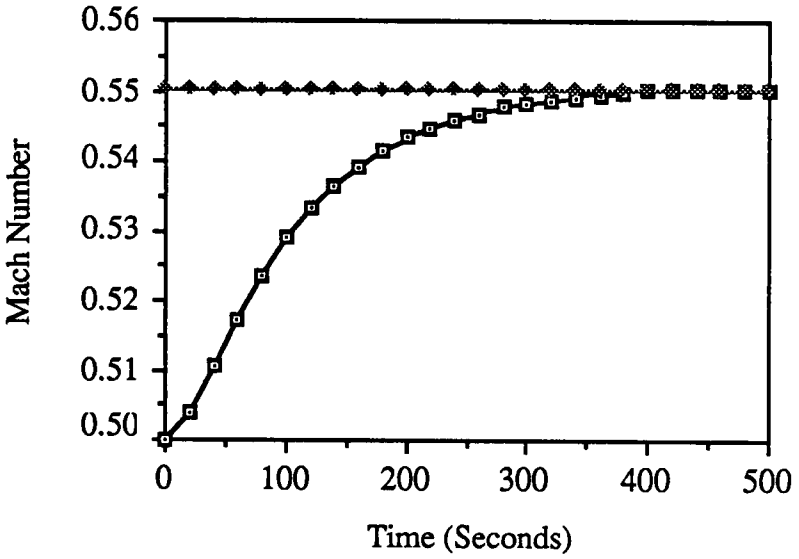



Figure C-20. Simulation Results for a Total Pressure of 1000 lb/ft$^2$ at Mach 0.5 and Two Motor Operation.

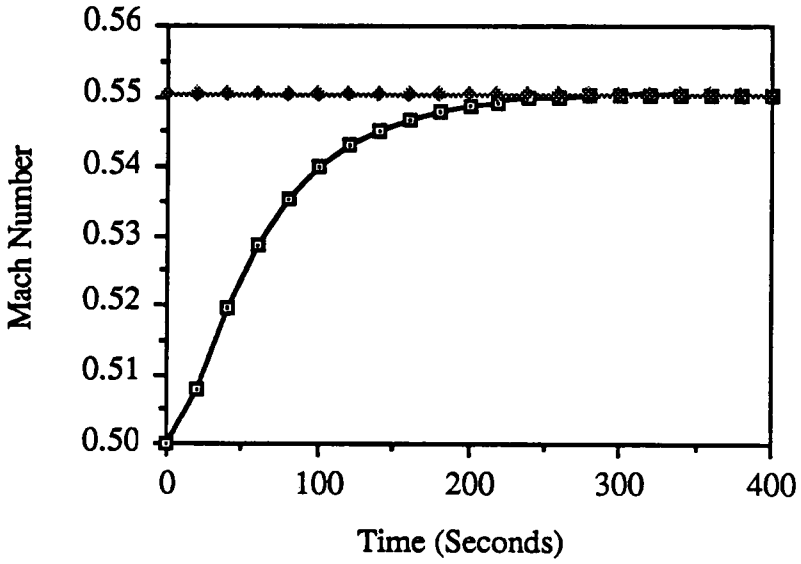



Figure C-21. Simulation Results for a Total Pressure of 2000 lb/ft$^2$ at Mach 0.5 and Two Motor Operation.

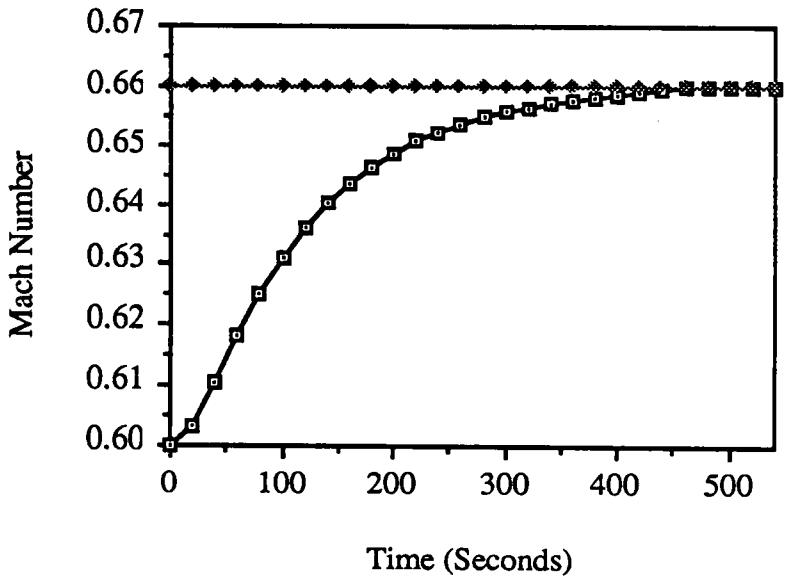



Figure C-22. Simulation Results for a Total Pressure of 750 lb/ft$^2$ at Mach 0.6 and Two Motor Operation.

# VITA

John Conrad Wysor was born in Birmingham, Alabama, on November 10, 1961. He graduated from Clinton Senior High School in Clinton, Tennessee, in May of 1980. He then entered the University of Tennessee in September 1980 where he studied mechanical engineering, receiving a Bachelor of Science degree in Mechanical Engineering in June of 1984.

After working for one year as a manufacturing engineer at Ferro Manufacturing in Pikeville, Tennessee, he returned to the University of Tennessee in January of 1986 to study electrical engineering. In June of 1987 he received a Bachelor of Science Degree in Electrical Engineering. In July of 1987 he obtained employment as a design engineer with Calspan Field Services, an operating contractor for Arnold Engineering Development Center, Arnold Air Force Station, Tennessee. Since September 1987 he has been attending the University of Tennessee Space Institute on a part-time basis working toward completion of a Master's Degree in Electrical Engineering.